

Dear editor,

In this document we include a point-by-point response to the reviews with a list of all relevant changes made in the manuscript, and a marked-up manuscript version.

We also include in the manuscript's introduction a more detailed discussion on the need and motivation for this work, as proposed by the editor: *"Overall, the importance of this work lies on an extended review and synthesis of the current knowledge of global atmospheric Fe deposition fluxes in the ocean, aiming to provide ensemble model data to the scientific community, able to be used in ocean biogeochemistry models and as comparative measures for atmospheric models."* (see p.7, lines 12-15).

We have also added 2 missing co-authors, acknowledgments (see marked-up manuscript), and we have corrected typos. The ensemble model fields from this work are now available online at <https://ecpl.chemistry.uoc.gr/GESAMP/>.

Kind regards,

S. Myriokefalitakis (on behalf of all co-authors)

We thank the Referee#1 for the careful reading of the paper. Please find below the point-by-point answers to the referee's general and specific comments and technical corrections.

1. General comments:

- Q: The authors state that this kind of modelling is the only way to estimate iron deposition (page 4 lines 11ff). But is it really impossible to utilise the large number of observations of Fe concentrations (listed in the SI) to estimate fluxes? I would like to see a better justification for this claim.
 - A: With our statement we do not want to devaluate the importance and the need of observations. We state that models are an excellent way to study atmospheric Fe supply to the oceans and to assess its impacts on a global scale, partly because of episodic nature of atmospheric deposition. Models enable the integration of knowledge and of discontinuous geographically and temporally observations and in synergy with observations are the appropriate tools to study the global spatial and temporal patterns of species such as Fe. We rephrased as: “*The use of global biogeochemical numerical models and surface observations is an excellent way to better understand past, present and future atmospheric supply to the oceans, as well as to quantify the resultant effect on the ocean biological productivity and the carbon uptake.*” (see page 4 lines 15-17).
- Q: The third aim of the work (page 7, top) seems circular – why would future modelling studies find the fluxes calculated in this modelling study useful, other than as comparative measures? I also miss an indication that the work described here is potentially useful in permitting prediction of changes in Fe deposition rates, for example due to anthropogenic activities.
 - A: The 3rd aim refers to the utility of the calculated ensemble Fe deposition as an input for the next-generation of ocean biogeochemistry modelling studies. Our study aims to provide to the scientific community with ensemble TFe and LFe deposition fluxes, as a result of state-of-the-art atmospheric models and satellite retrievals. Currently, most ocean biogeochemistry models use global dust deposition fields to derive the atmospheric Fe input (e.g., Aumont et al., 2015), usually by assuming a constant fraction by mass on dust. Furthermore, to take into account the labile fraction in Fe deposition fluxes, either a constant value is applied or Fe solubility maps from other atmospheric models are used (e.g., Mahowald et al., 2005). Such approaches mean that the ocean data will contain significant assumptions, which the current science no longer supports; e.g., the combustion Fe-containing aerosol and the heterogeneity of soil mineralogy are neglected as well as the explicitly calculation of the Fe solubilization processes (resulting in lower Fe solubility near the dust source regions and higher Fe solubility over the remote ocean than earlier estimates, bringing closer model results to observations).
Overall, models need to first be evaluated against observations though to have some level of confidence in their ability and then to use them in order to access for example the anthropogenic effects. We can further use the models for the predicting of changes in Fe deposition rates, especially for the past and the future.

2. Specific comments:

- Q: Page 21, line 10 states “*The TFe loading, Fe solubility, and LFe loading from the models are compared with the measurements and presented in Fig. 4.*” This confuses me, since I would use the term loading to mean a flux over time (mass per unit area). The axis labels refer to

concentrations, with units of mass per volume, but the text and the Figure caption use loading. Please clarify.

- A: We changed the term “loading” to “concentrations” (see page 21 line 26).
- Q: With reference to Figure 4, if I understand correctly (and if I don’t then please clarify the text) the MNB values indicate the overall bias of the predictions compared to the data, which would mean that the ensemble model overestimates LFe concentrations by a factor of five. Does it then follow that loadings to the ocean are overestimated by this factor? If so, then the proposed further work doesn’t seem to address the issue – Section 5 reads more like a series of minor tweaks than addressing a major quantification problem.

- A: As for the MNB values, overestimates are weighted more than equivalent underestimates. As was noted in p.24, l.24, a similar overestimate in the measured monthly averaged dust concentration from a the short-term cruise measurements was seen in the dust model intercomparison study of Huneus et al. (2011). The bias may be due to the short duration of the sampling frequencies. We added further work to address one of the major quantification problems in p.25, l.2, “due to to short of the sampling frequencies. *A comparison of long-term measurements with a multi-year modelling will allow assessment of the model performance to capture labile Fe concentrations under specific events*” after “Note, however, that evaluation of monthly mean model results by comparison with the shorter-term (e.g., daily) observations during different sampling periods introduces uncertainties”.

We also added the description of MNB in the text as following: “We use the monthly mean of model output to compare with the measurements. The normalized bias (NB) at a given grid box is calculated as follows:

$$NB_i = \frac{C_{model,i} - C_{obs,i}}{C_{obs,i}} \quad (2)$$

where, $C_{model,i}$ is the modelled aerosol concentration in grid box i , and $C_{obs,i}$ is the measured aerosol concentration in the same grid box. When discussing the multi-model results we use the mean of all models, while we also analyze the mean normalized bias (MNB) of the models against measurements (a perfect comparison would have a MNB of 0 and correlation, R , of 1). A model’s MNB is derived as the arithmetic mean of all NB_i values, thus overestimates are weighted more than equivalent underestimates.” (see page 21 lines 27-28 and page 22 lines 1-7).

- Q: Evaluating the importance of atmospherically deposited Fe depends greatly upon assessing the fate of the metal in ocean water. According to the authors “Upon deposition to the surface ocean, this fraction of Fe from the atmosphere can either enter the dissolved Fe pool, or precipitate-out as large oxy-hydroxide particles (Meskhidze et al., 2017)”. I am surprised that the cited study, which worked with high Fe concentrations and did not explore the influence of light on iron chemistry, is considered to represent the state of knowledge in this area. I am also surprised that neither this reference nor the paper under review cites the book by Turner and Hudson “The Biogeochemistry of Iron in Seawater” (Wiley 2001).

A: The study by Meskhidze et al. (2017) was designed to represent the processes affecting the soluble Fe deposited to the open oceans through atmospheric pathways on a time scale of sec to minutes. The concentrations were selected to be representative of wet removal (i.e., rainout and washout) which is the dominant removal mechanism over the remote oceans. The reference is used here, because, as far as we know, this is the first study that explored the role of atmospheric organic ligands on Fe solubility after deposition to the surface ocean. However, we agree with the reviewer tha additional references, particularly on the effects of oceanic ligands and

photochemistry need to be provided. The revised manuscript now reads: “*Upon deposition to the surface ocean, the soluble of Fe delivered through atmospheric pathways can either enter the dissolved Fe pool or precipitate-out as large oxy-hydroxide particles (de Baar and de Jong, 2001; Boyd and Ellwood, 2010; Meskhidze et al., 2017; Turner and Hunter, 2001).*” (see page 3 lines 27-29).

- Q: Is there any prospect of using the Fe loadings reported here to simulate Fe concentrations in the ocean? I realize that this may be outside the scope of the present paper, but some indication of possibilities would be welcome.
 - A: We included the following part in the conclusions: “*Although the calculation of the Fe concentrations in the ocean is outside the scope of this paper, we expect that the Fe deposition fluxes here provided will be used in oceanic models.*” (see page 27 lines 7-9).

- Q: It is not clear to me whether FeD deposited to the ocean is considered “inert” or whether it can yield significant dissolved. Maybe this could be explained. If it is not considered to be a source, then it is not so important to get the global fluxes correct, and the focus should be on the LFe.
 - A: Total Fe deposited in the ocean is important for the assessment of the fate of Fe in the ocean. Total Fe is needed for the comparison of particulate Fe with the measurements in the ocean biogeochemistry models (e.g., Ye and Völker, 2017). Additionally, less labile Fe in total Fe may be potentially utilized by marine organisms. Note that ocean biogeochemistry models (e.g., Aumont et al., 2015) take into account both the total and the soluble deposited Fe for chemistry calculations, assuming some fractions of less labile Fe in total Fe are dissolved in the ocean. For example, Aumont et al. (2015) considers that the particulate Fe from dust experiences dissolution in the water column, with the dissolution rate computed assuming that during sinking of mineral particles particulate Fe dissolves by about 0.01% per day (Bonnet, 2004). Therefore, both the total and the labile Fe deposition fluxes are needed. However, the dissolution of Fe from FeD is species depended and affected by spatiotemporal variations in the ocean. The following explanation has been added in the text in the introduction: “*Both the TFe and LFe atmospheric deposition can be used in ocean biogeochemical modelling. For example, total Fe is needed for comparisons of particulate Fe with the measurements in the ocean biogeochemistry models (e.g., Ye and Völker, 2017), while LFe can be assumed as readily available to the marine ecosystem. Note that the less labile fraction of Fe in TFe can be slowly dissolved from particulate Fe in the ocean during sinking of mineral particles (e.g., roughly 0.01% per day; Bonnet, 2004), with the dissolution of Fe, however being species depended and affected by spatiotemporal variations in the ocean.*” (see page 4 lines 26-31).

- Q: As I understand it, a similar loading (to LFe) of dissolved Fe to the oceans comes from rivers. Could the authors briefly explain why this is not considered as important as the atmospherically-deposited form?
 - A: According to the recent study of Tagliabue et al. (2016), riverine inputs are considering 1-2 order of magnitudes smaller than the atmospheric dust deposition to the global ocean. We included the following part in the manuscript (introduction), to further refer to the other known sources of Fe in the global ocean: “*However, significant Fe inputs from continental margins and hydrothermal vents are also supplied to the global*

ocean, regulating the ocean biogeochemical cycles. Moreover, riverine Fe inputs are currently estimated 1-2 orders of magnitudes smaller than the atmospheric pathway (e.g., Tagliabue et al., 2016), affecting mainly coastal regions, while icebergs and glaciers could also be important to the polar oceans (Raiswell et al., 2016).” (see page 3 lines 12-16).

- Q: Section 2.1.2 introduces the presence of oxalate in aerosols, without explanation of its sources and why other carboxylic acids are not considered. I am not at all expert in this area, it appears as though oxalate is assumed or known to be dominant – if so then its strong solubilising properties are clearly important. I would appreciate some references to justify the assumption that oxalate is truly dominant in governing aerosol Fe solubility.
 - A: Indeed, numerous organic compounds, such as acetate, formate, oxalate, malonate, succinate, glutarate, glycolate, lactate, tartrate and humic like substances (HULIS) can be found in atmospheric waters. However, oxalate, malonate, tartrate and humic acid have been observed to enhance Fe solubility (e.g., Paris et al., 2010, 2011). For all these organic ligands, positive dependences of iron solubility to organic concentrations were observed and revealed that the extent of organic complexation on iron solubility decreased in the following order: oxalate > malonate = tartrate > humic acid (Paris et al., 2011). Therefore, this study confirmed that among the known atmospheric organic binding ligands of Fe, oxalate is the most effective ligand in promoting dust iron solubility under atmospheric conditions. Furthermore, observations in the atmosphere, point to oxalate as the most abundant organic ligand (e.g., Kawamura and Ikushima, 1993; Kawamura and Sakaguchi, 1999). Oxalate originates from multiphase chemistry of organics, but has also weak anthropogenic primary sources (see Myriokefalitakis et al., 2011 and Lin et al., 2014 for a comprehensive global modelling study of atmospheric oxalate). Therefore, atmospheric models use oxalate to study the effect of organic ligands on Fe dissolution. However, the lack of experimental data for Fe-containing minerals mixed with a variety of organic ligands in solution is an important source of uncertainty. For clarity, in Sect. 2.1.2 we added after the first sentence the following explanatory text: “*Oxalate is, however, used in models as a proxy of all organic ligands for ligand-promoted dissolution since 1) it is the most abundant in the atmosphere (e.g., Kawamura and Ikushima, 1993; Kawamura and Sakaguchi, 1999) originating mainly from secondary sources and only a weak contribution from combustion primary sources (e.g., Myriokefalitakis et al., 2011) and 2) it is the most effective ligand in promoting iron solubilisation (e.g., Paris et al., 2011). We note, however, that more work is required to elucidate the role of other ligands that may promote Fe dissolution in future studies.*” (see page 12 lines 3-9).
- Q: The right-hand maps in Figure S4 are not informative. Is it possible – or do the authors consider it worthwhile? – to show primary sources of LFe?
 - A: As we state in the text, not all the models simulate the LFe primary and secondary sources in the same manner of dust and combustion aerosols. For a fairer comparison in Fig. S4, we show the primary (i.e., emissions) and secondary (i.e., atmospheric processing) sources together. As we state in the manuscript “*The models use significantly different assumptions to describe the total LFe source to the atmosphere and therefore primary (emissions) and secondary (atmospheric processing) sources cannot be accurately separated from rapid formation assumed in coarse-scale models.*” (see page 17 lines 9-12). A detailed description of models’ parameterizations as well as the differences among them with regard to the LFe sources, are also presented in Sect. 2.1.

3. Technical Corrections:

- Q: Page 5 line 15 This sentence needs improvement.
 - A: We rephrased the text between lines 13-19 as follows: “*During atmospheric transport, coating of Fe-containing dust particles by acidic compounds (e.g., sulfates and nitrates) increases the Fe solubility. When this process is taken into account in model simulations (e.g., Meskhidze et al., 2005) it aids in explaining the observations. Indeed, measurements of the fresh dust particles present low (<<1%) initial solubilities (Chuang et al., 2005; Fung et al., 2000; Hand et al., 2004; Sedwick et al., 2007), while high aerosol solubilities are commonly observed at lower dust concentrations far from sources (Baker and Jickells, 2006; Sholkovitz et al., 2012; Oakes et al., 2012). Atmospheric processing of dust (Kumar et al., 2010; Meskhidze et al., 2003; Srinivas et al., 2014) is considered as the best candidate to explain these observations.*” (see page 5 lines 21-28).

- Q: Table S3. What does “NaN” mean? (not analysed I guess, but please say).
 - A: NaN is replaced with “-”, which means that data are not available. We have also modified and explain it now in the Table S3 caption.

- Q: Figure S7 should have “continuous” not “*continues*”.

A: Done

- Q: Page 21 line 19. I assume that SH = southern hemisphere? Is this so very well known?

A: We replaced “SH” with “*the Southern Hemisphere*”.

- Q: Page 21 line 22. Should it read 0.50-0.56?
 - A: The value is correct. The differences in Fe solubility trend between CAM4 and TM4-ECPL can be partly seen from Fig. 5.

4. References

- Aumont, O., Ethé, C., Tagliabue, A., Bopp, L. and Gehlen, M.: PISCES-v2: an ocean biogeochemical model for carbon and ecosystem studies, *Geosci. Model Dev.*, 8(8), 2465–2513, doi:10.5194/gmd-8-2465-2015, 2015.
- de Baar, H. J. and de Jong, J. T.: ‘Distributions, sources and sinks of iron in seawater, ’, 2001.
- Baker, A. R. and Jickells, T. D.: Mineral particle size as a control on aerosol iron solubility, *Geophys. Res. Lett.*, 33(17), L17608, doi:10.1029/2006GL026557, 2006.
- Baker, A. R., French, M. and Linge, K. L.: Trends in aerosol nutrient solubility along a west–east transect of the Saharan dust plume, *Geophys. Res. Lett.*, 33(7), L07805, doi:10.1029/2005GL024764, 2006.
- Bonnet, S.: Dissolution of atmospheric iron in seawater, *Geophys. Res. Lett.*, 31(3), L03303, doi:10.1029/2003GL018423, 2004.

Boyd, P. W. and Ellwood, M. J.: The biogeochemical cycle of iron in the ocean, *Nat. Geosci.*, 3(10), 675–682, doi:10.1038/ngeo964, 2010.

Chuang, P. Y., Duvall, R. M., Shafer, M. M. and Schauer, J. J.: The origin of water soluble particulate iron in the Asian atmospheric outflow, *Geophys. Res. Lett.*, 32(7), L07813, doi:10.1029/2004GL021946, 2005.

Fung, I. Y., Meyn, S. K., Tegen, I., Doney, S. C., John, J. G. and Bishop, J. K. B.: Iron supply and demand in the upper ocean, *Global Biogeochem. Cycles*, 14(1), 281–295, doi:10.1029/1999GB900059, 2000.

Hand, J. L., Mahowald, N. M., Chen, Y., Siefert, R. L., Luo, C., Subramaniam, A. and Fung, I.: Estimates of atmospheric-processed soluble iron from observations and a global mineral aerosol model: Biogeochemical implications, *J. Geophys. Res.*, 109(D17), D17205, doi:10.1029/2004JD004574, 2004.

Kawamura, K. and Ikushima, K.: Seasonal changes in the distribution of dicarboxylic acids in the urban atmosphere, *Environ. Sci. Technol.*, 27(10), 2227–2235, doi:10.1021/es00047a033, 1993.

Kawamura, K. and Sakaguchi, F.: Molecular distributions of water soluble dicarboxylic acids in marine aerosols over the Pacific Ocean including tropics, *J. Geophys. Res. Atmos.*, 104(D3), 3501–3509, doi:10.1029/1998JD100041, 1999.

Kumar, A., Sarin, M. M. and Srinivas, B.: Aerosol iron solubility over Bay of Bengal: Role of anthropogenic sources and chemical processing, *Mar. Chem.*, 121(1–4), 167–175, doi:10.1016/j.marchem.2010.04.005, 2010.

Lin, G., Sillman, S., Penner, J. E. and Ito, A.: Global modeling of SOA: the use of different mechanisms for aqueous-phase formation, *Atmos. Chem. Phys.*, 14(11), 5451–5475, doi:10.5194/acp-14-5451-2014, 2014.

Mahowald, N. M., Baker, A. R., Bergametti, G., Brooks, N., Duce, R. A., Jickells, T. D., Kubilay, N. N., Prospero, J. M. and Tegen, I.: Atmospheric global dust cycle and iron inputs to the ocean, *Global Biogeochem. Cycles*, 19(4), GB4025, doi:10.1029/2004GB002402, 2005.

Meskhidze, N., Chameides, W. L., Nenes, A. and Chen, G.: Iron mobilization in mineral dust: Can anthropogenic SO₂ emissions affect ocean productivity?, *Geophys. Res. Lett.*, 30(21), 2085, doi:10.1029/2003GL018035, 2003.

Meskhidze, N., Chameides, W. L. and Nenes, A.: Dust and pollution: A recipe for enhanced ocean fertilization?, *J. Geophys. Res. D Atmos.*, 110(3), 1–23, doi:10.1029/2004JD005082, 2005.

Meskhidze, N., Hurley, D., Royalty, T. M. and Johnson, M. S.: Potential effect of atmospheric dissolved organic carbon on the iron solubility in seawater, *Mar. Chem.*, 194, 124–132, doi:10.1016/j.marchem.2017.05.011, 2017.

Myriokefalitakis, S., Tsigaridis, K., Mihalopoulos, N., Sciare, J., Nenes, A., Kawamura, K., Segers, A. and Kanakidou, M.: In-cloud oxalate formation in the global troposphere: a 3-D modeling study, *Atmos. Chem. Phys.*, 11(12), 5761–5782, doi:10.5194/acp-11-5761-2011, 2011.

Oakes, M., Ingall, E. D., Lai, B., Shafer, M. M., Hays, M. D., Liu, Z. G., Russell, A. G. and Weber, R. J.: Iron Solubility Related to Particle Sulfur Content in Source Emission and Ambient Fine Particles, *Environ. Sci. Technol.*, 46(12), 6637–6644, doi:10.1021/es300701c, 2012.

Paris, R., Desboeufs, K. V., Formenti, P., Nava, S. and Chou, C.: Chemical characterisation of iron in dust and biomass burning aerosols during AMMA-SOP0/DABEX: implication for iron solubility, *Atmos. Chem. Phys.*, 10(9), 4273–4282, doi:10.5194/acp-10-4273-2010, 2010.

Paris, R., Desboeufs, K. V. and Journet, E.: Variability of dust iron solubility in atmospheric waters: Investigation of the role of oxalate organic complexation, *Atmos. Environ.*, 45(36), 6510–6517, doi:10.1016/j.atmosenv.2011.08.068, 2011.

Raiswell, R., Hawkings, J. R., Benning, L. G., Baker, A. R., Death, R., Albani, S., Mahowald, N., Krom, M. D., Poulton, S. W., Wadham, J. and Tranter, M.: Potentially bioavailable iron delivery by iceberg-hosted sediments and atmospheric dust to the polar oceans, *Biogeosciences*, 13(13), 3887–3900, doi:10.5194/bg-13-3887-2016, 2016.

Sedwick, P. N., Sholkovitz, E. R. and Church, T. M.: Impact of anthropogenic combustion emissions on the fractional solubility of aerosol iron: Evidence from the Sargasso Sea, *Geochemistry, Geophys. Geosystems*, 8(10), 1–21, doi:10.1029/2007GC001586, 2007.

Sholkovitz, E. R., Sedwick, P. N., Church, T. M., Baker, A. R. and Powell, C. F.: Fractional solubility of aerosol iron: Synthesis of a global-scale data set, *Geochim. Cosmochim. Acta*, 89, 173–189, doi:10.1016/j.gca.2012.04.022, 2012.

Srinivas, B., Sarin, M. M. and Rengarajan, R.: Atmospheric transport of mineral dust from the Indo-Gangetic Plain: Temporal variability, acid processing, and iron solubility, *Geochemistry, Geophys. Geosystems*, 15(8), 3226–3243, doi:10.1002/2014GC005395, 2014.

Tagliabue, A., Aumont, O., DeAth, R., Dunne, J. P., Dutkiewicz, S., Galbraith, E., Misumi, K., Moore, J. K., Ridgwell, A., Sherman, E., Stock, C., Vichi, M., Völker, C. and Yool, A.: How well do global ocean biogeochemistry models simulate dissolved iron distributions?, *Global Biogeochem. Cycles*, 30(2), 149–174, doi:10.1002/2015GB005289, 2016.

Turner, D. R. and Hunter, K. A.: The biogeochemistry of iron in seawater, J. Wiley. [online] Available from: <https://www.wiley.com/en-us/The+Biogeochemistry+of+Iron+in+Seawater-p-9780471490685> (Accessed 27 August 2018), 2001.

Ye, Y. and Völker, C.: On the Role of Dust-Deposited Lithogenic Particles for Iron Cycling in the Tropical and Subtropical Atlantic, *Global Biogeochem. Cycles*, 31(10), 1543–1558, doi:10.1002/2017GB005663, 2017.

Zhu, X., Prospero, J. M., Savoie, D. L., Millero, F. J., Zika, R. G. and Saltzman, E. S.: Photoreduction of iron(III) in marine mineral aerosol solutions, *J. Geophys. Res. Atmos.*, 98(D5), 9039–9046, doi:10.1029/93JD00202, 1993.

Zhuang, G., Yi, Z., Duce, R. A. and Brown, P. R.: Link between iron and sulphur cycles suggested by detection of Fe(n) in remote marine aerosols, *Nature*, 355(6360), 537–539, doi:10.1038/355537a0, 1992.

We thank the Referee #2 for the careful reading of the manuscript. Please find below the point-by-point answers to the referee's general, specific and technical comments.

1. General comments:

- Q: My main concern is about the interannual variability of the models. As stated in Table 1, the simulated years are different for each model but the interannual variability of each model is not presented nor discussed.
 - A: This work uses single year model results only. Therefore, no year-to-year variability is possible to be presented in our post-processed analysis for the present atmosphere. However, our analysis shows the variability derived from the structural differences between models.

- Q: Moreover, no requests for meteorological conditions or emission inventories have been set to the model simulations and the sensitivity of each model to these parameters are also not discussed.
 - A: The aim of this work is to describe the current state of Fe global atmospheric deposition modeling and provide a multi-model ensemble of Fe atmospheric deposition fluxes of the current estimates, characterized with regard to observations (see introduction). It aims also to understand the origin of the respective model differences over the oceanic regions among the participating models and not to conclude which model is the best. As discussed in the model description (section 2), the participating models use different parameterizations to simulate the Fe-cycle in the atmosphere. Although using the same meteorology and the same emission inventories in the participating models would have been a very interesting exercise this is out of the scope of the present study. All models are driven by publicly available meteorological datasets that have been used and evaluated in numerous studies. As shown in Table 1, two models are using GEOS-5, one model GEOS-FP and one ERA interim meteorology (see in Table 1).

2. Specific comments:

- Q: P2, line 1: please add min and max for TFe and LFe deposition fluxes.
 - A: The minimum and maximum values for the global mean of the deposition fluxes TFe and LFe are added. This part now reads: “*The mean global deposition fluxes into the global ocean is here estimated in the range of 10-30 Tg-Fe yr⁻¹ and 0.2-0.4 Tg-Fe yr⁻¹ for TFe and LFe, corresponding to roughly ~15 Tg-Fe yr⁻¹ and ~0.3 Tg-Fe yr⁻¹, respectively, for the for the multi model ensemble model mean.*” (see page 2 lines 3-6).

- Q: P3, lines 18-22: the fraction of Fe that is bioavailable is still not well known and also depends on phytoplankton species, so I suggest that the authors do not write that labile Fe is a good approximation for bioavailable Fe.
 - A: We agree with the reviewer that Fe bioavailability is a complex issue and for this we clearly stated this in the manuscript (pp3, lines: 16-22). However to make it more clear we rephrased this part as (please see also our reply to Reviewer 1): “*The bioavailability of Fe is a complex issue (e.g., Lis et al., 2015; Morel et al., 2008) and several naming conventions and abbreviations were used to characterize the*

atmospheric supply of potentially bioavailable Fe to the global ocean (Baker and Croot, 2010; Shi et al., 2012). It has been widely assumed that soluble Fe can be considered, as a first approximation, to be bioavailable (Baker et al., 2006a, 2006b) and a common experimental practice to determine the bioavailable Fe fraction in Fe-containing aerosols is the quantification of Fe in a leachate solution that passes through 0.45 μm , 0.2 μm or 0.02 μm sized filter (see Meskhidze et al., 2016 and ref. therein). However, due to its operational definition, it has been shown that this filterable Fe may contain both the soluble Fe and colloidal forms (Jickells and Spokes, 2001; Raiswell and Canfield, 2012). Upon deposition to the surface ocean, the soluble of Fe delivered through atmospheric pathways can either enter the dissolved Fe pool in the ocean, or precipitate-out as large oxy-hydroxide particles (de Baar and de Jong, 2001; Boyd and Ellwood, 2010; Meskhidze et al., 2017; Turner and Hunter, 2001). Consequently, the impact of atmospheric Fe on marine biogeochemistry depends on both the total Fe (TFe) deposition and its solubility, keeping in mind that the bioavailable fraction of Fe in seawater will then also change due to post-atmospheric deposition ocean processes (e.g., Baker and Croot, 2010; Chen and Siefert, 2004; Meskhidze et al., 2017; Rich and Morel, 1990).” (see page 3 lines 19-30 and page 4 lines 1-3).

○

- Q: P4, line 8: “can be also be”
 - A: Corrected.

- Q: P6, lines 2-5: for the role of oxalate on Fe solubility, Paris et al. (2011) could be cited as well (<https://doi.org/10.1016/j.atmosenv.2011.08.068>) .
 - A: Reference added (see page 6 line 13).

- Q: P7, line 29: please change “in (Albani et al., 2014)” by “in Albani et al. (2014)”
 - A: Typo corrected.

- Q: P18, lines 28-30: “LFe sources are mainly driven by mineral dust aerosols, although a significant fraction (6 to 62%) is due to LFe combustion aerosols, especially over the high-latitudes of the Northern Hemisphere (Ito et al. 2018; companion manuscript to be submitted).” I would rather put this sentence in the previous section.
 - A: We agree with the reviewer. The sentence has been moved into the previous section.

- Q: P19, lines 1-5: the authors compare the seasonal variability of LFe, but I would have liked to see the error bars on Fig. 1, as well as more information on the statistical test (which one was used, P value, n, . . .).
 - A: Error bars in Fig. 1 are added. For the individual models, however, the results here correspond to one year of simulation. Therefore, no statistics can be derived for the seasonal deposition fluxes which are calculated as the sum of monthly deposition fluxes. We provide further statistics for the ensemble model; the median bias correction factors are presented in Table 3 for each model, together with the lower and upper 95% confidence interval.

- Q: Moreover, the authors state that “in most of the cases IMPACT and GEOS-Chem present similar seasonal variation.” However, IMPACT is higher in JJA, while GEOS is higher in MAM.
 - A: We thank the reviewer for pointing this inconsistency. We now corrected this part as: “*However, significant differences in the magnitude of the deposition fluxes are calculated between models (Fig. 1). A seasonal maximum in the deposition fluxes is calculated by CAM4 and GEOS-Chem during MAM, attributed to Saharan mineral dust aerosols, while IMPACT and TM4-ECPL present a seasonal maximum during JJA.*” (see page 9 lines 16-19).

- Q: P19, lines 9-11: the authors state that “in the other seasons the 30N maximum is not clearly present”, but in JJA, a clear maximum for IMPACT is seen at 30°N.
 - A: We now rephrased this part as: “*In DJF, and to a lesser extent in JJA, two zonal maxima are shown near the equator and around 30N.*” (see page 19 lines 22-23).

- Q: P21, line 12: the authors should explain how they calculate the mean normalized bias. Why would a value of 2.4 mean that the concentrations are underestimated? This is not clear to me.
 - A: We agree with the reviewer that this sentence is confusing. We have rephrased for clarity as follows: “*This reflects that overall the models overestimate TFe surface mass concentrations. However, from Fig. 4 we can see that this overestimate is higher for the highest TFe concentrations near the dust source regions and tend to turn to an underestimate for the lowest concentrations observed over remote oceans.*” (see page 22 lines 10-12).
A detailed description of MNB calculations has been also added in the manuscript (please see Eq. 2, page 22, line 2 and our reply to Referee#1).

- Q: P22, line 3 and Fig. 5: the authors discuss the relationship between Fe solubility and aerosol Fe concentrations but these 2 variables are not independent as the latter one is used to calculate the former one. How do the authors deal with that?
 - A: This is a good question. We are aware that concentrations and solubility are not independent variables in the calculations since solubility is the ratio of Labile to Total Fe concentrations. At low Fe concentration, for example, Fe solubility of TM4 is similar to ensemble model (red triangles in Fig. 5). This is because the mean Fe solubility is weighted by Fe concentration. More specifically, Fe concentration at low concentration of TM4 is much higher than other models, resulting in similar Fe solubility between TM4 and ensemble model. This indicates that a small number of aerosols with high Fe concentration can determine Fe solubility in bulk samples. We added further work to address one of the major quantification problems due to the sampling issues: “*Note, however, that evaluation of monthly mean model results by comparison with the shorter-term (e.g., daily) observations during different sampling periods introduces uncertainties, due to short of the sampling frequencies; a comparison of long-term measurements with a multi-year modelling will allow assessment of the model performance to capture labile Fe concentrations under specific events.*” (page 26, lines 4-9).
 - At the same time, models consider the process of enhancement of Fe solubility. It is therefore interesting to see whether the models are able to capture the fraction of LFe

to TFe correctly and this is what we are evaluating in Fig. 5. This figure shows that the models have difficulties to simulate the 4 orders of magnitude variability from 0.02% to 98% in the Fe solubility observed in the atmosphere (Fig. 5a). IMPACT simulates almost 3 orders of magnitude variability in Fe solubility. In the other models including the ensemble model, Fe solubility is less variable (one to two orders of magnitude only). In particular, low solubilities (high concentrations near sources) are overestimated and high solubilities (low concentrations at remote locations) are underestimated. This may indicate that the primary LFe in the models is overestimated and that models are missing solubilisation processes during transport or that those considered in the models are not sufficient effective. The discussion has been added appropriately in the manuscript.

- Q: P23, line 12-: How is the lifetime (turnover time) calculated? Is it calculated by dividing the concentration by the deposition flux, both estimated by the model? This could be added in the text.
 - A: We explain in the caption of Fig. 6 that lifetimes are the calculated atmospheric concentrations (or burdens) divided by total sinks”, but for clarity we also added the following explanation in the manuscript:
“Figure 6 presents the spatial distribution of TFe lifetime over the ocean (i.e., atmospheric concentrations divided by total sinks), as calculated for the ensemble model.” (page 24, lines 16-17).

- Q: P24, lines 26-27: please change “similar to what it was pointed out in (Albani et al., 2014) and seen in the dust model intercomparison study of Huneus et al. (2011).” By “similar to what was pointed out in Albani et al. (2014) and seen in the dust model intercomparison study of Huneus et al. (2011)”.
 - A: We corrected the typos (page 26, lines 1-2).

The GESAMP atmospheric iron deposition model intercomparison study

Stelios Myriokefalitakis^{1,a}, Akinori Ito², Maria Kanakidou³, Athanasios Nenes⁴, Maarten C. Krol¹, Natalie M. Mahowald⁵, Rachel A. Scanza⁵, Douglas S. Hamilton⁵, Matthew S. Johnson⁶, Nicholas Meskhidze⁷, Jasper F. Kok⁸, Cecile Guieu⁹, Alex R. Baker¹⁰, Timothy D. Jickells¹⁰, Manmohan M. Sarin¹¹, Srinivas Bikina¹¹, [Rachel Shelley¹²](#), [Andrew Bowie^{13,14}](#), Morgane M. G. Perron¹³ and Robert A. Duce¹⁵

¹ Institute for Marine and Atmospheric Research (IMAU), Utrecht University, 3584 CC Utrecht, The Netherlands

² Yokohama Institute for Earth Sciences, JAMSTEC, Yokohama, Kanagawa 236-0001, Japan

³ Environmental Chemical Processes Laboratory (ECPL), Department of Chemistry, University of Crete, 70013 Heraklion, Greece

⁴ School of Earth & Atmospheric Sciences, Georgia Institute of Technology, Atlanta, GA 30332, USA

⁵ Department of Earth and Atmospheric Sciences, Cornell University, Ithaca NY, 14853, USA

⁶ Earth Science Division, NASA Ames Research Center, Moffett Field, CA, USA

⁷ Marine, Earth, and Atmospheric Sciences, North Carolina State University, Raleigh, NC, USA

⁸ Department of Atmospheric and Oceanic Sciences, University of California, Los Angeles, CA 90095, USA

⁹ Laboratoire d'Océanographie de Villefranche (LOV), UMR7093, CNRS-INSU-Université Paris 6, Villefranche sur Mer, France, France

¹⁰ Centre for Ocean and Atmospheric Sciences, School of Environmental Sciences, University of East Anglia, Norwich, UK

¹¹ Geosciences Division, Physical Research Laboratory, Ahmedabad, India

¹² [Florida State University, Tallahassee, USA](#)

¹³ Institute for Marine and Antarctic Studies, University of Tasmania, Hobart, Tasmania, Australia

¹⁴ [Antarctic Climate & Ecosystems CRC, Hobart, Tasmania, Australia](#)

¹⁵ Departments of Oceanography and Atmospheric Sciences, Texas A&M University, College Station, TX, USA

^a now at: [Institute for Environmental Research & Sustainable Development \(IERSD\), National Observatory of Athens, GR-15236 Palea Penteli, Greece](#)

Correspondence to: Stelios Myriokefalitakis (steliosm@noa.gr) and Akinori Ito (akinorii@jamstec.go.jp)

Abstract.

This work reports on the current status of global modelling of iron (Fe) deposition fluxes and atmospheric concentrations and analyses of the differences between models, as well as between models and observations. A total of four global 3-D chemistry-transport (CTMs) and general circulation (GCMs) models have participated in this intercomparison, in the framework of the United Nations Joint Group of Experts on the Scientific Aspects of Marine Environmental Protection (GESAMP) Working Group 38, “The Atmospheric Input of Chemicals to the Ocean”. The global total Fe (TFe) emissions strength in the models is equal to ~ 72 Tg-Fe yr⁻¹ (38–134 Tg-Fe yr⁻¹) from mineral dust sources and around 2.1 Tg-Fe yr⁻¹ (1.8–2.7 Tg-Fe yr⁻¹) from combustion processes (sum

Deleted: ²

Deleted: ³

Deleted: ¹²

Deleted: ¹³

Deleted:

Deleted: s.myriok@uu.nl

of anthropogenic combustion/biomass burning and wildfires). The mean global labile Fe (LFe) source strength in the models, considering both the primary emissions and the atmospheric processing, is calculated to be 0.7 (± 0.3) Tg-Fe yr⁻¹, accounting for mineral dust and combustion aerosols together. The mean global deposition fluxes into the global ocean is estimated in the range of 10-30 Tg-Fe yr⁻¹ and 0.2-0.4 Tg-Fe yr⁻¹ for TFe and LFe,
5 corresponding to roughly 15 Tg-Fe yr⁻¹ and 0.3 Tg-Fe yr⁻¹, respectively, for the multi model ensemble model mean.

The model intercomparison analysis indicates that the representation of the atmospheric Fe cycle varies among models, in terms of both the magnitude of natural and combustion Fe emissions as well as the complexity of atmospheric processing parametrizations of Fe-containing aerosols. The model comparison with aerosol Fe
10 observations over oceanic regions indicate that most models overestimate surface level TFe mass concentrations near the dust source regions and tend to underestimate the low concentrations observed in remote ocean regions. All models are able to simulate the tendency of higher Fe concentrations near and downwind from the dust
15 source regions, with the mean normalized bias for the Northern Hemisphere (~14), larger than the Southern Hemisphere (~2.4) for the ensemble model mean. This model intercomparison and model-observation comparison study reveals two critical issues in LFe simulations that require further exploration: 1) the Fe-containing aerosol size distribution and 2) the relative contribution of dust and combustion sources of Fe to labile Fe in atmospheric aerosols over the remote oceanic regions.

Deleted: multi model ensemble

Deleted: TFe and LFe

Deleted: are calculated

Deleted: be ~

Deleted: ~

Deleted: .

Deleted: loading

1 Introduction

Oceans are important for the Earth System's functioning, currently absorbing roughly 27% of total CO₂ emissions (e.g., Le Quéré et al., 2013), providing about half of atmospheric oxygen and being a source of biomass needed to help sustain life on our planet. Iron (Fe) is a key element for marine life (Duce and Tindale, 1991; Fung et al., 2000) being required for photosynthesis and respiration. As an essential micronutrient, Fe (co-)limits ocean productivity over large regions (Boyd et al., 2005; Jickells et al., 2005; Martin et al., 1991; Moore et al., 2013), influences the nitrogen fixation capability of diazotrophs in oligotrophic regions (Falkowski, 1997; Falkowski et al., 2000) and overall affects the transport and sequestration of carbon into the deep ocean (Maher et al., 2010). Atmospheric deposition is considered an important external Fe source to the open ocean (Jickells et al., 2005; Tagliabue et al., 2017). Micronutrient Fe delivered through atmospheric pathways may influence the primary and export production of carbon over the High-Nutrient Low-Chlorophyll (HNLC) oceanic regions (i.e., the oceanic regions where Fe is the limiting factor for phytoplankton productivity). However, significant Fe inputs from continental margins and hydrothermal vents are also supplied to the global ocean, regulating the ocean biogeochemical cycles. Moreover, riverine Fe inputs are currently estimated 1-2 orders of magnitudes smaller than the atmospheric pathway (e.g., Tagliabue et al., 2016), affecting mainly coastal regions, while icebergs and glaciers could also be important to the polar oceans (Raiswell et al., 2016).

Understanding of the impact of Fe on global marine productivity requires knowledge of the rates and locations of Fe supply to the ocean, and of the physicochemical forms of Fe that can be utilized by marine biota (i.e., those that are bioavailable). The bioavailability of Fe is a complex issue (e.g., Lis et al., 2015; Morel et al., 2008) and several naming conventions and abbreviations were used to characterize the atmospheric supply of potentially bioavailable Fe to the global ocean (Baker and Croot, 2010; Shi et al., 2012). It has been widely assumed that soluble Fe can be considered, as a first approximation, to be bioavailable (Baker et al., 2006a, 2006b) and a common experimental practice to determine the bioavailable Fe fraction in Fe-containing aerosols is the quantification of Fe in a leachate solution that passes through 0.45 µm, 0.2 µm or 0.02 µm sized filter (see Meskhidze et al., 2016 and ref. therein). However, due to its operational definition, it has been shown that this filterable Fe may contain both the soluble Fe and colloidal forms (Jickells and Spokes, 2001; Raiswell and Canfield, 2012). Upon deposition to the surface ocean, the soluble Fe delivered through atmospheric pathways can either enter the dissolved Fe pool or precipitate-out as large oxy-hydroxide particles (de Baar and de Jong, 2001; Boyd and Ellwood, 2010; Meskhidze et al., 2017; Turner and Hunter, 2001). Consequently, the impact of atmospheric Fe on marine biogeochemistry depends on both the total Fe (TFe) deposition and its solubility,

Deleted: (Boyd et al., 2005; Jickells et al., 2005; Martin et al., 1991; Moore et al., 2013), influences the nitrogen fixation capability of diazotrophs in oligotrophic regions (Falkowski, 2000, 1997) and overall affects the transport and sequestration of carbon into the deep ocean

Deleted: Atmospheric deposition is considered an important external Fe source to the open ocean (Jickells et al., 2005; Tagliabue et al., 2017). Micronutrient Fe delivered through atmospheric pathways may influence the primary and export production of carbon over the High-Nutrient Low-Chlorophyll (HNLC) oceanic regions (i.e., the oceanic regions where Fe is the limiting factor for phytoplankton productivity) (Fung et al., 2000; Krishnamurthy et al., 2009)

Deleted: a

Deleted: the

Deleted: fraction of

Deleted: However, it

Deleted: for

Deleted: Fe

Deleted: po

Deleted: (see Meskhidze et al., 2017 and ref. therein). This filterable Fe contains both the soluble Fe and the particulate Fe of diameter smaller than 0.45, 0.2 or 0.02 µm. Upon deposition to the surface ocean, this fraction of Fe from the atmosphere can either enter the dissolved Fe pool,

Formatted: Font: Times New Roman, English (UK)

Deleted: (Meskhidze et al., 2017).

Formatted: Font: Times New Roman

keeping in mind that the bioavailable fraction of Fe in seawater will then also change due to post-atmospheric deposition ocean processes (e.g., Baker and Croot, 2010; Chen and Siefert, 2004; Meskhidze et al., 2017; Rich and Morel, 1990).

On the global scale mineral dust is the dominant source of Fe to the atmosphere (~95%; Mahowald et al., 2009)

5 The average Fe content in upper crustal minerals is 3.5% (e.g., Duce and Tindale, 1991), but this can vary considerably, depending on the underlying mineralogy (and geography) of the dust source (Journet et al., 2014; Nickovic et al., 2012, 2013). According to Journet et al. (2014), the Fe content of various minerals is as follows: hematite (69.9%), goethite (62.8%), chlorite (12.3%), vermiculite (6.71%), illite (4.3%), smectite (2.6%), feldspars (0.34%) and kaolinite (0.23%) in clay- and silt-sized soil particles (i.e., soil particles with diameters < 10 2µm and 2 - 50 µm, respectively). Fe-containing aerosols also originate from wildfires and biomass burning (Guieu et al., 2005; Mahowald et al., 2005; Oakes et al., 2012; Paris et al., 2010) and anthropogenic combustion processes, such as coal and oil fly ash (Luo et al., 2008), including ship oil combustion (Ito, 2013). Other sources of Fe-oxides can be also identified in the atmosphere, attributed to volcanic eruptions (Benitez-Nelson et al., 2003; Langmann et al., 2010) and to lesser extent meteors (Johnson, 2001).

15 The use of global biogeochemical numerical models and surface observations is an excellent way to better understand past, present and future atmospheric supply to the oceans, as well as to quantify the resultant effect on the ocean biological productivity and the carbon uptake. Modelling of the atmospheric supply of soluble Fe to the global ocean is challenging, due to the multitude and complexity of the forms under which Fe can be present in aerosol emitted to the atmosphere (Meskhidze et al., 2017), as well as the variety and complexity of processes which alter the solubility of Fe during its transport through the atmosphere (Baker and Croot, 2010). Indeed, the soluble fraction of Fe in atmospheric aerosols may include different Fe forms in the ferric oxidation state (Fe(III)) (Fu et al., 2012), ferrihydrite and amorphous precipitates, Fe-oxide nanoparticles (Shi et al., 2009), Fe-organic complexes (Cheize et al., 2012) and Fe in the ferrous oxidation state (Fe(II)) (Raiswell and Canfield, 2012). The atmospheric modelling community is mostly focused on the soluble fraction of the deposited Fe over the oceans and for this work the general term labile Fe (LFe) will be used to represent the overall soluble Fe in simulated atmospheric aerosol. Both the TFe and LFe atmospheric deposition can be used in ocean biogeochemical modelling. For example, total Fe is used for comparisons of particulate Fe with the measurements in the ocean biogeochemistry models (e.g., Ye and Völker, 2017), while LFe can be assumed as readily available to the marine ecosystem. Note that the less labile fraction of TFe can be slowly dissolved from particulate Fe in the ocean during sinking of mineral particles (e.g., roughly 0.01% per day; Bonnet, 2004), with the dissolution of Fe, however, being species depended and affected by spatiotemporal variations in the ocean.

Deleted: f

Deleted: be

Deleted: Numerical

Deleted: are currently the only feasible means to study

Deleted: Fe

Deleted: and the only way to assess its impacts

Deleted: large (regional and greater) scales in response to changes in past and future climate. However, modelling

Deleted: (Raiswell and Canfield, 2012).

During recent decades, intensive research has been carried out to elucidate the origin, nature and magnitude of LFe fluxes to the surface ocean. Soils may include a small fraction of LFe - roughly 0.1%; e.g., Ito and Shi (2016) - considered as impurities attached on minerals such as illite, smectite, kaolinite and feldspars (e.g., Ito and Xu, 2014). Fe-containing fly ash has been observed to be present as ferric sulfate salts or nanoparticulate Fe and thus is highly soluble (Fu et al., 2012; Schroth et al., 2009), since it is mainly formed via high-temperature combustion followed by sulfuric acid condensation (Sippula et al., 2009). However, the form and the chemical properties of Fe in emissions can vary substantially for each combustion source (Ito, 2013; Wang et al., 2015), with the initial soluble fraction in combustion emissions to be about 77–81% in oil fly ash (Schroth et al., 2009), 20–25% in coal fly ash (Chen et al., 2012) and 18–46% in biomass fly ash (Bowie et al., 2009; Oakes et al., 2012). Recently, Matsui et al. (2018) suggested, based on observed magnetite concentrations, that emissions of anthropogenic combustion Fe in global models could be significantly underestimated, and show that the atmospheric burden of Fe is potentially up to 8 times greater than previous estimates have suggested (Luo et al., 2008). LFe can be also formed in the atmosphere during atmospheric processing of mineral dust and combustion aerosols (Ito, 2012; Ito and Feng, 2010; Johnson and Meskhidze, 2013; Meskhidze et al., 2005; Myriokefalitakis et al., 2015). We use here the general term “solubilisation” to describe the process that converts Fe from relatively insoluble minerals to the soluble Fe during atmospheric transport and photo-chemical transformation in the aqueous solution of aerosols and clouds.

Iron solubility (i.e., the fraction of total Fe that is soluble) in atmospheric aerosols over the Atlantic and Pacific Oceans has been observed to be in the range of 0.1–67% during oceanographic cruises (Baker et al., 2006a; Furutani et al., 2010), with even higher solubilities (up to 80%) measured in precipitation samples in the Southern Ocean (Heimbürger et al., 2013). During atmospheric transport, coating of Fe-containing dust particles by acidic compounds (e.g., sulfates and nitrates) increases the Fe solubility. When this process is taken into account in model simulations (e.g., Meskhidze et al., 2005), it aids in explaining the observations. Indeed, measurements of the fresh dust particles present low (<<1%) initial solubilities (Chuang et al., 2005; Fung et al., 2000; Hand et al., 2004; Sedwick et al., 2007), while high aerosol solubilities are commonly observed at lower dust concentrations far from sources (Baker and Jickells, 2006; Sholkovitz et al., 2012; Oakes et al., 2012). Atmospheric processing of dust (Kumar et al., 2010; Meskhidze et al., 2003; Srinivas et al., 2014) is considered as the best candidate to explain these observations. These processes may alter also the global pattern of LFe deposition (Fan et al., 2004), especially within remote regions, such as the Atlantic, the Pacific (e.g., Sedwick et al., 2007) and the Southern Ocean (Ito and Kok, 2017; Johnson et al., 2010, 2011).

Deleted: ¶

Deleted: Acidic
Formatted: Font: Times New Roman, English (UK)

Deleted: coating dust particles increase
Formatted: Font: Times New Roman, English (UK)

Deleted: during atmospheric transport of Fe-containing particles
Formatted: Font: Times New Roman, English (UK)

Formatted: Font: Times New Roman

Deleted: .
Formatted: Font: Times New Roman, English (UK)

Deleted: since in direct
Formatted: Font: Times New Roman, English (UK)

Formatted: Font: Times New Roman, English (UK)

Formatted: Font: Times New Roman

Deleted: the atmospheric processing of dust (Kumar et al., 2010; Meskhidze et al., 2003; Srinivas et al., 2014) is considered as the best candidate to explain the high aerosol solubilities commonly observed at lower loadings
Formatted: Font: Times New Roman

Formatted: Font: Times New Roman, English (UK)

Formatted: Font: Times New Roman

There is clear experimental evidence that atmospheric acidity - which is mainly driven by air pollution over high populated regions especially over the Northern Hemisphere (e.g., Seinfeld and Pandis, 2006) as well as natural sources such as volcanic sulfur emissions and the oceanic emissions of dimethylsulfide (DMS) in relatively pristine ecosystems (e.g., Benitez-Nelson et al., 2003) - increases the dust solubility. Laboratory studies indicate that Fe solubilisation from minerals under acidic conditions in aerosol or rain droplets (Brandt et al., 2003; Shi et al., 2011; Spokes et al., 1994) occurs on different timescales; from hours to weeks depending on the size and the type of the Fe-containing minerals (Shi et al., 2011), with amorphous and ultrafine Fe solubilized much faster in acidic solutions (Brandt et al., 2003) compared to the aluminosilicates (roughly 10-14 days). Other laboratory studies also support the occurrence of photo-induced reductive Fe solubilisation under acidic conditions (e.g., Fu et al., 2010), a mechanism that involves electron transfer to Fe(III) atoms on the particle surface to produce Fe(II) (Larsen and Postma, 2001). The reductive solubilisation of minerals that are rich in Fe is also observed to be accelerated in the presence of Fe(II) or Fe(II)-ligand complexes (Litter et al., 1994). ~~The oxalate-promoted solubilisation (e.g., Paris et al., 2011)~~ is controlled by the breaking of Fe-O bonds at the minerals surface due to the formation of a mononuclear bidentate ligand with surface Fe (Yoon et al., 2004), with the solubilisation rate significantly increased as the pH decreases. Luo and Gao (2010) further prescribed pH and oxalate/hematite ratio dependent solubilisation rates for mineral dust, based on the laboratory experiments of Xu and Gao (2008). For weakly acidic conditions (pH=4.7) and various oxalate concentrations, a positive linear correlation between oxalate concentrations and the released LFe from different minerals has been also observed (Paris et al., 2011; Paris and Desboeufs, 2013). Laboratory investigations (Chen and Grassian, 2013; Siffert and Sulzberger, 1991) indicated that even under highly acidic solutions (pH=2-3), the oxalic acid can be more important for the Fe solubilisation process of dust and combustion aerosols than the sulfuric acid through the formation of Fe(III)-oxalate complexes. Thus the minerals' solubilisation depends mainly on the proton concentration, the mineral surface concentration of organic ligands (such as oxalate), the sunlight and the ambient temperature (e.g., Hamer et al., 2003; Lanzl et al., 2012; Lasaga et al., 1994; Zhu et al., 1993).

The first modelling efforts that took into account the mixing of mineral dust with such anthropogenic acidic trace gases like sulfur dioxide (SO₂) (Fan et al., 2004; Meskhidze et al. 2003; Meskhidze et al., 2005; Solmon et al., 2009) showed considerable enhancements of atmospheric soluble Fe concentrations. A review by Mahowald et al. (2009) pointed out that human activity may have significantly modified the soluble Fe oceanic deposition flux, because anthropogenic combustion processes increased both Fe emissions and the acidity of atmospheric aerosols. Recent studies (Meskhidze et al., 2017; Tagliabue et al., 2017) further show that atmospheric and oceanic organic ligands may increase the Fe solubilisation in the atmosphere and in the ocean, by forming Fe

Deleted: The oxalate-promoted solubilisation

complexes that further increases the Fe bioavailability for the marine ecosystems. State-of-the-art global models clearly indicate a strong spatial and temporal variability of atmospheric LFe supply to the global ocean, that can be partly attributed to atmospheric processing. The global LFe deposition flux is currently estimated in the range of 0.4–1.1 Tg-Fe yr⁻¹ (Ito and Kok, 2017; Ito and Shi, 2016; Ito and Xu, 2014; Johnson and Meskhidze, 2013; Luo et al., 2008; Myriokefalitakis et al., 2015; Wang et al., 2015).

In order to constrain a global picture of the influence of present atmospheric composition on the Fe supply to the oceans, we perform here a systematic comparison between models and between models and observations. We identify possible similarities and differences among models and between models and observations. The goals of the present study are to (1) quantify the magnitude of the atmospheric TFe and LFe fluxes to the global ocean as calculated by four state-of-the-art global atmospheric aerosol models, (2) explain the differences of the simulated LFe among the participating models, as well as (3) to provide multi-model ensemble TFe and LFe atmospheric Fe deposition fluxes for the next-generation of ocean biogeochemistry modelling studies. Overall, the importance of this work lies on an extended review and synthesis of the current knowledge of global atmospheric Fe deposition fluxes in the ocean, aiming to provide ensemble model data to the scientific community, able to be used in ocean biogeochemistry models and as comparative measures for atmospheric models.

The following discussion is organized in four sections: Section 2 describes the participating models and the observations used in this study. To build a concise view of the present-day understanding on the magnitude as well as the distribution of the TFe and LFe simulated deposition fluxes to the global ocean, ensemble model calculations are also presented. Section 3 presents and discusses the simulated global Fe atmospheric budgets and distributions. In Sect. 4, the uncertainties in the calculated surface aerosol Fe concentrations and deposition fluxes are discussed and the potential model biases are analyzed by attributing them to their major contributors. Finally, in Sect. 5 the findings of the present study are summarized together with recommendations for future research directions.

2 Methods

2.1 Description of models

The global models participating in this study differ in the spatial horizontal and vertical resolution, the meteorology, the emissions used for gas and aerosol species, as well as, the aerosol microphysics (i.e., size distribution and refractive properties). They also differ in the gas- and aqueous- phase chemical schemes and the parameterisations of atmospheric transport and deposition processes. The main characteristics of the participating

Formatted: Greek

models are summarized in Table 1. Note, however, that for this intercomparison no requirements of specific year, meteorological conditions or emission inventories have been set to the model simulations. Presented data are therefore mainly based on earlier published (or soon to be published) modeling experiments, which are evaluated and systematically analyzed here.

- 5 **1.** The Community Atmosphere Model version 4 (CAM4) is embedded within the National Center for Atmospheric Research (NCAR) Community Earth System Model version 1.0.5 (CESM 1.0.5; Hurrell et al., 2013). The CAM4 simulations are conducted with a horizontal resolution of $2.0^\circ \times 1.9^\circ$ (longitude x latitude) and 56 vertical layers up to 2 hPa and forced by NASA's Goddard Earth Observing System (GEOS-5) meteorology. The emission data sets for anthropogenic activities, such as fossil fuel and
10 biofuel combustion, are taken from the Aerosol Comparison between Observations and Models (AeroCom) database (Dentener et al., 2006). Desert dust is modeled following the Dust Entrainment and Deposition (DEAD) module (Zender et al., 2003) with updates in size fractions (Kok, 2011) and optics as described in [Albani et al. \(2014\)](#). The bin widths are prescribed at 0.1-1.0, 1.0-2.5, 2.5-5.0, and 5.0-10.0
15 μm diameter and with fixed lognormal sub-bin distributions. Dust in CAM4 is speciated into six minerals, clays (illite, kaolinite and montmorillonite), feldspar, calcite and hematite (Scanza et al., 2015), with a total dust source of about 1767 Tg yr^{-1} calculated for the present day. Further details on the CAM4 model used for this work are provided in Scanza et al. (2018) and references therein.
- 20 **2.** The GEOS-Chem model is driven by assimilated meteorological fields from the Goddard Earth Observing System (GEOS-5) of the NASA Global Modeling Assimilation at a horizontal $2.0^\circ \times 2.5^\circ$ (latitude x longitude) grid resolution and 47 vertical levels up to 0.01 hPa. GEOS-Chem simulates the emissions and chemical transformation of sulfur compounds, carbonaceous aerosols, and sea salt, and includes H_2SO_4 - HNO_3 - NH_3 aerosol thermodynamics solved by the ISORROPIA II thermodynamic model ([Fountoukis and Nenes, 2007](#)) coupled to an O_3 - NO_x -hydrocarbon-aerosol chemical mechanism.
25 GEOS-Chem combines the DEAD scheme with the source function used in the Goddard Chemistry Aerosol Radiation and Transport (GOCART) model. Once mineral dust is mobilized from the surface, the model uses four standard dust bins with diameter boundaries of 0.2–2.0, 2.0–3.6, 3.6–6.0 and 6.0–12.0 μm to simulate global dust transport and deposition, emitting 1614 Tg yr^{-1} of mineral dust globally. Further details on the GEOS-Chem model used for the this work can be found in Johnson and Meskhidze (2013) and references therein.
- 30 **3.** The Integrated Massively Parallel Atmospheric Chemical Transport (IMPACT) model (Rotman et al., 2004) is also driven by assimilated meteorological fields from the Goddard Earth Observation System –

Deleted: (Albani et al., 2014).

Deleted: (Fountoukis and Nenes, 2007) coupled to an O_3 - NO_x -hydrocarbon-aerosol chemical mechanism.

Forward Processing (GEOS-FP) of the NASA Global Modeling and Assimilation Office (Lucchesi, 2017) with a horizontal resolution of $2.0^{\circ} \times 2.5^{\circ}$ and 59 vertical layers up to 0.01 hPa. The model simulates the emissions, chemistry, transport, and deposition of major aerosol species (Liu et al., 2005) and their precursor gases (Ito et al., 2007). IMPACT takes into account emissions of primary aerosols and precursor gases of secondary aerosols such as sulfate, nitrate, ammonium and oxalate. The emission data sets for anthropogenic activities such as fossil fuel use and biofuel combustion are taken from the Community Emission Data System (CEDS) (Hoesly et al., 2018). Fe-containing combustion and dust aerosols are distributed among 4 bins in the model, with diameters: <1.26 , $1.26-2.5$, $2.5-5$, and $5-20$ μm , respectively (Ito, 2015; Ito and Feng, 2010). The present-day emission estimates for natural sources as well as combustion aerosols from biomass burning are used together with anthropogenic emissions (Dentener et al., 2006; Ito et al., 2018). A total dust source of 5070 Tg yr^{-1} is dynamically calculated by a physically-based dust emission scheme (Kok et al., 2014a, 2014b) in the model for the present day (Experiments 3 in Ito and Kok, 2017). The chemical composition of mineral dust and combustion aerosols can change dynamically from that in the originally emitted aerosols due to reactions with gaseous species. Aerosol pH is calculated from the internal particle composition (H^+ and H_2O) for each size bin by the thermodynamic equilibrium module (Jacobson, 1999). The aerosol acidity depends on the aerosol types, mineralogy, particle size, meteorological conditions, and transport pathway of aerosols (Ito and Feng, 2010; Ito and Xu, 2014; Ito, 2015). A more detailed description of the IMPACT model used for this work can be found in Ito (2015), Ito and Kok (2017), Ito and Shi (2016) and references therein.

Deleted: (Ito, 2015; Ito and Feng, 2010).

4. The TM4-ECPL global chemistry transport model simulates the oxidant ($\text{O}_3/\text{NO}_x/\text{HO}_x/\text{CH}_4/\text{CO}$) chemistry, accounting for non-methane volatile organic compounds, including isoprene, terpenes and aromatics, multiphase chemistry in clouds and aerosol water, as well as all major primary and secondary aerosol components, including sulfate, nitrate and secondary organic aerosols. TM4-ECPL is coupled with the ISORROPIA II thermodynamic model (Fountoukis and Nenes, 2007) and it uses modal size (lognormal) distributions to describe the evolution of fine and coarse aerosols in the atmosphere. Dust emissions, for the present version of the model, are calculated online based on the dust source parameterization of Tegen et al. (2002), as described in Myriokefalitakis et al. (2016); with the updated dust source calculations to produce slightly higher ($\sim 7\%$) dust emissions of around 1181 Tg yr^{-1} compared to the modified AeroCom inventory (Dentener et al., 2006) taken into account in the previous version of the model (Myriokefalitakis et al., 2015). Dust is emitted in the fine and coarse mode with mass median radii (lognormal standard deviation) of $0.34 \mu\text{m}$ (1.59) and $1.75 \mu\text{m}$ (2.00), respectively.

Deleted: (Ito, 2015; Ito and Kok, 2017; Ito and Shi, 2016) and references therein.

Deleted: (Fountoukis and Nenes, 2007) and it uses modal size (lognormal) distributions to describe the evolution of fine and coarse aerosols in the atmosphere.

Deleted: Myriokefalitakis et al. (2016)

Note also that in the updated version of the model, the mineral-containing combustion aerosols are emitted with a number mode radius (lognormal standard deviation) of 0.04 μm (1.8) and 0.5 μm (2.0) for the fine and coarse mode, respectively (~~Dentener et al., 2006; Myriokefalitakis et al., 2016~~). All aerosol species in the model are subject to hygroscopic growth and removal processes that overall affect the mass median radius. The aerosol hygroscopic growth in the model is treated as a function of ambient relative humidity and the composition of soluble aerosol components and the uptake of water on aerosols change the particle size. TM4-ECPL model is driven by ECMWF (European Center for Medium-Range Weather Forecasts) Interim re-analysis project (ERA-Interim) meteorology and it has a horizontal resolution of $3.0^\circ \times 2.0^\circ$ in longitude by latitude, 34 hybrid layers from the surface up to 0.1 hPa and a model time step of 30 min. Further details on the TM4-ECPL model used for this study can be found in ~~Myriokefalitakis et al. (2015, 2016)~~ and references therein.

Deleted: (Dentener et al., 2006; Myriokefalitakis et al., 2016)

Deleted: Myriokefalitakis et al. (2015, 2016)

2.1.1 Iron emission parameterizations

The primary Fe sources taken into account by the models can be roughly grouped as 1) mineral dust and 2) combustion sources. Various parameterizations or simplifications of Fe emission are adopted by the models, with the most important in the context of this paper being the Fe content and initial Fe solubility in emissions. The mean Fe content in dust emissions, as well as the initial Fe solubility in emissions taken into account by the participating models, are presented in the supplement (Fig. S1 and Fig. S2, respectively). In more details:

- 1. Mineral dust emissions:** Mineral-Fe primary sources are derived from the total mineral dust emissions, the fraction of specific Fe-containing minerals in dust emissions and the Fe content of each mineral (Table S1). CAM4 uses a soil mineralogy map and the Fe content in soils is estimated based on mineralogical content (Claquin et al., 1999; Scanza et al., 2015, 2018; Zhang et al., 2015). GEOS-Chem and TM4-ECPL take into account the global soil mineralogy data set developed by Nickovic et al. (2012). GEOS-Chem prescribes an initial Fe solubility of 0.45% for the most reactive and poorly crystalline pool of Fe in desert top soils (Fig. S1), based on the synthesis of data from the Saharan and Sahel regions of northern Africa (Shi et al., 2012). The IMPACT model uses the mineralogy map and the Fe content in soils as estimated by Journet et al. (2014). All the Fe-containing minerals in the model (i.e., hematite, goethite, illite, smectite, kaolinite, chlorite, vermiculite, and feldspars) are considered to be in the clay-sized (diameters $<2 \mu\text{m}$), with only goethite, chlorite, and feldspars to be also present in the silt-sized soils (diameters between 2-50 μm ; Journet et al., 2014). The Fe content averaged in size bins 1–3 (3.6%) is higher than in the size bin 4 (2.3%). IMPACT applies an initial Fe solubility of 0.1% (Ito and

Shi, 2016) to the mineral dust aerosols emitted in the atmosphere (Fig. S1). In TM4-ECPL, the Fe content of the different Fe-containing minerals of dust (i.e., illite, kaolinite, smectite, goethite and hematite and feldspars) is based on the recommendations of Nickovic et al. (2013) and the assumption that is equally distributed between clay- and silt-sized soils, while for GEOS-Chem the Fe content of mineral dust was set to the widely accepted global mean value of 3.5% (Duce and Tindale, 1991). The initial solubility of the emitted Fe-containing dust particles in TM4-ECPL is prescribed as 4.3% on kaolinite and 3% on feldspars emissions (Ito and Xu, 2014), while other minerals are considered to be emitted containing only insoluble Fe. The resulted annual global mean TFe content of emitted dust particles in TM4-ECPL is calculated to be 3.2% on average (Fig. S2).

2. Combustion emissions: All models but one (i.e., GEOS-Chem) include Fe-combustion emissions. These are considered to be emitted from different combustion sectors with various initial Fe solubilities, with the most important ones to be those from biomass burning, coal and oil combustion (Table S2). The CAM4 simulation includes the combustion Fe sources derived from industrial, biofuels (e.g., residential heating) and fires (sum of wildfires and anthropogenic biomass burning), as described in Luo et al. (2008), with an assumption that 4% is soluble at emission, and atmospheric processing occurs as for dust. Shipping Fe emissions are not currently represented within CAM4. IMPACT takes into account Fe emissions from biomass burning, coal combustion and oil combustion (Ito et al., 2018), while an initial Fe solubility (58±22%) which is only applied to the primary Fe emission of ship oil combustion aerosols ~~(Ito, 2015) assuming other Fe combustion emission sectors as insoluble~~. TM4-ECPL takes into account Fe emissions from biomass burning, coal combustion and oil combustion, based on the recommendations of Luo et al. (2008) for biomass burning and coal combustion and by Ito (2013) for oil combustion, assuming fixed Fe-solubilities of 12% for biomass-burning Fe emissions, 8% for coal combustion and 81% for oil combustion from shipping. Note that none of the current models considered here take into account volcanic emissions, although it may be an important source of LFe to some regions of the ocean (e.g., Duggen et al., 2010).

2.1.2 Iron solubilisation parameterizations

The conversion of insoluble-to-soluble Fe in the models can be parameterized as an aqueous-phase kinetic process that depends on (1) the proton activity (also termed as acid-promoted solubilisation), (2) the oxalate concentration (also termed as oxalate-promoted Fe solubilisation) and (3) the actinic flux (also termed as photo-reductive solubilisation). The simplification of the applied parameterisations differs among models; from the

Deleted: (Ito, 2015) assuming other Fe combustion emission sectors as insoluble.

models used in this study, only IMPACT takes into account all three solubilisation processes, but only in aerosol water for both dust and combustion aerosols. TM4-ECPL and GEOS-Chem apply an acid- and oxalate-solubilisation scheme only for dust aerosols, both in aerosol and cloud water. Oxalate is, however, used in models as a proxy of all organic ligands for the ligand-promoted dissolution since 1) it is the most abundant in the atmosphere (e.g., Kawamura and Ikushima, 1993; Kawamura and Sakaguchi, 1999) originating mainly from secondary sources and only a weak contribution from combustion primary sources (e.g., Myriokefalitakis et al., 2011) and 2) it is the most effective ligand in promoting Fe solubilisation (e.g., Paris et al., 2011). We note, however, that more work is required to elucidate the role of other ligands that may promote Fe dissolution in future studies.

10 CAM4 accounts for the atmospheric processing of both dust and combustion aerosols, based on the acid- (Meskhidze et al., 2005) and oxalate- (Paris et al., 2011) driven solubilisation processes in a simplified manner appropriate for use in an earth system model (Scanza et al., 2018). The method is described in more detail in Scanza et al. (2018), but generally the acid promoted iron dissolution depends explicitly on modeled temperature and an assumed acidity, which is either high (i.e., pH=2) or low (i.e., pH=7.5) based on the relative model
15 concentrations of sulfate and calcite, while the oxalate concentrations in cloud water required for ligand promoted iron dissolution are not explicitly calculated, but instead assumed to be proportional to the modeled organic carbon aerosol concentration. CAM4 also assumes Fe from dust to be in either a slow, medium or readily soluble state based on Shi et al. (2011) and Ito and Xu (2014), while Fe from combustion is assumed to be in a medium soluble state.

20 The other three models (i.e., GEOS-Chem, IMPACT and TM4-ECPL) calculate the proton-promoted solubilisation rate of minerals by applying an empirical parameterization of Meskhidze et al. (2005) and Johnson and Meskhidze (2013), that takes into account the degree of saturation of the solution, the type of each mineral and the ambient temperature. The thermodynamic equilibrium modules are used to estimate the water content in the aqueous phase of hygroscopic particles (Jacobson, 1999; Fountoukis and Nenes, 2007). In addition to the
25 mineral types, IMPACT and TM4-ECPL consider three dust-Fe pools associated with mineral source materials as measured by Ito and Shi (2016) and Shi et al. (2011), respectively, and the solubilisation rates calculated by Ito and Shi (2016) and Ito and Xu (2014), respectively. Despite the different mineral databases used by the two models (see Sect. 2.1), the three Fe-pools are roughly similarly characterized in the models as ferrihydrite, nano-sized Fe oxides and heterogeneous inclusion of nano-Fe grains in aluminosilicates, respectively. For GEOS-
30 Chem, the Fe containing mineral (i.e., hematite, goethite, and illite) solubilisation rate is based on the temperature-dependent equations of Meskhidze et al. (2005) and Johnson and Meskhidze (2013).

Deleted: (Jacobson, 1999; Fountoukis and Nenes, 2007).

For the oxalate-promoted solubilisation, CAM4, GEOS-Chem and TM4-ECPL apply a linear relationship between solubilisation rates and oxalate concentration in the solution, based on the laboratory data of Paris et al. (2011), who measured the initial soluble Fe release rates of Fe-oxides and aluminosilicates (i.e., at pH = 4.7, and for one hour). TM4-ECPL applied this oxalate-solubilisation relationship for three Fe-containing minerals (hematite, goethite, and illite), using illite as a proxy for all Fe-containing aluminosilicate minerals (Johnson and Meskhidze, 2013). In TM4-ECPL the formation of oxalate in cloud and aerosol water is explicitly simulated in the model (Myriokefalitakis et al., 2011), in contrast to GEOS-Chem in which the sulfate concentrations are used as a proxy for the oxalate production (Yu et al., 2005). However, in TM4-ECPL the oxalate Fe-solubilisation is applied only in cloud droplets, where in GEOS-Chem it is applied both in cloud and aerosol water. IMPACT also takes into account an explicit scheme of oxalate formation both in cloud and aerosol water (Lin et al., 2014), applying however the oxalate-promoted Fe-solubilisation only in aerosol water (Ito, 2015). The constants used to calculate these Fe solubilisation rates in IMPACT are fitted to experimental data for coal fly ash (Chen and Grassian, 2013), while the rate of the photo-induced solubilisation is based on the Fe-dissolution rates of coal fly ash (Chen and Grassian, 2013), scaled on the photolysis rate of H₂O₂ estimated in the model.

Deleted: (Ito, 2015).

2.1.3 Deposition parameterizations

The dry and wet deposition are considered as loss processes for all Fe-containing aerosols in the models. For this work, the dry deposition fluxes include both the gravitational settling and the turbulent deposition and the wet deposition takes into account both the in-cloud nucleation scavenging and the below- cloud scavenging in all models. For CAM4, the dry removal of dust aerosols involves parameterizations for gravitational settling and turbulent mix out, and wet removal includes in-cloud and below-cloud scavenging (Rasch et al., 2000; Zender et al., 2003). For GEOS-Chem, the removal of mineral dust occurs through dry deposition processes such as gravitational settling (Seinfeld and Pandis, 2006) and turbulent dry transfer of particles to the surface (Zhang et al., 2001). Dust removal by wet deposition processes includes both convective updraft scavenging and rainout/washout from large-scale precipitation (Liu et al., 2001).

Deleted: (Rasch et al., 2000; Zender et al., 2003)

For IMPACT, the dry deposition of aerosol particles uses a resistance-in-series parameterization (Zhang et al., 2001). Gravitational settling is also taken into account (Rotman et al., 2004; Seinfeld and Pandis, 2006). Aerosols and soluble gases can be incorporated into cloud drops and ice crystals within cloud (rainout), collected by falling rain and snow (washout), and be entrained into wet convective updrafts (Ito et al., 2007; Ito and Kok, 2017; Liu et al., 2001; Rotman et al., 2004). The aging of dust and combustion aerosols from hydrophobic to hydrophilic enhances their dry and wet deposition. Hygroscopic growth of mineral dust and combustion aerosols in

gravitational settling uses the (Gerber, 1991) scheme, including the particle growth due to sulfate, ammonium and nitrate associated with the particles (Liu et al., 2005; Xu and Penner, 2012). Scavenging efficiencies for mineral dust and combustion aerosols in wet deposition are calculated based on the amount of sulfate, ammonium and nitrate coated on the particles (Liu et al., 2005; Xu and Penner, 2012). For TM4-ECPL, the dry deposition parameterizations are based on an online scheme that takes into account series of surface and atmospheric resistances (Ganzeveld and Lelieveld, 1995). The aerosol hygroscopic growth in the model is treated as a function of ambient relative humidity and the composition of soluble aerosol components (Gerber, 1985) changing thus the particle size and impact on aerosols gravitational settling. For the wet deposition in TM4-ECPL, both the liquid and ice precipitation are taken into account, with a distinction between scavenging due to large-scale and convective precipitation. In-cloud scavenging in stratiform precipitation uses an altitude dependent precipitation formation rate and the scavenging efficiency is calculated taking into account the aerosols lognormal distributions. Note that in TM4-ECPL, all soluble aerosols are assumed to be completely scavenged in the convective updrafts producing rainfall rates of >1 mm/h, and exponentially scaled down for lower rainfall rates.

15 2.2 The ensemble model

Ensemble model calculations of this study aim overall to provide robust results of the simulated atmospheric Fe concentrations and deposition fluxes. For these calculations, all fields for TFe and LFe in mineral dust and combustion aerosols (as well as for dust aerosols) are first converted to a common $1.0^\circ \times 1.0^\circ$ horizontal resolution grid, by using the freely available Climate Data Operators (CDO v.1.9.1) software. The CDO is a collection of operators for standard processing of climate and forecast model data developed by the Max Planck Institute for Meteorology and for this work were applied with a bilinear interpolation to all fields, assuring an exact mass conservation. Further details about CDO can be found online in <https://code.mpimet.mpg.de/projects/cdo/embedded/cdo.pdf>.

The ensemble atmospheric concentrations and deposition fluxes of mineral dust Fe have been calculated from 4 models, while for the Fe originating from combustion sources, 3 models were used (see Table 2). For Fe-contained combustion aerosols, we simply use the mean of the respective fields of each model to derive the ensemble model, since no considerable differences appeared among the participating models. However, since model simulations of the global dust cycle are well known to have substantial biases in the size distribution relative to *in situ* measurements and remote sensing observations (e.g., Huneeus et al., 2011; Kok et al., 2017; Ridley et al., 2016), we here attempt to reduce these biases by correcting the loading and deposition flux in each

model's particle bin, using state-of-the-art constraints on size-resolved dust loading, as recently derived in Kok et al. (2017).

Specifically, a correction factor $c_{i,j}$ is applied to each particle bin j of model i , which equals:

$$c_{i,j} = \frac{\int_{D_{i,j-}}^{D_{i,j+}} \frac{dM_{atm}}{dD} dD}{L_{i,j}} \quad (1)$$

5 where, $\frac{dM_{atm}}{dD}$ is the mass size distribution of the global atmospheric dust (see Figs. 2b and S1b in Kok et al. (2017)). This mass size distribution was obtained from measurements, modeling, and remote sensing constraints on the size distribution of emitted dust, the atmospheric lifetime and extinction efficiency of atmospheric dust, and the global dust aerosol optical depth (Kok et al., 2017; Ridley et al., 2016). Furthermore, $D_{i,j-}$ and $D_{i,j+}$ are respectively the lower and upper size limits of particle bin j in model i , and $L_{i,j}$ is the (not bias corrected) 10 simulated global dust loading in that particle bin. Since emission and deposition fluxes scale with atmospheric dust loading, we correct these fluxes as well as the atmospheric load in each particle bin of each of the contributing models by multiplying the flux by the correction factor of Eq. (1). Note, however, that the bias correction calculated in this work is expected to correct only the part of the regional bias that stems from a bias in 15 the global deposition fluxes. Biases in the regional scales are affected by biases on the global scale, but also by other biases, for instance caused by uncertainties in the deposition scheme. The global mean bias correction factors (i.e., median, lower 95% confidence interval and upper 95% confidence interval) for each model and each aerosol size (bin or mode) are presented in Table 3.

For TM4-ECPL, which uses modal size distributions for dust (see Table 2), we also redistributed the fine and coarse aerosols into 4 bins, in order to apply the same methodology. Specifically, the new aerosol modes are re- 20 calculated using the error function and based on the characteristic (radius and sigma lognormal) of each mode (see Table 2) to derive binned data for diameters bin 1: 0-1 μm , bin 2: 1-4 μm , bin 3: 4-10 μm and bin 4: 10-20 μm . This bias correction indicates biases mainly in the small modes, with the median correction factors for bins 1 - 4 being 0.134, 0.692, 1.257, and 1.81, respectively. Note also that for the ensemble model calculations of this study, the TFe and LFe depositions fluxes have been calculated as the sum of Fe from the corrected mineral dust 25 and the mean combustion aerosols.

2.3 Iron atmospheric observations

To evaluate the models' ability to reproduce the observed distributions of surface TFe and LFe aerosol concentrations over oceans, the model results have been compared with available observations from Achterberg

et al. (2018), Baker et al. (2006a, 2006b, 2007, 2013), Baker and Jickells (2017), Bowie et al. (2009), Buck et al. (2006, 2010, 2013, pers. com. 2018), Chance et al. (2015), Gao et al. (2013), Guieu et al. (2005, pers. com. 2018), Jickells et al. (2016), Kumar et al. (2010), Longo et al. (2016), Powell et al. (2015), Shelley et al. (2015), Shelley et al. (2018), Sholkovitz et al. (2012), Srinivas et al. (2012), Srinivas and Sarin (2013), Wagener (2008) and Wagener et al. (2008). A total of 818 observations of TFe and 795 daily observations of LFe over the ocean performed from September 1999 to March 2015 have been used for this purpose. The global distribution of the observed aerosol Fe-concentrations used for this study is presented in Fig. S3 and the respective coordinates in Table S3. A bulk dust deposition flux data set compiled by Albani et al. (2014) is also used for comparison of Fe deposition flux after multiplying by the averaged Fe content in upper crustal minerals of 3.5%.

TFe were obtained from sampling aerosols in air mainly on board oceanographic cruises, and for some studies at sampling stations located on shore or on islands with no local anthropogenic influence. A variety of samplers (small or high volume) have been used to collect particulate Fe, using different types of filters. TFe was either measured on whole filter or part of filter by X-ray fluorescence or after acid digestion. LFe was obtained following several protocols, e.g. contact time, volume of media, and type of media (ultra-pure water or filtered surface seawater for different pH conditions and various amounts of Fe ligands). As highlighted in Baker and Croot (2010), these diverse experimental approaches used for determination of aerosol Fe solubility cause part of the variability observed. Although there is still no consensus in the experimental way to determine LFe, this data set provides valuable and robust data in all oceanic region to be compared to model outputs. Here the results from the different protocols are all combined together. Overall, the results are analyzed with regard to the role of the different model complexities, providing insight to directions for future model improvements.

3 Results

3.1 Global budgets

All participating models have submitted results to enable the analysis of the TFe and LFe global budgets and atmospheric concentrations, both for dust and combustion aerosols, for emissions, dry and wet deposition fluxes, atmospheric processing and atmospheric loads (see Sect. 2). Concerning the temporal resolution, daily mean spatially-resolved budget terms have been submitted for IMPACT, while for GEOS-Chem, CAM4 and TM4-ECPL monthly mean fields for all budget terms are provided. For atmospheric concentrations however, all models provided daily mean fields. Concerning the aerosol size distribution (see Table 2), IMPACT and CAM4 submitted budget fields for four size bins, TM4-ECPL for two size modes, while GEOS-Chem provided results

as bulk aerosols. CAM4 and TM4-ECPL submitted separate fields for proton and oxalate Fe solubilisation, while IMPACT and GEOS-Chem provided total fields. IMPACT and CAM4 have also submitted atmospheric processing terms for dust and combustion aerosols, while TM4-ECPL only for dust aerosols since no solubilisation processes are calculated for Fe combustion aerosol in the model. GEOS-Chem does not take into account Fe from combustion aerosols.

3.1.1 Iron sources and deposition

The computed TFe and LFe emissions together with the deposition fluxes for all models are presented in Table 4. Note however that for LFe, both from mineral dust and combustion sources, the total sources (sum of primary and secondary sources) are here discussed rather than the primary emissions alone. The models use significantly different assumptions to describe the total LFe source to the atmosphere and therefore primary (emissions) and secondary (atmospheric processing) sources cannot be accurately separated from rapid formation assumed in coarse-scale models. The computed annual TFe emissions and LFe sources (emissions and atmospheric processing) from 1) mineral dust and 2) combustion sources for each model are presented in Table 4 and the corresponding global emission/sources distributions are shown in Fig. S4 and Fig. S5, respectively.

The importance of wet versus dry deposition as removal processes for atmospheric aerosols depends on the aerosol solubility and size distribution (and the presence/amount of precipitation). Focusing however on the deposition to oceans for this study, the apportionment of the total atmospheric deposition within different oceanic regions is presented in Table 5 (for this deposition analysis we use here the ocean classification as provided by HTAP phase-2: available online via the HTAP Wiki). Moreover, the computed annual deposition flux distributions of TFe and LFe from mineral dust and combustion sources together for each model are further presented in Fig. S6.

Overall, the Fe sources and deposition in the models are here classified as:

- 1. Total Fe:** The modelled annual mean emission fluxes of TFe from mineral dust (TFeD) are calculated to be in the range of 38 - 134 Tg-Fe yr⁻¹. CAM4 and GEOS-Chem calculate similar annual TFeD emission fluxes (around 57 Tg-Fe yr⁻¹), TM4-ECPL emissions are about 40% lower (~38 Tg-Fe yr⁻¹) and IMPACT is about 2.4 times higher (around 134 Tg-Fe yr⁻¹). Note that IMPACT takes into account the largest flux among the participating models (Table S1) mainly due to the largest upper size. However, dust fluxes in the same size range for the different models are comparable after the bias correction based on the analysis by Kok et al. (2017) (see Sect. 2.2). TFe emissions from combustion sources (TFeC) range between 1.8 and 2.7 Tg-Fe yr⁻¹, with CAM4 and TM4-ECPL calculating annual mean fluxes of around

1.8 Tg-Fe yr⁻¹ globally, and IMPACT having a 35% higher estimate. On a global scale, dry deposition is the most important removal mechanism, across all models for the TFeD; IMPACT has the highest dry deposition flux of all models (~68 Tg-Fe yr⁻¹), followed by GEOS-Chem (~40 Tg-Fe yr⁻¹), CAM4 (~33 Tg-Fe yr⁻¹) and TM4-ECPL (~30 Tg-Fe yr⁻¹). Submicron aerosols are removed mostly by wet removal while for supermicron aerosols the gravitational settling is important (e.g., Seinfeld and Pandis, 2006). Consequently, the wet removal of TFeD across almost all models (except for IMPACT) is smaller than dry deposition flux - mainly due to the high contribution of coarse aerosol sedimentation to the dry removal processes (Table 4). The simulated wet deposition flux of TFeD ranges over about one order of magnitude (from about 8 to 66 Tg-Fe yr⁻¹); IMPACT calculates the highest TFeD wet deposition flux of all models of about 66 Tg-Fe yr⁻¹ (~49% of total removal), followed by CAM4 (24 Tg-Fe yr⁻¹; 42%), GEOS-Chem (16 Tg-Fe yr⁻¹; ~29%) and TM4-ECPL of roughly 8 Tg-Fe yr⁻¹ (~20%). In contrast to TFeD, due to the similar assumptions of the size distribution and scavenging efficiency in the models, the wet deposition is the larger removal pathway for TFe from combustion processes (TFeC), (except for TM4-ECPL, probably due to the different solubility factors in primary emissions and the different atmospheric processing parameterizations), responsible overall for about 60% of the total TFeC removal across models and amounting to about 1 Tg-Fe yr⁻¹.

2. Labile Fe: The global annual mean LFe sources from mineral dust (LFeD) range between 0.3 and 1.0 Tg-Fe yr⁻¹. IMPACT and GEOS-Chem calculate similar LFeD sources, close to 0.7-0.8 Tg-Fe yr⁻¹, where CAM4 calculates the highest annual source and TM4-ECPL the lowest. However, these differences are mainly attributed to the secondary processes leading to LFeD production rather than the primary emissions. For example, despite the large difference between IMPACT and TM4-ECPL in TFeD sources, the models consider similar emission amounts of LFeD emissions of about 0.12-0.13 Tg-Fe yr⁻¹. In contrast, the secondary LFeD produced due to atmospheric processing is calculated to vary by a factor of 3-4 between 0.57 Tg-Fe yr⁻¹ (IMPACT) and 0.17 Tg-Fe yr⁻¹ (TM4-ECPL), respectively. CAM4 takes into account LFeD emissions of around 0.18 Tg-Fe yr⁻¹, but the highest annual LFeD atmospheric processing (0.8 Tg-Fe yr⁻¹), and GEOS-Chem about 0.25 Tg-Fe yr⁻¹ and 0.54 Tg-Fe yr⁻¹ for LFeD emissions and atmospheric processing, respectively. The LFe source from combustion aerosols (LFeC), with a range of about 0.1-0.2 Tg-Fe yr⁻¹, shows smaller differences than that from mineral dust (0.3-1.0 Tg-Fe yr⁻¹). Although the differences are not large, these clearly depict the different assumptions followed by these two models; IMPACT does not account for primary LFe sources from combustion (except those from oil ship combustion of about 0.009 Tg-Fe yr⁻¹), thus almost all the LFeC sources over

land are attributed to secondary production via atmospheric processing ($0.091 \text{ Tg-Fe yr}^{-1}$). In contrast, TM4-ECPL does not take into account atmospheric processing of Fe from combustion sources, attributing all the LFeC sources to direct emissions ($\sim 0.2 \text{ Tg-Fe yr}^{-1}$). Finally, CAM4 that includes both direct emissions and atmospheric processing of LFeC, calculates a total source of about $0.13 \text{ Tg-Fe yr}^{-1}$, corresponding to roughly $0.075 \text{ Tg-Fe yr}^{-1}$ and $0.053 \text{ Tg-Fe yr}^{-1}$, for primary LFeC emissions and atmospheric processing respectively.

3.1.2 Iron seasonal variability

Figure 1 presents the global LFe sources (positive) and oceanic deposition fluxes (negative) for all participating models and their ensemble mean (see Sect. 3.2), for the four seasons, i.e., December, January and February (DJF), March, April and May (MAM), June, July and August (JJA) and September, October and November (SON). LFe sources are mainly driven by mineral dust aerosols, although a significant fraction (6 to 62%) is due to LFe combustion aerosols, especially over the high-latitudes of the Northern Hemisphere (Ito et al. 2018; companion manuscript to be submitted). For LFe sources, despite the different assumptions applied in the models (i.e., atmospheric processing and direct LFe emissions), maximum sources are calculated for MAM and JJA due to intense dust emissions and biomass burning, respectively. The models with the highest LFe sources, also exhibit the highest deposition fluxes to the ocean. However, significant differences in the magnitude of the deposition fluxes are calculated between models (Fig. 1). A seasonal maximum in the deposition fluxes is calculated by CAM4 and GEOS-Chem during MAM, attributed to Saharan mineral dust aerosols, while IMPACT and TM4-ECPL present a seasonal maximum during JJA.

Figure S7 (supplement) further presents the zonal mean seasonal variability of the LFe global sources and oceanic deposition fluxes. Most of LFe emissions are calculated to occur over the mid-latitudes of the Northern Hemisphere (NH) for all seasons, with maximum during MAM and JJA and minima during SON. In DJF, and to a lesser extent in JJA, two zonal maxima are shown near the equator and around 30N . The equatorial maximum in DJF is, however, shifted to the Northern Hemisphere in JJA following the Intertropical Convergence Zone (ITCZ) migration and the subsequent geographic change in the location of biomass burning emissions. Again, all models appear to have similar LFe seasonality, with the highest LFe oceanic deposition fluxes across all models calculated by CAM4 (Table 5).

Deleted: , mainly for DJF and JJA.

Deleted: and in most of the cases

Deleted: GEOS-Chem

Deleted: similar

Deleted: variation

Deleted: , while in the other seasons the 30N maximum is not clearly present.

Deleted: NH

3.2 Ensemble model calculations

3.2.1 Iron surface concentrations

The annual mean surface TFe aerosol concentrations for the ensemble model exceed $100 \mu\text{g-Fe m}^{-3}$ over the major dust source regions such as the Sahara Desert, where mineral dust particles dominate the atmospheric Fe burden (Fig. 2a). Relatively high TFe concentrations (e.g., up to $10 \mu\text{g-Fe m}^{-3}$ over the tropical Atlantic Ocean) are calculated for ocean regions at the outflow from these source regions. High TFe concentrations of around $6 \mu\text{g-Fe m}^{-3}$ are also calculated over heavily polluted areas like China, while secondary maxima up to $2\text{-}5 \mu\text{g-Fe m}^{-3}$ are calculated over the central Africa, Asia and Indonesia, where Fe-containing aerosols are associated with biomass burning emissions (Fig. 2b).

Model Fe solubility calculations (Fig. 2c) clearly suggest the impact of atmospheric processing on the derived LFe ensemble surface concentrations, with high Fe solubilities calculated far from source regions over the remote tropical oceans, corresponding to low TFe concentrations. Ensemble annual mean LFe concentrations around $0.5 \mu\text{g-Fe m}^{-3}$ occur downwind of the Sahara and around $0.1 \mu\text{g-Fe m}^{-3}$ downwind of the Arabian and Gobi Deserts. At the outflow of these regions, the Fe solubility over the global ocean is calculated to be about 1-1.5%, with the highest Fe solubilities (4-5%) over the tropical Atlantic Ocean (Fig. 2c). Additionally, LFe concentrations over polluted regions may range up to $0.05 \mu\text{g-Fe m}^{-3}$, indicating a significant anthropogenic contribution via direct combustion emissions and atmospheric processing (Fig. 2b). Over central South America, Asia and Indonesia, LFe concentrations of about $0.03\text{-}0.05 \mu\text{g-Fe m}^{-3}$ (corresponding to high Fe solubilities up to 5%) are found due to both direct biomass-burning emissions and due to ligand-promoted dissolution. The latter process is enhanced in these areas by the respective enhanced oxalate production upon the oxidation of emitted biogenic VOCs precursors, such as isoprene, under cloudy conditions (Lin et al., 2014; Myriokefalitakis et al., 2011).

3.2.2 Iron deposition fluxes

Model calculations indicate that about $71.5 (\pm 43) \text{Tg-Fe yr}^{-1}$ of TFe from mineral dust are deposited to the Earth's surface (Table 4), with ensemble deposition fluxes of around $5000\text{-}8000 \text{mg-Fe m}^{-2} \text{yr}^{-1}$ calculated downwind of the main desert source regions (Fig. 3a). However, within the Northern Atlantic Ocean in the outflow of the Sahara, the model mean indicates deposition fluxes up to $2400 \text{mg-Fe m}^{-2} \text{yr}^{-1}$, while within the Northern Pacific Ocean in the outflow of Gobi Desert and within the Southern Ocean downwind of the Patagonia Desert the ensemble model shows annual mean fluxes of ~ 34 and $\sim 10 \text{mg-Fe m}^{-2} \text{yr}^{-1}$, respectively (Fig. 3a). The TFe annual mean global deposition flux from combustion sources (Table 4) is calculated to be about $2.2 (\pm 0.5)$

Tg-Fe yr⁻¹, with two main regions where TFe concentrations exceed 2500 mg-Fe m⁻² yr⁻¹, one near biomass burning regions (e.g., southern Africa, South America and southeast Asia) with up to ~3000 mg-Fe m⁻² yr⁻¹, and a second near highly populated regions with Fe released from coal and oil combustion processes (India and China) with up to ~3500 mg-Fe m⁻² yr⁻¹ (Fig. 3b).

5 A global mean LFe deposition flux of 0.7 (± 0.2) Tg-Fe yr⁻¹ is derived from all models (Table 4), with about one third (~0.24 Tg-Fe yr⁻¹) calculated to be deposited to the global ocean for the ensemble model (Table 5). The highest annual mean LFe deposition fluxes (up to 36 mg-Fe m⁻² yr⁻¹) are simulated within dust source regions (Fig. 3c), owing mainly to the LFe content of the emissions (e.g., see Fig. 2d). The global model-mean LFe deposition fluxes from combustion sources are calculated at about 0.2 (± 0.04) Tg-Fe yr⁻¹ (Table 4), with maximum global deposition rates of 4-5 mg-Fe m⁻² yr⁻¹ (Fig. 3c) simulated in the outflow of tropical biomass burning regions (i.e., South America, Africa and Indonesia), clearly reflecting the contribution of combustion processes. Focusing on the marine environment, annual mean LFe deposition rates of 15 mg-Fe m⁻² yr⁻¹ are calculated for the tropical Atlantic Ocean and for the Indian Ocean (up to 16 mg-Fe m⁻² yr⁻¹) under the influence of the Arabian and Indian peninsulas, but up to ~29 mg-Fe m⁻² yr⁻¹ for the Mediterranean Sea downwind of the Sahara Desert. Deposition rates around 1 mg-Fe m⁻² yr⁻¹ are calculated to occur within the Northern Pacific in the outflow from the Gobi Desert as well as within the Southern Hemisphere downwind of Patagonia to the Southern Ocean (up to 0.1 mg-Fe m⁻² yr⁻¹) and downwind of the dust source regions of Australia and South America (up to ~4 mg-Fe m⁻² yr⁻¹). The LFe deposition rates to the Southern Ocean are associated mainly with the Patagonian, Southern African and Australian deserts, with a smaller contribution in the subtropical ocean from biomass burning sources (Fig. 3d). Note, that the largest fluxes of LFe deposited to the HNLC region of the Southern Ocean (e.g., south of the Antarctic circumpolar current) are simulated to be originating from a Patagonian mineral dust source, with rates reaching 0.1 mg-Fe m⁻² yr⁻¹. The ensemble annual mean deposition fluxes to various oceanic regions are further presented in Table 5.

4 Uncertainties

25 4.1. Comparison with measurements

The TFe ~~concentrations~~, Fe solubility, and LFe ~~concentrations~~ from the models are compared with the measurements and presented in Fig. 4. We use the monthly mean of model output to compare with the measurements. The normalized bias (NB) at a given grid box is calculated as follows:

Deleted: loading

Deleted: loading

Formatted: Font: +Body (Times New Roman)

$$NB_i = \frac{c_{model,i} - c_{obs,i}}{c_{obs,i}} \quad (2)$$

where,

$C_{model,i}$ is the modelled aerosol concentration in grid box i and $C_{obs,i}$ is the measured aerosol concentration in the same grid box. When discussing the multi-model results we use the mean of all models, while we also analyze the mean normalized bias (MNB) of the models against measurements (a perfect comparison would have an MNB of 0 and correlation, R , of 1). A model's MNB is derived as the arithmetic mean of all NB_i values, thus, overestimates are weighted more than equivalent underestimates.

All models captured a tendency of higher Fe concentrations near and downwind of the major dust source regions. The MNB for the Northern Hemisphere (14 for ensemble model) is larger than that for the Southern Hemisphere (2.4 for ensemble model). This reflects that overall the models overestimate TFe surface mass concentrations. However, from Fig. 4 we can see that this overestimate is higher for the highest TFe concentrations near the dust

source regions and tend to turn to an underestimate for the lowest concentrations observed over remote oceans. Overall, bias correction for ensemble model improves agreement of the ensemble model against measurements (Fig. S8). We note, however, that matching the atmospheric concentrations may cause a high bias in simulated Fe depositions at low values in the Southern Hemisphere (Albani et al., 2014; Huneus et al., 2011) (Fig. S9). The computed correlation coefficients of the ensemble model against measurements at the surface are 0.13 for TFe, 0.05 for Fe solubility, and 0.25 for LFe, respectively, which are much smaller than those between the participating models (0.57–0.90 for TFe (GEOS-Chem vs. IMPACT)–(CAM4 vs. TM4-ECPL), 0.05–0.56 for Fe solubility (CAM4 vs. TM4-ECPL)–(CAM4 vs. IMPACT), and 0.40–0.75 for LFe (GEOS-Chem vs. IMPACT)–(CAM4 vs. GEOS-Chem)). This indicates a linear dependence of the model results and that the models have similar behavior accounting for the same key processes that affect Fe deposition. The small positive correlation between models and observations indicates that the models miss –or do not accurately represent- important processes that drive the variability in the observations. Indeed, when comparing the computed and observed solubilities of Fe, all models overestimate the lowest solubilities (<0.1%) observed close to the source regions (14 samples in Arabian Sea and 2 samples in tropical Atlantic). This is primarily due to the assumed solubility of the dust aerosols at emissions, and the subsequent enhancement of Fe solubility estimated from the simulated amount of atmospheric processing during transport in the models. It is noted, however, that the lowest solubilities in the measurements are outliers in the negative slope of Fe concentrations versus Fe solubility in the Northern Hemisphere (Fig. 5). Our calculations show that the models have difficulties to simulate the 4 orders of

Deleted: loading

Deleted: The mean normalized biases (MNB) between the models and observations are also presented.

Deleted: most

Formatted: Font: +Body (Times New Roman)

Deleted: This might also indicate an inaccurate transport from the continental source areas to the observational sites or a too fast loss via deposition in the models.

Formatted: Font: +Body (Times New Roman)

Formatted: Font: +Body (Times New Roman)

Formatted: Font: +Body (Times New Roman)

Deleted: SH

Deleted: loading versus Fe solubility in the NH (Figure 5).

magnitude variability from 0.02% to 98% in the Fe solubility observed in the atmosphere (Fig. 5a). IMPACT simulates almost 3 orders of magnitude variability in Fe solubility. In the other models including the ensemble model, Fe solubility is less variable (one to two orders of magnitude only). In particular, low solubilities (high concentrations near sources) are overestimated and high solubilities (low concentrations at remote locations) are underestimated. This may indicate that the primary LFe in the models is overestimated and that models are missing solubilisation processes during transport or that those considered in the models are not sufficient effective.

All models underestimate the high end of the observed values (>10%) in the Southern Ocean, which are mainly associated with transported and aged aerosols and this is potentially a significant shortcoming because this is an oceanic HNLC region where atmospheric Fe supply has a potentially important impact on ocean productivity in past and future climate. In GEOS-Chem, IMPACT, and TM4-ECPL, Fe dissolution over the Southern Ocean is suppressed mainly due to the lack of anthropogenic emissions and the subsequent acidification of the aerosols. CAM4 is relatively insensitive to the acidity, since most labile Fe is formed by in-cloud processes. Thus, the model results from CAM4 can in part test whether in-cloud processing can realistically describe the observed pattern of solubility over the Southern Ocean. CAM4 shows higher Fe solubility than field data for most samples in the Southern Ocean (69% in CAM4, 7% in GEOS-Chem, 55% in IMPACT and 5% in TM4 TM4-ECPL) (Figs. 4 and 5). Thus, the wide range in observed Fe solubility cannot be explained by excluding the effect of modelled aerosol acidity over the Southern Ocean. It is worth mentioning that IMPACT, which has the highest complexity in simulating labile Fe, reproduces the widest range of observed Fe solubility. It should be noted, however, that the comparison of monthly mean model results with the shorter-term (e.g., daily) observations during different sampling periods introduces inaccuracies due to an episodic nature of high Fe solubility. A more detailed comparison of Fe solubility between models and observations is presented in a separate companion paper to this work (Ito et al. 2018; in preparation).

4.2. Model-to-model comparison

Model budget analysis and model evaluation indicate that even though the models are able to reproduce surface Fe measurements to some extent, large differences existed among models in processes such as emissions, transport and deposition. A large diversity is here documented between models in terms of LFe primary sources (i.e., emissions) and secondary processes (i.e., atmospheric processing) which introduce uncertainties in the estimated oceanic deposition. There are many intrinsic reasons, however, for this diversity in the Fe simulations among models; besides the emitted Fe mass in the atmosphere (especially from dust aerosols), the aerosol size

distribution, the soil mineralogy, the strength of combustion aerosol sources, as well as the parameterizations used to calculate the pH of the aerosol water and the oxalate production are large sources of uncertainty in model simulations.

The aerosol size and solubility are important factors driving the atmospheric cycle of Fe, since they both control the removal processes from the atmosphere via the dry deposition (including gravitational settling) and the wet scavenging (e.g., Albani et al., 2014). It is well documented that the lifetime of Fe-containing aerosols ranges between less than one day for the coarse mode (with diameters larger than 1 μm) particles to weeks for the fine mode (with diameters less than 1 μm) (e.g., Ginoux et al., 2012; Luo et al., 2008; Mahowald et al., 2009; Tegen and Fung, 1994), with the overall lifetime of dust aerosols to usually range between 1.6 and 7.1 days in the models (Huneeus et al., 2011). Fine particles have longer lifetimes and thus experience more atmospheric processing. The conversion of insoluble minerals content to soluble forms as a result of aging during atmospheric transport increases aerosols' solubility. Lifetime calculations can thus provide a valuable tool to determine the Fe persistence in the atmosphere, overall integrating sources, transport and deposition differences among models, especially over remote areas such as the open ocean.

15 4.2.1 Iron atmospheric lifetime (turnover time)

Figure 6 presents the spatial distribution of TFe lifetime over the ocean ([i.e., atmospheric concentrations divided by total sinks](#)), as calculated for the ensemble model. For TFe originating from dust sources, the calculated global mean lifetime over the oceans is $\sim 6 (\pm 4)$ days (Fig. 6a). The lifetime of combustion TFe over oceans is longer, at around $14 (\pm 9)$ days (Fig. 6c), due to the overall smaller size of the combustion Fe aerosols compared to that of mineral dust (affecting their sedimentation processes, their horizontal and vertical transport in the atmosphere), but also because of the low precipitation over part of the regions in which mineral dust and combustion aerosols are transported. The ensemble model indicates long TFe lifetimes over remote oceanic regions, such as in the outflow of South America, in the outflow of South Africa, as well as in the outflow of Australia (Fig. 6c). Over these so-called ocean deserts, where precipitation is low and thus the wet deposition rates are low, the ensemble model results overall in longer lifetimes for Fe containing aerosols, although the LFe atmospheric concentrations can be extremely low.

To further analyze the differences among the models, the standard deviation (STD) of the TFe lifetime is calculated for each grid for dust aerosols (Fig. 6b), combustion aerosols (Fig. 6d), and the combined TFe lifetime (Fig. 6f). Over remote oceanic regions, the high STD can be related to the different assumptions used by the models to parameterize 1) the long-range transport of Fe-containing aerosols of different parameterizations of the

sizes, 2) the wet and dry deposition parameterizations, and 3) the soluble fraction of Fe-containing combustion aerosols (e.g., the differences in ship oil combustion and biomass burning emissions). From the models that include Fe from combustion processes, IMPACT assumes that only ship oil combustion emissions have an initial fraction of soluble Fe, and thus all the LFe from continental sources is produced due to atmospheric processing.

5 CAM4 does not take into account ship emissions but includes both primary and secondary sources for LFe from other combustion sources. TM4-ECPL although includes continental and ship oil combustion emissions both for TFe and LFe but, it does not take into account any dissolution processes for combustion aerosols, although continental and ship oil combustion emissions both for TFe and LFe are considered. Differences in the precipitation patterns or parameterization for wet or dry deposition in the models can also partially explain the

10 models' diversity. In addition, less constrained parameters like dissolution, long-range transport and Fe removal (which affect Fe solubility) can further increase the model diversity, and thus the STD, over these remote areas.

5 Conclusions and future directions

We here present the first model intercomparison study of the atmospheric Fe-cycle by assessing aerosol simulations of total and labile Fe with four state-of-the-art global aerosol models (CAM4, IMPACT, GEOS-15 Chem and TM4-ECPL). The TFe emissions from dust sources in the models range from ~38 to ~134 Tg-Fe yr⁻¹, with a mean value of 71.5 (±43) Tg-Fe yr⁻¹. The models simulate the secondary formation of soluble Fe in the atmosphere, as a result of mineral Fe atmospheric processing by acids, organic ligands and photochemistry, but the absolute amount of the simulated LFe remains highly uncertain. The simulated LFe deposition fluxes from mineral dust span from 0.3 to 1.0 Tg-Fe yr⁻¹, with a mean value of around 0.7 (±0.3) Tg-Fe yr⁻¹. All models

20 capture the main features of the distribution of TFe and LFe: i.e., large deposition rates to the Sahara and Gobi Desert and regions downwind of strong dust sources. Models also show significant LFe deposition to the oceans downwind from the Middle East and the continents of South America, Africa and Australia in the Southern Hemisphere; the Middle East has large dust sources and while South America, Africa and Australia experience strong biomass burning emissions.

25 The models are able to simulate the main features of TFe and LFe atmospheric concentrations and deposition fluxes. On average, the ensemble model computes roughly 50% higher lifetime with respect to the deposition flux for combustion aerosol (~14 days) than for dust aerosol, reflecting differences in size distribution and in the location of emitted aerosols. Ensemble model calculations present overestimate of the observed TFe surface mass concentrations near the dust source regions and underestimate the Fe concentrations over the Southern Ocean

compared with cruise measurements; similar to what was pointed out in [Albani et al. \(2014\)](#) and seen in the dust model intercomparison study of Huneus et al. (2011). Note that the latter is important because of the key role of Fe in the biogeochemistry of these ocean waters. For the ensemble model mean, the MNB for the Northern Hemisphere (about 14) is larger than for the Southern Hemisphere (about 2.4). Note, however, that evaluation of monthly mean model results by comparison with the shorter-term (e.g., daily) observations during different sampling periods introduces uncertainties, due to short of the sampling frequencies; a comparison of long-term measurements with a multi-year modelling will allow assessment of the model performance to capture labile Fe concentrations under specific events.

The model intercomparison and model–observation comparison revealed the Fe size distribution and the relative contribution of the dust and combustion sources, as two critical issues for LFe simulations that now require further study. The diversity of how the models represent Fe emissions as well as of deposition fluxes among the models can be thus large, especially over source regions. The model diversity over remote oceans reflects uncertainty in Fe content parameterizations of dust emissions (e.g., soil mineralogy and the initial Fe soluble content in primary sources) and combustion aerosols, and/or in the parameterizations of the size distribution of the transported aerosol Fe, and thus the representation of deposition fluxes - which overall control the atmospheric lifetime of Fe. On the other hand, there are many other intrinsic reasons for this diversity especially for the LFe aerosol fraction, since it involves complex atmospheric chemical processes driven by atmospheric acidity. For example, detailed chemical mechanisms need to be invoked to simulate a multi-phase, multi-component solution system, since such a system may not be solved accurately using a thermodynamic equilibrium approach for the entire grid box due to sub-grid processes, e.g., when the dust plume is not well mixed with surrounding pollutants. Consequently, a reasonable aerosol pH simulation further depends on the representation of soluble acidic and basic compounds, as well as the water content of hygroscopic particles.

In this respect, new field observations are needed to improve understanding of Fe solubilisation process, and how this process alters in the presence of anthropogenic pollution. Modelling studies together with their evaluation based on a greater number of atmospheric observations, especially over the remote ocean, are deemed necessary in order to reduce the uncertainty associated to the model performance in simulating the atmospheric Fe deposition. For example, the participating models here predict that wet deposition processes are important for the LFe atmospheric cycle but, it is rather hard to test that well due to the lack of respective field data. Moreover, although the models do well in higher dust and pollution regions, from an oceanographer’s perspective, the regions with the lowest Fe supply is of the greatest interest, because that creates the HNLC situation in the water column. Model evaluation can be further more difficult, however, due to a lack of standardization in the protocols

Deleted: it

Deleted: (Albani et al., 2014)

used to determine the soluble Fe fraction in marine aerosol samples (e.g., Baker and Croot, 2010). Protocols that involve different solutes, aerosol – solution contact times and filter pore sizes, among other differences, are in use by different investigators and these presumably introduce some, as yet unquantified, uncertainties into the available databases of aerosol soluble Fe concentrations and Fe solubility. Model developments related to atmospheric Fe cycle must be performed in parallel with an extensive model evaluation in order to better understand the underlying mechanisms and to provide, overall, realistic labile Fe deposition fluxes for the next-generation of ocean biogeochemistry modelling studies. Although the calculation of the Fe concentrations in the ocean is outside the scope of this paper, we expect that the Fe deposition fluxes here provided will be used in oceanic models.

10

Data availability: Global 1.0x1.0 fields for TFe and LFe deposition fluxes (i.e. from combustion and dust origin and their sum) as well as the Fe solubility (SFe) derived from the ensemble model calculations are available online at <https://ecpl.chemistry.uoc.gr/GESAMP/> (contact: S. Myriokefalitakis steliosm@noa.gr; M. Kanakidou mariak@uoc.gr).

5 **Author contribution:** This paper resulted from the deliberations of United Nations GESAMP Working Group 38, “The Atmospheric Input of Chemicals to the Ocean” (SM, AI, MK, AN, NM, AB, TJ, MS, YG, RS, MP, CG, RD), February 2017, University of East Anglia, Norwich, UK. SM manipulated all model fields, analyzed the data and prepared the respective figures and fields of this work. AI performed the model evaluation and the respective statistical analysis. JFK provided the analysis for dust correction factors for model data. SM, AI, MK, 10 MCK, AN, NM, RAS, DSH, NM and MSJ, provided the model products, AB, TJ, MS, BS, YG, RS, CB, WL, AB, TW, CG and YF contributed to the measured data. All authors contributed to the manuscript preparation.

Acknowledgments: SM acknowledges financial support for this research by the [European Union’s Horizon 2020 research and innovation programme under the Marie Skłodowska-Curie grant agreement No 705652 - ODEON](#). Support for this research was provided to AI by JSPS KAKENHI Grant Number JP16K00530 and Integrated 15 Research Program for Advancing Climate Models (MEXT). NM, RS and DH acknowledge support from DOE DE-SC0006791. [A.R.B. and M.M.G.P. were funded by an Australian Research Council Future Fellowship \(FT130100037\)](#). We are grateful to T. Wagener for kindly providing field data set. This work is prepared in the framework of the Joint Group of Experts on the Scientific Aspects of Marine Environmental Protection (GESAMP; <http://www.gesamp.org/>), Working Group 38, the Atmospheric Input of Chemicals to the Ocean. We 20 thank the Global Atmosphere Watch and the World Weather Research Programme of the World Meteorological Organization, the International Maritime Organization, the U.S. National Science Foundation, the ICSU Scientific Committee on Oceanic Research (SCOR), and the University of East Anglia for their financial support, and SOLAS for their sponsorship. [Data post-processing was carried out on the Dutch national e-infrastructure with the support of SURF Cooperative. The publication of this work was financed by Utrecht University and by the European Union’s Horizon 2020 research and innovation programme under the Marie Skłodowska-Curie grant agreement No 705652 - ODEON.](#) 25

Competing interests: The authors declare that they have no conflict of interest.

Deleted: the

Deleted: corresponding

Deleted: will be freely

Deleted: after the final publication of this work

Deleted: s.myriok@uu.nl

Deleted: H2020-MSCA-IF-2015

Deleted: ODEON (ID

Deleted:).

Formatted: Font: 11 pt

References

- Achterberg, E. P., Steigenberger, S., Marsay, C. M., Lemoigne, F. A. C., Painter, S. C., Baker, A. R., Connelly, D. P., Moore, C. M., Tagliabue, A. and Tanhua, T.: Iron Biogeochemistry in the High Latitude North Atlantic Ocean, *Sci. Rep.*, 8(1), doi:10.1038/s41598-018-19472-1, 2018.
- 5 Albani, S., Mahowald, N. M., Perry, A. T., Scanza, R. A., Zender, C. S., Heavens, N. G., Maggi, V., Kok, J. F. and Otto-Bliessner, B. L.: Improved dust representation in the Community Atmosphere Model, *J. Adv. Model. Earth Syst.*, 6(3), 541–570, doi:10.1002/2013MS000279, 2014.
- de Baar, H. J. W. and de Jong, J. T. M.: Distributions, sources and sinks of iron in seawater, in *The Biogeochemistry of Iron in Seawater. IUPAC Series on Analytical and Physical Chemistry of Environmental Systems*, pp. 123–253., 2001.
- 10 Baker, A. R. and Croot, P. L.: Atmospheric and marine controls on aerosol iron solubility in seawater, *Mar. Chem.*, 120(1–4), 4–13, doi:10.1016/j.marchem.2008.09.003, 2010.
- Baker, A. R. and Jickells, T. D.: Mineral particle size as a control on aerosol iron solubility, *Geophys. Res. Lett.*, 33(17), L17608, doi:10.1029/2006GL026557, 2006.
- 15 Baker, A. R. and Jickells, T. D.: Atmospheric deposition of soluble trace elements along the Atlantic Meridional Transect (AMT), *Prog. Oceanogr.*, 158, 41–51, doi:10.1016/j.pocean.2016.10.002, 2017.
- Baker, A. R., French, M. and Linge, K. L.: Trends in aerosol nutrient solubility along a west–east transect of the Saharan dust plume, *Geophys. Res. Lett.*, 33(7), L07805, doi:10.1029/2005GL024764, 2006a.
- Baker, A. R., Jickells, T. D., Witt, M. and Linge, K. L.: Trends in the solubility of iron, aluminium, manganese and phosphorus in aerosol collected over the Atlantic Ocean, *Mar. Chem.*, 98(1), 43–58, doi:10.1016/j.marchem.2005.06.004, 2006b.
- 20 Baker, A. R., Weston, K., Kelly, S. D., Voss, M., Streu, P. and Cape, J. N.: Dry and wet deposition of nutrients from the tropical Atlantic atmosphere: Links to primary productivity and nitrogen fixation, *Deep Sea Res. Part I Oceanogr. Res. Pap.*, 54(10), 1704–1720, doi:10.1016/j.dsr.2007.07.001, 2007.
- 25 Baker, A. R., Adams, C., Bell, T. G., Jickells, T. D. and Ganzeveld, L.: Estimation of atmospheric nutrient inputs to the Atlantic Ocean from 50°N to 50°S based on large-scale field sampling: Iron and other dust-associated elements, *Global Biogeochem. Cycles*, 27(3), 755–767, doi:10.1002/gbc.20062, 2013.
- Benitez-Nelson, C. R., Vink, S. M., Carrillo, J. H. and Huebert, B. J.: Volcanically influenced Fe and Al cloud water deposition to Hawaii, *Atmos. Environ.*, 37(4), 535–544, doi:10.1016/S1352-2310(02)00892-0, 2003.
- 30 Bonnet, S.: *Dissolution of atmospheric iron in seawater, Geophys. Res. Lett.*, 31(3), L03303,

[doi:10.1029/2003GL018423](https://doi.org/10.1029/2003GL018423), 2004.

Bowie, A. R., Lannuzel, D., Remenyi, T. A., Wagener, T., Lam, P. J., Boyd, P. W., Guieu, C., Townsend, A. T. and Trull, T. W.: Biogeochemical iron budgets of the Southern Ocean south of Australia: Decoupling of iron and nutrient cycles in the subantarctic zone by the summertime supply, *Global Biogeochem. Cycles*, 23(4), GB4034, doi:10.1029/2009GB003500, 2009.

Boyd, P. W. and Ellwood, M. J.: [The biogeochemical cycle of iron in the ocean](https://doi.org/10.1038/ngeo964), *Nat. Geosci.*, 3(10), 675–682, doi:10.1038/ngeo964, 2010.

Boyd, P. W., Strzepek, R., Takeda, S., Jackson, G., Wong, C. S., McKay, R. M., Law, C., Kiyosawa, H., Saito, H. and Sherry, N.: The evolution and termination of an iron-induced mesoscale bloom in the northeast subarctic Pacific, *Limnol. Oceanogr.*, 50(6), 1872–1886, doi:10.4319/lo.2005.50.6.1872, 2005.

Brandt, F., Bosbach, D., Krawczyk-Barsch, E., Arnold, T. and Bernhard, G.: Chlorite dissolution in the acid pH-range: a combined microscopic and macroscopic approach, *Geochim. Cosmochim. Acta*, 67(8), 1451–1461, doi:10.1016/S0016-7037(02)01293-0, 2003.

Buck, C. S., Landing, W. M., Resing, J. A. and Lebon, G. T.: Aerosol iron and aluminum solubility in the northwest Pacific Ocean: Results from the 2002 IOC cruise, *Geochemistry, Geophys. Geosystems*, 7(4), 1–21, doi:10.1029/2005GC000977, 2006.

Buck, C. S., Landing, W. M., Resing, J. A. and Measures, C. I.: The solubility and deposition of aerosol Fe and other trace elements in the North Atlantic Ocean: Observations from the A16N CLIVAR/CO2 repeat hydrography section, *Mar. Chem.*, 120(1–4), 57–70, doi:10.1016/j.marchem.2008.08.003, 2010.

Buck, C. S., Landing, W. M. and Resing, J.: Pacific Ocean aerosols: Deposition and solubility of iron, aluminum, and other trace elements, *Mar. Chem.*, 157(2013), 117–130, doi:10.1016/j.marchem.2013.09.005, 2013.

Chance, R., Jickells, T. D. and Baker, A. R.: Atmospheric trace metal concentrations, solubility and deposition fluxes in remote marine air over the south-east Atlantic, *Mar. Chem.*, 177, 1–12, doi:10.1016/j.marchem.2015.06.028, 2015.

Cheize, M., Sarthou, G., Croot, P. L., Bucciarelli, E., Baudoux, A.-C. and Baker, A. R.: Iron organic speciation determination in rainwater using cathodic stripping voltammetry, *Anal. Chim. Acta*, 736, 45–54, doi:10.1016/j.aca.2012.05.011, 2012.

Chen, H. and Grassian, V. H.: Iron Dissolution of Dust Source Materials during Simulated Acidic Processing: The Effect of Sulfuric, Acetic, and Oxalic Acids, *Environ. Sci. Technol.*, 130829091001000, doi:10.1021/es401285s, 2013.

Chen, H., Laskin, A., Baltrusaitis, J., Gorski, C. A., Scherer, M. M. and Grassian, V. H.: Coal Fly Ash as a

- Source of Iron in Atmospheric Dust, *Environ. Sci. Technol.*, 46(4), 2112–2120, doi:10.1021/es204102f, 2012.
- Chen, Y. and Siefert, R. L.: Seasonal and spatial distributions and dry deposition fluxes of atmospheric total and labile iron over the tropical and subtropical North Atlantic Ocean, *J. Geophys. Res.*, 109(D9), D09305, doi:10.1029/2003JD003958, 2004.
- 5 Chuang, P. Y., Duvall, R. M., Shafer, M. M. and Schauer, J. J.: The origin of water soluble particulate iron in the Asian atmospheric outflow, *Geophys. Res. Lett.*, 32(7), L07813, doi:10.1029/2004GL021946, 2005.
- Claquin, T., Schulz, M. and Balkanski, Y. J.: Modeling the mineralogy of atmospheric dust sources, *J. Geophys. Res. Atmos.*, 104(D18), 22243–22256, doi:10.1029/1999JD900416, 1999.
- Dentener, F., Kinne, S., Bond, T., Boucher, O., Cofala, J., Generoso, S., Ginoux, P., Gong, S., Hoelzemann, J. J.,
10 Ito, A., Marelli, L., Penner, J. E., Putaud, J.-P., Textor, C., Schulz, M., van der Werf, G. R. and Wilson, J.: Emissions of primary aerosol and precursor gases in the years 2000 and 1750 prescribed data-sets for AeroCom, *Atmos. Chem. Phys.*, 6(12), 4321–4344, doi:10.5194/acp-6-4321-2006, 2006.
- Duce, R. A. and Tindale, N. W.: Atmospheric transport of iron and its deposition in the ocean, *Limnol. Oceanogr.*, 36(8), 1715–1726, doi:10.4319/lo.1991.36.8.1715, 1991.
- 15 Duggen, S., Olgun, N., Croot, P., Hoffmann, L., Dietze, H., Delmelle, P. and Teschner, C.: The role of airborne volcanic ash for the surface ocean biogeochemical iron-cycle: a review, *Biogeosciences*, 7(3), 827–844, doi:10.5194/bg-7-827-2010, 2010.
- Falkowski, P. G.: [Evolution of the nitrogen cycle and its influence on the biological sequestration of CO₂ in the ocean](#), *Nature*, 387(6630), 272–275, doi:10.1038/387272a0, 1997.
- 20 [Falkowski, P. G., Scholes, R. J., Boyle, E., Canadell, J., Canfield, D., Elser, J., Gruber, N., Hibbard, K., Högberg, P., Linder, S., Mackenzie, F. T., Moore, B., Pedersen, T., Rosenthal, Y., Seitzinger, S., Smetacek, V. and Steffen, W.](#): The Global Carbon Cycle: A Test of Our Knowledge of Earth as a System, *Science* (80-.), 290(5490), 291–296, doi:10.1126/science.290.5490.291, 2000.
- [Fan, S.-M., Horowitz, L. W., Levy, H. and Moxim, W. J.](#): Impact of air pollution on wet deposition of mineral
25 dust aerosols, *Geophys. Res. Lett.*, 31(2), doi:10.1029/2003GL018501, 2004.
- Fountoukis, C. and Nenes, A.: ISORROPIA II: a computationally efficient thermodynamic equilibrium model for
 $K^+ - Ca^{2+} - Mg^{2+} - NH_4^+ - Na^+ - SO_4^{2-} - NO_3^-$, *Atmos. Chem. Phys.*, 7(17), 4639–4659, doi:10.5194/acp-7-
4639-2007, 2007.
- Fu, H., Cwiertny, D. M., Carmichael, G. R., Scherer, M. M. and Grassian, V. H.: Photoreductive dissolution of
30 Fe-containing mineral dust particles in acidic media, *J. Geophys. Res.*, 115(D11), D11304, doi:10.1029/2009JD012702, 2010.

Deleted: Falkowski, P. G.: Evolution of the nitrogen cycle and its influence on the biological sequestration of CO₂ in the ocean, *Nature*, 387(6630), 272–275, doi:10.1038/387272a0, 1997.

Deleted: "–Ca²⁺–Mg²⁺–";

Deleted: "–";

Deleted: "–SO₄²⁻–";

Formatted: Not Superscript/ Subscript

Formatted: Not Superscript/ Subscript

Deleted: [;]

- Fu, H., Lin, J., Shang, G., Dong, W., Grassian, V. H., Carmichael, G. R., Li, Y. and Chen, J.: Solubility of Iron from Combustion Source Particles in Acidic Media Linked to Iron Speciation, *Environ. Sci. Technol.*, 46(20), 11119–11127, doi:10.1021/es302558m, 2012.
- 5 Fung, I. Y., Meyn, S. K., Tegen, I., Doney, S. C., John, J. G. and Bishop, J. K. B.: Iron supply and demand in the upper ocean, *Global Biogeochem. Cycles*, 14(1), 281–295, doi:10.1029/1999GB900059, 2000.
- Furutani, H., Meguro, A., Iguchi, H. and Uematsu, M.: Geographical distribution and sources of phosphorus in atmospheric aerosol over the North Pacific Ocean, *Geophys. Res. Lett.*, 37(3), L03805, doi:10.1029/2009GL041367, 2010.
- 10 Ganzeveld, L. and Lelieveld, J.: Dry deposition parameterization in a chemistry general circulation model and its influence on the distribution of reactive trace gases, *J. Geophys. Res. Atmos.*, 100(D10), 20999–21012, doi:10.1029/95jd02266, 1995.
- Gao, Y., Xu, G., Zhan, J., Zhang, J., Li, W., Lin, Q., Chen, L. and Lin, H.: Spatial and particle size distributions of atmospheric dissolvable iron in aerosols and its input to the Southern Ocean and coastal East Antarctica, *J. Geophys. Res. Atmos.*, 118(22), 12,634–12,648, doi:10.1002/2013JD020367, 2013.
- 15 Gerber, H.: Supersaturation and Droplet Spectral Evolution in Fog, *J. Atmos. Sci.*, 48(24), 2569–2588, doi:10.1175/1520-0469(1991)048<2569:SADSEI>2.0.CO;2, 1991.
- Gerber, H. E.: Relative Humidity Parameterization of the Navy Aerosol Model (NAM), 1985.
- Ginoux, P., Prospero, J. M., Gill, T. E., Hsu, N. C. and Zhao, M.: Global-scale attribution of anthropogenic and natural dust sources and their emission rates based on MODIS Deep Blue aerosol products, *Rev. Geophys.*, 50(3), 20 RG3005, doi:10.1029/2012RG000388, 2012.
- 20 Guieu, C. C., Bonnet, S., Wagener, T., Lo?e-Pilot, M.-D. and Lo?e-Pilot, M. D.: Biomass burning as a source of dissolved iron to the open ocean?, *Geophys. Res. Lett.*, 32(19), L19608, doi:10.1029/2005GL022962, 2005.
- Hamer, M., Graham, R. C., Amrhein, C. and Bozhilov, K. N.: Dissolution of Ripidolite (Mg, Fe-Chlorite) in Organic and Inorganic Acid Solutions, *Soil Sci. Soc. Am. J.*, 67(2), 654, doi:10.2136/sssaj2003.6540, 2003.
- 25 Hand, J. L., Mahowald, N. M., Chen, Y., Siefert, R. L., Luo, C., Subramaniam, A. and Fung, I.: Estimates of atmospheric-processed soluble iron from observations and a global mineral aerosol model: Biogeochemical implications, *J. Geophys. Res.*, 109(D17), D17205, doi:10.1029/2004JD004574, 2004.
- Heimbürger, A., Losno, R. and Triquet, S.: Solubility of iron and other trace elements in rainwater collected on the Kerguelen Islands (South Indian Ocean), *Biogeosciences*, 10(10), 6617–6628, doi:10.5194/bg-10-6617-2013, 30 2013.
- Hoesly, R. M., Smith, S. J., Feng, L., Klimont, Z., Janssens-Maenhout, G., Pitkanen, T., Seibert, J. J., Vu, L.,

- Andres, R. J., Bolt, R. M., Bond, T. C., Dawidowski, L., Kholod, N., Kurokawa, J., Li, M., Liu, L., Lu, Z., Moura, M. C. P., O'Rourke, P. R. and Zhang, Q.: Historical (1750–2014) anthropogenic emissions of reactive gases and aerosols from the Community Emissions Data System (CEDS), *Geosci. Model Dev.*, 11(1), 369–408, doi:10.5194/gmd-11-369-2018, 2018.
- 5 Huneeus, N., Schulz, M., Balkanski, Y., Griesfeller, J., Prospero, J., Kinne, S., Bauer, S., Boucher, O., Chin, M., Dentener, F., Diehl, T., Easter, R., Fillmore, D., Ghan, S., Ginoux, P., Grini, A., Horowitz, L., Koch, D., Krol, M. C., Landing, W., Liu, X., Mahowald, N., Miller, R., Morcrette, J.-J., Myhre, G., Penner, J., Perlwitz, J., Stier, P., Takemura, T. and Zender, C. S.: Global dust model intercomparison in AeroCom phase I, *Atmos. Chem. Phys.*, 11(15), 7781–7816, doi:10.5194/acp-11-7781-2011, 2011.
- 10 Hurrell, J. W., Holland, M. M., Gent, P. R., Ghan, S., Kay, J. E., Kushner, P. J., Lamarque, J.-F., Large, W. G., Lawrence, D., Lindsay, K., Lipscomb, W. H., Long, M. C., Mahowald, N., Marsh, D. R., Neale, R. B., Rasch, P., Vavrus, S., Vertenstein, M., Bader, D., Collins, W. D., Hack, J. J., Kiehl, J. and Marshall, S.: The Community Earth System Model: A Framework for Collaborative Research, *Bull. Am. Meteorol. Soc.*, 94(9), 1339–1360, doi:10.1175/BAMS-D-12-00121.1, 2013.
- 15 Ito, A.: Contrasting the Effect of Iron Mobilization on Soluble Iron Deposition to the Ocean in the Northern and Southern Hemispheres, *J. Meteorol. Soc. Japan*, 90A(0), 167–188, doi:10.2151/jmsj.2012-A09, 2012.
- Ito, A.: Global modeling study of potentially bioavailable iron input from shipboard aerosol sources to the ocean, *Global Biogeochem. Cycles*, 27(1), 1–10, doi:10.1029/2012GB004378, 2013.
- Ito, A.: Atmospheric Processing of Combustion Aerosols as a Source of Bioavailable Iron, *Environ. Sci. Technol. Lett.*, 2(3), 70–75, doi:10.1021/acs.estlett.5b00007, 2015.
- 20 Ito, A. and Feng, Y.: Role of dust alkalinity in acid mobilization of iron, *Atmos. Chem. Phys.*, 10(19), 9237–9250, doi:10.5194/acp-10-9237-2010, 2010.
- Ito, A. and Kok, J. F.: Do dust emissions from sparsely vegetated regions dominate atmospheric iron supply to the Southern Ocean?, *J. Geophys. Res. Atmos.*, 122(7), 3987–4002, doi:10.1002/2016JD025939, 2017.
- 25 Ito, A. and Shi, Z.: Delivery of anthropogenic bioavailable iron from mineral dust and combustion aerosols to the ocean, *Atmos. Chem. Phys.*, 16(1), 85–99, doi:10.5194/acp-16-85-2016, 2016.
- Ito, A. and Xu, L.: Response of acid mobilization of iron-containing mineral dust to improvement of air quality projected in the future, *Atmos. Chem. Phys.*, 14(7), 3441–3459, doi:10.5194/acp-14-3441-2014, 2014.
- Ito, A., Sillman, S. and Penner, J. E.: Effects of additional nonmethane volatile organic compounds, organic nitrates, and direct emissions of oxygenated organic species on global tropospheric chemistry, *J. Geophys. Res.*, 112(D6), D06309, doi:10.1029/2005JD006556, 2007.
- 30

- Ito, A., Lin, G. and Penner, J. E.: Radiative forcing by light-absorbing aerosols of pyrogenetic iron oxides, *Sci. Rep.*, 8(1), 7347, doi:10.1038/s41598-018-25756-3, 2018.
- Ito, A., Myriokefalitakis, S., Kanakidou, M., Mahowald, N., Scanza, R. A., Hamilton, D. S., Baker, A., Jickells, T., Sarin, M., Srinivas, B., Gao, Y., Shelley, R., Buck, C., Landing, W., Bowie, A., Perron, M., Wagener, T.,
5 Guieu, C., Meskhidze, N., Johnson, M. S., Feng, Y., Kok, J. F. and Duce, R.: Observationally-constrained attribution of labile iron in aerosols to combustion sources, to be Submitt., n.d.
- Jickells, T. D. and Spokes, L. J.: [Atmospheric iron inputs to the ocean, J. Wiley., 2001.](#)
- Jickells, T. D., An, Z. S., Andersen, K. K., Baker, A. R., Bergametti, G., Brooks, N., Cao, J. J., Boyd, P. W.,
Duce, R. A., Hunter, K. A., Kawahata, H., Kubilay, N., laRoche, J., Liss, P. S., Mahowald, N., Prospero, J. M.,
10 Ridgwell, A. J., Tegen, I. and Torres, R.: Global Iron Connections Between Desert Dust, Ocean Biogeochemistry, and Climate, *Science* (80-), 308(5718), 67 LP-71, doi:10.1126/science.1105959, 2005.
- Jickells, T. D., Baker, A. R. and Chance, R.: Atmospheric transport of trace elements and nutrients to the oceans, *Philos. Trans. R. Soc. A Math. Phys. Eng. Sci.*, 374(2081), 20150286, doi:10.1098/rsta.2015.0286, 2016.
- Johnson, K. S.: Iron supply and demand in the upper ocean: Is extraterrestrial dust a significant source of
15 bioavailable iron?, *Global Biogeochem. Cycles*, 15(1), 61–63, doi:10.1029/2000GB001295, 2001.
- Johnson, M. S. and Meskhidze, N.: Atmospheric dissolved iron deposition to the global oceans: effects of oxalate-promoted Fe dissolution, photochemical redox cycling, and dust mineralogy, *Geosci. Model Dev.*, 6(4), 1137–1155, doi:10.5194/gmd-6-1137-2013, 2013.
- Johnson, M. S., Meskhidze, N., Solmon, F., Gassó, S., Chuang, P. Y., Gaiero, D. M., Yantosca, R. M., Wu, S.,
20 Wang, Y. and Carouge, C.: Modeling dust and soluble iron deposition to the South Atlantic Ocean, *J. Geophys. Res.*, 115(D15), D15202, doi:10.1029/2009JD013311, 2010.
- Johnson, M. S., Meskhidze, N., Kiliyanpilakkil, V. P. and Gassó, S.: Understanding the transport of Patagonian dust and its influence on marine biological activity in the South Atlantic Ocean, *Atmos. Chem. Phys.*, 11(6), 2487–2502, doi:10.5194/acp-11-2487-2011, 2011.
- 25 Journet, E., Balkanski, Y. and Harrison, S. P.: A new data set of soil mineralogy for dust-cycle modeling, *Atmos. Chem. Phys.*, 14(8), 3801–3816, doi:10.5194/acp-14-3801-2014, 2014.
- [Kawamura, K. and Ikushima, K.: Seasonal changes in the distribution of dicarboxylic acids in the urban atmosphere, *Environ. Sci. Technol.*, 27\(10\), 2227–2235, doi:10.1021/es00047a033, 1993.](#)
- [Kawamura, K. and Sakaguchi, F.: Molecular distributions of water soluble dicarboxylic acids in marine aerosols over the Pacific Ocean including tropics, *J. Geophys. Res. Atmos.*, 104\(D3\), 3501–3509, doi:10.1029/1998JD100041, 1999.](#)
- 30

- Kok, J. F.: A scaling theory for the size distribution of emitted dust aerosols suggests climate models underestimate the size of the global dust cycle, *Proc. Natl. Acad. Sci.*, 108(3), 1016–1021, doi:10.1073/pnas.1014798108, 2011.
- Kok, J. F., Mahowald, N. M., Fratini, G., Gillies, J. A., Ishizuka, M., Leys, J. F., Mikami, M., Park, M.-S., Park, S.-U., Van Pelt, R. S. and Zobeck, T. M.: An improved dust emission model – Part 1: Model description and comparison against measurements, *Atmos. Chem. Phys.*, 14(23), 13023–13041, doi:10.5194/acp-14-13023-2014, 2014a.
- Kok, J. F., Albani, S., Mahowald, N. M. and Ward, D. S.: An improved dust emission model – Part 2: Evaluation in the Community Earth System Model, with implications for the use of dust source functions, *Atmos. Chem. Phys.*, 14(23), 13043–13061, doi:10.5194/acp-14-13043-2014, 2014b.
- Kok, J. F., Ridley, D. A., Zhou, Q., Miller, R. L., Zhao, C., Heald, C. L., Ward, D. S., Albani, S. and Haustein, K.: Smaller desert dust cooling effect estimated from analysis of dust size and abundance, *Nat. Geosci.*, 10(4), 274–278, doi:10.1038/ngeo2912, 2017.
- Kumar, A., Sarin, M. M. and Srinivas, B.: Aerosol iron solubility over Bay of Bengal: Role of anthropogenic sources and chemical processing, *Mar. Chem.*, 121(1–4), 167–175, doi:10.1016/j.marchem.2010.04.005, 2010.
- Langmann, B., Zakšek, K., Hort, M. and Duggen, S.: Volcanic ash as fertiliser for the surface ocean, *Atmos. Chem. Phys.*, 10(8), 3891–3899, doi:10.5194/acp-10-3891-2010, 2010.
- Lanzl, C. A., Baltrusaitis, J. and Cwiertny, D. M.: Dissolution of Hematite Nanoparticle Aggregates: Influence of Primary Particle Size, Dissolution Mechanism, and Solution pH, *Langmuir*, 28(45), 15797–15808, doi:10.1021/la3022497, 2012.
- Larsen, O. and Postma, D.: Kinetics of reductive bulk dissolution of lepidocrocite, ferrihydrite, and goethite, *Geochim. Cosmochim. Acta*, 65(9), 1367–1379, doi:10.1016/S0016-7037(00)00623-2, 2001.
- Lasaga, A. C., Soler, J. M., Ganor, J., Burch, T. E. and Nagy, K. L.: Chemical weathering rate laws and global geochemical cycles, *Geochim. Cosmochim. Acta*, 58(10), 2361–2386, doi:10.1016/0016-7037(94)90016-7, 1994.
- Lin, G., Sillman, S., Penner, J. E. and Ito, A.: Global modeling of SOA: the use of different mechanisms for aqueous-phase formation, *Atmos. Chem. Phys.*, 14(11), 5451–5475, doi:10.5194/acp-14-5451-2014, 2014.
- Lis, H., Shaked, Y., Kranzler, C., Keren, N. and Morel, F. M. M.: Iron bioavailability to phytoplankton: An empirical approach, *ISME J.*, 9, 1003–1013, doi:10.1038/ismej.2014.199, 2015.
- Litter, M. I., Villegas, M. and Blesa, M. A.: Photodissolution of iron oxides in malonic acid, *Can. J. Chem.*, 72(10), 2037–2043, doi:10.1139/v94-260, 1994.
- Liu, H., Jacob, D. J., Bey, I. and Yantosca, R. M.: Constraints from ^{210}Pb and ^7Be on wet deposition and

Deleted: Krishnamurthy, A., Moore, J. K., Mahowald, N., Luo, C., Doney, S. C., Lindsay, K. and Zender, C. S.: Impacts of increasing anthropogenic soluble iron and nitrogen deposition on ocean biogeochemistry, *Global Biogeochem. Cycles*, 23(3), GB3016, doi:10.1029/2008GB003440, 2009.

- transport in a global three-dimensional chemical tracer model driven by assimilated meteorological fields, *J. Geophys. Res. Atmos.*, 106(D11), 12109–12128, doi:10.1029/2000JD900839, 2001.
- Liu, X., Penner, J. E. and Herzog, M.: Global modeling of aerosol dynamics: Model description, evaluation, and interactions between sulfate and nonsulfate aerosols, Wiley-Blackwell., 2005.
- 5 Longo, A. F., Feng, Y., Lai, B., Landing, W. M., Shelley, R. U., Nenes, A., Mihalopoulos, N., Violaki, K. and Ingall, E. D.: Influence of Atmospheric Processes on the Solubility and Composition of Iron in Saharan Dust, *Environ. Sci. Technol.*, 50(13), 6912–6920, doi:10.1021/acs.est.6b02605, 2016.
- Lucchesi, R.: File Specification for GEOS-5 FP, GMAO Office Note No. 4 (Version 1.1), GMAO - Glob. Model. Assim. Off. Res. Site [online] Available from: https://gmao.gsfc.nasa.gov/GMAO_products/ (Accessed 14 May
10 2018), 2017.
- Luo, C., Mahowald, N., Bond, T., Chuang, P. Y., Artaxo, P., Siefert, R., Chen, Y. and Schauer, J.: Combustion iron distribution and deposition, *Global Biogeochem. Cycles*, 22(1), GB1012, doi:10.1029/2007GB002964, 2008.
- Luo, C., Gao, Y., Pio, C. A., Duarte, A. C., Laës, A., Ussher, S., Achterberg, E. P., Baar, H. J. W. de,
15 Timmermans, K. R. and Blain, S.: Aeolian iron mobilisation by dust-acid interactions and their implications for soluble iron deposition to the ocean: a test involving potential anthropogenic organic acidic species, *Environ. Chem.*, 7(2), 153, doi:10.1071/EN09116, 2010.
- Maher, B. A., Prospero, J. M., Mackie, D., Gaiero, D., Hesse, P. P. and Balkanski, Y.: Global connections between aeolian dust, climate and ocean biogeochemistry at the present day and at the last glacial maximum,
20 *Earth-Science Rev.*, 99(1–2), 61–97, doi:10.1016/j.earscirev.2009.12.001, 2010.
- Mahowald, N. M., Artaxo, P., Baker, A. R., Jickells, T. D., Okin, G. S., Randerson, J. T. and Townsend, A. R.: Impacts of biomass burning emissions and land use change on Amazonian atmospheric phosphorus cycling and deposition, *Global Biogeochem. Cycles*, 19(4), GB4030, doi:10.1029/2005GB002541, 2005.
- Mahowald, N. M., Engelstaedter, S., Luo, C., Sealy, A., Artaxo, P., Benitez-Nelson, C., Bonnet, S., Chen, Y.,
25 Chuang, P. Y., Cohen, D. D., Dulac, F., Herut, B., Johansen, A. M., Kubilay, N., Losno, R., Maenhaut, W., Paytan, A., Prospero, J. M., Shank, L. M. and Siefert, R. L.: Atmospheric iron deposition: global distribution, variability, and human perturbations., *Ann. Rev. Mar. Sci.*, 1, 245–278, doi:10.1146/annurev.marine.010908.163727, 2009.
- Martin, J. H., Gordon, M. and Fitzwater, S. E.: The case for iron, *Limnol. Oceanogr.*, 36(8), 1793–1802,
30 doi:10.4319/lo.1991.36.8.1793, 1991.
- Matsui, H., Mahowald, N. M., Moteki, N., Hamilton, D. S., Ohata, S., Yoshida, A., Koike, M., Scanza, R. A. and

- Flanner, M. G.: Anthropogenic combustion iron as a complex climate forcer, *Nat. Commun.*, 9(1), 1593, doi:10.1038/s41467-018-03997-0, 2018.
- Meskhidze, N., Chameides, W. L., Nenes, A. and Chen, G.: Iron mobilization in mineral dust: Can anthropogenic SO₂ emissions affect ocean productivity?, *Geophys. Res. Lett.*, 30(21), 2085, doi:10.1029/2003GL018035, 2003.
- 5 Meskhidze, N., Chameides, W. L. and Nenes, A.: Dust and pollution: A recipe for enhanced ocean fertilization?, *J. Geophys. Res. D Atmos.*, 110(3), 1–23, doi:10.1029/2004JD005082, 2005.
- Meskhidze, N., [Johnson, M. S., Hurley, D. and Dawson, K.: Influence of measurement uncertainties on fractional solubility of iron in mineral aerosols over the oceans, *Aeolian Res.*, 22, 85–92, doi:10.1016/j.aeolia.2016.07.002, 2016.](#)
- 10 [Meskhidze, N., Hurley, D., Royalty, T. M. and Johnson, M. S.:](#) Potential effect of atmospheric dissolved organic carbon on the iron solubility in seawater, *Mar. Chem.*, 194, 124–132, doi:10.1016/j.marchem.2017.05.011, 2017.
- Moore, J. K., Lindsay, K., Doney, S. C., Long, M. C. and Misumi, K.: Marine Ecosystem Dynamics and Biogeochemical Cycling in the Community Earth System Model [CESM1(BGC)]: Comparison of the 1990s with the 2090s under the RCP4.5 and RCP8.5 Scenarios, *J. Clim.*, 26(23), 9291–9312, doi:10.1175/JCLI-D-12-
- 15 00566.1, 2013.
- Morel, F. M. M., Kustka, A. B. and Shaked, Y.: The role of unchelated Fe in the iron nutrition of phytoplankton, *Limnol. Oceanogr.*, 53(1), 400–404, doi:10.4319/lo.2008.53.1.0400, 2008.
- Myriokefalitakis, S., Tsigaridis, K., Mihalopoulos, N., Sciare, J., Nenes, A., Kawamura, K., Segers, A. and Kanakidou, M.: In-cloud oxalate formation in the global troposphere: a 3-D modeling study, *Atmos. Chem. Phys.*, 11(12), 5761–5782, doi:10.5194/acp-11-5761-2011, 2011.
- 20 Myriokefalitakis, S., Daskalakis, N., Mihalopoulos, N., Baker, A. R., Nenes, A. and Kanakidou, M.: Changes in dissolved iron deposition to the oceans driven by human activity: a 3-D global modelling study, *Biogeosciences*, 12(13), 3973–3992, doi:10.5194/bg-12-3973-2015, 2015.
- Myriokefalitakis, S., Nenes, A., Baker, A. R., Mihalopoulos, N. and Kanakidou, M.: Bioavailable atmospheric phosphorous supply to the global ocean: a 3-D global modeling study, *Biogeosciences*, 13(24), 6519–6543, doi:10.5194/bg-13-6519-2016, 2016.
- 25 Nickovic, S., Vukovic, A., Vujadinovic, M., Djurdjevic, V. and Pejanovic, G.: Technical Note: High-resolution mineralogical database of dust-productive soils for atmospheric dust modeling, *Atmos. Chem. Phys.*, 12(2), 845–855, doi:10.5194/acp-12-845-2012, 2012.
- 30 Nickovic, S., Vukovic, A. and Vujadinovic, M.: Atmospheric processing of iron carried by mineral dust, *Atmos. Chem. Phys.*, 13(18), 9169–9181, doi:10.5194/acp-13-9169-2013, 2013.

Oakes, M., Ingall, E. D., Lai, B., Shafer, M. M., Hays, M. D., Liu, Z. G., Russell, A. G. and Weber, R. J.: Iron Solubility Related to Particle Sulfur Content in Source Emission and Ambient Fine Particles, *Environ. Sci. Technol.*, 46(12), 6637–6644, doi:10.1021/es300701c, 2012.

Paris, R. and Desboeufs, K. V.: Effect of atmospheric organic complexation on iron-bearing dust solubility, *Atmos. Chem. Phys.*, 13(9), 4895–4905, doi:10.5194/acp-13-4895-2013, 2013.

Paris, R., Desboeufs, K. V., Formenti, P., Nava, S. and Chou, C.: Chemical characterisation of iron in dust and biomass burning aerosols during AMMA-SOP0/DABEX: implication for iron solubility, *Atmos. Chem. Phys.*, 10(9), 4273–4282, doi:10.5194/acp-10-4273-2010, 2010.

Paris, R., Desboeufs, K. V. and Journet, E.: Variability of dust iron solubility in atmospheric waters: Investigation of the role of oxalate organic complexation, *Atmos. Environ.*, 45(36), 6510–6517, doi:10.1016/j.atmosenv.2011.08.068, 2011.

Powell, C. F., Baker, A. R., Jickells, T. D., Bange, H. W., Chance, R. J. and Yodanis, C.: Estimation of the Atmospheric Flux of Nutrients and Trace Metals to the Eastern Tropical North Atlantic Ocean, *J. Atmos. Sci.*, 72(10), 4029–4045, doi:10.1175/JAS-D-15-00111.1, 2015.

15 Le Quéré, C., Andres, R. J., Boden, T., Conway, T., Houghton, R. A., House, J. I., Marland, G., Peters, G. P., van der Werf, G. R., Ahlström, A., Andrew, R. M., Bopp, L., Canadell, J. G., Ciais, P., Doney, S. C., Enright, C., Friedlingstein, P., Huntingford, C., Jain, A. K., Jourdain, C., Kato, E., Keeling, R. F., Klein Goldewijk, K., Levis, S., Levy, P., Lomas, M., Poulter, B., Raupach, M. R., Schwinger, J., Sitch, S., Stocker, B. D., Viovy, N., Zaehle, S. and Zeng, N.: The global carbon budget 1959–2011, *Earth Syst. Sci. Data*, 5(1), 165–185, doi:10.5194/essd-5-165-2013, 2013.

20 Raiswell, R. and Canfield, D. E.: The Iron Biogeochemical Cycle Past and Present, *Geochemical Perspect.*, 1(1), 1–220, doi:10.7185/geochempersp.1.1, 2012.

[Raiswell, R., Hawkins, J. R., Benning, L. G., Baker, A. R., Death, R., Albani, S., Mahowald, N., Krom, M. D., Poulton, S. W., Wadham, J. and Tranter, M.: Potentially bioavailable iron delivery by iceberg-hosted sediments and atmospheric dust to the polar oceans, *Biogeosciences*, 13\(13\), 3887–3900, doi:10.5194/bg-13-3887-2016, 2016.](#)

Rasch, P. J., Feichter, J., Law, K., Mahowald, N., Penner, J., Benkovitz, C., Genthon, C., Giannakopoulos, C., Kasibhatla, P., Koch, D., Levy, H., Maki, T., Prather, M., Roberts, D. L., Roelofs, G.-J., Stevenson, D., Stockwell, Z., Taguchi, S., Kritz, M., Chipperfield, M., Baldocchi, D., McMurry, P., Barrie, L., Balkanski, Y., Chatfield, R., Kjellstrom, E., Lawrence, M., Lee, H. N., Lelieveld, J., Noone, K. J., Seinfeld, J., Stenchikov, G., Schwartz, S., Walcek, C. and Williamson, D.: A comparison of scavenging and deposition processes in global

- Deleted: FEICHTER
- Deleted: LAW
- Deleted: MAHOWALD
- Deleted: PENNER
- Deleted: BENKOVITZ
- Deleted: GENTHON
- Deleted: GIANNAKOPOULOS
- Deleted: KASIBHATLA
- Deleted: KOCH
- Deleted: LEVY
- Deleted: MAKI
- Deleted: PRATHER, M., ROBERTS, D. L., ROELOFS, G.-J., STEVENSON, D., STOCKWELL, Z., TAGUCHI, S., KRITZ, M., CHIPPERFIELD
- Deleted: BALDOCCHI
- Deleted: McMURRY
- Deleted: BARRIE
- Deleted: BALKANSKI
- Deleted: CHATFIELD
- Deleted: KJELLSTROM
- Deleted: LAWRENCE
- Deleted: LEE
- Deleted: N., LELIEVELD, J., NOONE, K. J., SEINFELD
- Deleted: STENCHIKOV
- Deleted: SCHWARTZ
- Deleted: WALCEK
- Deleted: WILLIAMSON

- models: results from the WCRP Cambridge Workshop of 1995, *Tellus B*, 52(4), 1025–1056, doi:10.1034/j.1600-0889.2000.00980.x, 2000.
- Rich, H. W. and Morel, F. M. M.: Availability of well-defined iron colloids to the marine diatom *Thalassiosira weissflogii*, *Limnol. Oceanogr.*, 35(3), 652–662, doi:10.4319/lo.1990.35.3.0652, 1990.
- 5 Ridley, D. A., Heald, C. L., Kok, J. F. and Zhao, C.: An observationally constrained estimate of global dust aerosol optical depth, *Atmos. Chem. Phys.*, 16(23), 15097–15117, doi:10.5194/acp-16-15097-2016, 2016.
- Rotman, D. A., Atherton, C. S., Bergmann, D. J., Cameron-Smith, P. J., Chuang, C. C., Connell, P. S., Dignon, J. E., Franz, A., Grant, K. E., Kinnison, D. E., Molenkamp, C. R., Proctor, D. D. and Tannahill, J. R.: IMPACT, the LLNL 3-D global atmospheric chemical transport model for the combined troposphere and stratosphere: Model
10 description and analysis of ozone and other trace gases, *J. Geophys. Res. Atmos.*, 109(D4), D04303, doi:10.1029/2002JD003155, 2004.
- Scanza, R. A., Mahowald, N., Ghan, S., Zender, C. S., Kok, J. F., Liu, X., Zhang, Y. and Albani, S.: Modeling dust as component minerals in the Community Atmosphere Model: development of framework and impact on radiative forcing, *Atmos. Chem. Phys.*, 15(1), 537–561, doi:10.5194/acp-15-537-2015, 2015.
- 15 Scanza, R. A., Mahowald, N. M., Perez Garcia-Pando, C., Buck, C., Baker, A. and Hamilton, D. S.: Atmospheric Processing of Iron in Mineral and Combustion Aerosols: Development of an Intermediate-Complexity Mechanism Suitable for Earth System Models, *Atmos. Chem. Phys. Discuss.*, in review(February), 1–39, doi:10.5194/acp-2018-80, 2018.
- Schroth, A. W., Crusius, J., Sholkovitz, E. R. and Bostick, B. C.: Iron solubility driven by speciation in dust
20 sources to the ocean, *Nat. Geosci.*, 2(5), 337–340, doi:10.1038/ngeo501, 2009.
- Sedwick, P. N., Sholkovitz, E. R. and Church, T. M.: Impact of anthropogenic combustion emissions on the fractional solubility of aerosol iron: Evidence from the Sargasso Sea, *Geochemistry, Geophys. Geosystems*, 8(10), 1–21, doi:10.1029/2007GC001586, 2007.
- Seinfeld, J. H. and Pandis, S. N.: *Atmospheric Chemistry and Physics: From Air Pollution to Climate Change.*,
25 2006.
- Shelley, R. U., Morton, P. L. and Landing, W. M.: Elemental ratios and enrichment factors in aerosols from the US-GEOTRACES North Atlantic transects, *Deep Sea Res. Part II Top. Stud. Oceanogr.*, 116, 262–272, doi:10.1016/j.dsr2.2014.12.005, 2015.
- Shelley, R. U., Landing, W. M., Ussher, S. J., Planquette, H. and Sarthou, G.: Regional trends in the fractional
30 solubility of Fe and other metals from North Atlantic aerosols (GEOTRACES cruises GA01 and GA03) following a two-stage leach, *Biogeosciences*, 15(8), 2271–2288, doi:10.5194/bg-15-2271-2018, 2018.

- Shi, Z., Krom, M. D., Bonneville, S., Baker, A. R., Jickells, T. D. and Benning, L. G.: Formation of Iron Nanoparticles and Increase in Iron Reactivity in Mineral Dust during Simulated Cloud Processing, *Environ. Sci. Technol.*, 43(17), 6592–6596, doi:10.1021/es901294g, 2009.
- Shi, Z., Bonneville, S., Krom, M. D., Carslaw, K. S., Jickells, T. D., Baker, A. R. and Benning, L. G.: Iron dissolution kinetics of mineral dust at low pH during simulated atmospheric processing, *Atmos. Chem. Phys.*, 11(3), 995–1007, doi:10.5194/acp-11-995-2011, 2011.
- Shi, Z., Krom, M. D., Jickells, T. D., Bonneville, S., Carslaw, K. S., Mihalopoulos, N., Baker, A. R. and Benning, L. G.: Impacts on iron solubility in the mineral dust by processes in the source region and the atmosphere: A review, *Aeolian Res.*, 5, 21–42, doi:10.1016/j.aeolia.2012.03.001, 2012.
- 10 Sholkovitz, E. R., Sedwick, P. N., Church, T. M., Baker, A. R. and Powell, C. F.: Fractional solubility of aerosol iron: Synthesis of a global-scale data set, *Geochim. Cosmochim. Acta*, 89, 173–189, doi:10.1016/j.gca.2012.04.022, 2012.
- Siffert, C. and Sulzberger, B.: Light-Induced Dissolution of Hematite in the Presence of Oxalate: A Case Study, *Langmuir*, 7(8), 1627–1634, doi:10.1021/la00056a014, 1991.
- 15 Sippula, O., Hokkinen, J., Puustinen, H., Yli-Pirila, P. and Jokiniemi, J.: Comparison of particle emissions from small heavy fuel oil and wood-fired boilers, *Atmos. Environ.*, 43(32), 4855–4864, doi:10.1016/j.atmosenv.2009.07.022, 2009.
- Solmon, F., Chuang, P. Y., Meskhidze, N. and Chen, Y.: Acidic processing of mineral dust iron by anthropogenic compounds over the north Pacific Ocean, *J. Geophys. Res.*, 114(D2), D02305, doi:10.1029/2008JD010417, 2009.
- 20 Spokes, L. J., Jickells, T. D. and Lim, B.: Solubilisation of aerosol trace metals by cloud processing: A laboratory study, *Geochim. Cosmochim. Acta*, 58(15), 3281–3287, doi:10.1016/0016-7037(94)90056-6, 1994.
- Srinivas, B. and Sarin, M. M.: Atmospheric deposition of N, P and Fe to the Northern Indian Ocean: Implications to C- and N-fixation, *Sci. Total Environ.*, 456–457, 104–114, doi:10.1016/j.scitotenv.2013.03.068, 2013.
- Srinivas, B., Sarin, M. M. and Kumar, A.: Impact of anthropogenic sources on aerosol iron solubility over the Bay of Bengal and the Arabian Sea, *Biogeochemistry*, 110(1–3), 257–268, doi:10.1007/s10533-011-9680-1, 2012.
- Srinivas, B., Sarin, M. M. and Rengarajan, R.: Atmospheric transport of mineral dust from the Indo-Gangetic Plain: Temporal variability, acid processing, and iron solubility, *Geochemistry, Geophys. Geosystems*, 15(8), 3226–3243, doi:10.1002/2014GC005395, 2014.
- 30 Tagliabue, A., [Aumont, O.](#), [DeAth, R.](#), [Dunne, J. P.](#), [Dutkiewicz, S.](#), [Galbraith, E.](#), [Misumi, K.](#), [Moore, J. K.](#), [Ridgwell, A.](#), [Sherman, E.](#), [Stock, C.](#), [Vichi, M.](#), [Völker, C.](#) and [Yool, A.](#): [How well do global ocean](#)

- [biogeochemistry models simulate dissolved iron distributions? Global Biogeochem. Cycles, 30\(2\), 149–174, doi:10.1002/2015GB005289, 2016.](#)
- [Tagliabue, A.,](#) Bowie, A. R., Boyd, P. W., Buck, K. N., Johnson, K. S. and Saito, M. A.: The integral role of iron in ocean biogeochemistry, *Nature*, 543(7643), 51–59, doi:10.1038/nature21058, 2017.
- 5 Tegen, I. and Fung, I.: Modeling of mineral dust in the atmosphere: Sources, transport, and optical thickness, *J. Geophys. Res.*, 99(D11), 22897, doi:10.1029/94JD01928, 1994.
- Tegen, I., Harrison, S. P., Kohfeld, K., Prentice, I. C., Coe, M. and Heimann, M.: Impact of vegetation and preferential source areas on global dust aerosol: Results from a model study, *J. Geophys. Res. Atmos.*, 107(D21), AAC 14-1-AAC 14-27, doi:10.1029/2001JD000963, 2002.
- 10 [Turner, D. R. and Hunter, K. A.: The biogeochemistry of iron in seawater, J. Wiley. \[online\] Available from: <https://www.wiley.com/en-us/The+Biogeochemistry+of+Iron+in+Seawater-p-9780471490685> \(Accessed 27 August 2018\), 2001.](#)
- Wagener, T.: Le fer à l'interface océan-atmosphère: Flux et processus de dissolution dans l'eau de mer, Université de la Méditerranée. [online] Available from: <https://tel.archives-ouvertes.fr/tel-00270558>, 2008.
- 15 Wagener, T., Guieu, C., Losno, R., Bonnet, S. and Mahowald, N.: Revisiting atmospheric dust export to the Southern Hemisphere ocean: Biogeochemical implications, *Global Biogeochem. Cycles*, 22(2), GB2006, doi:10.1029/2007GB002984, 2008.
- Wang, R., Balkanski, Y., Boucher, O., Bopp, L., Chappell, A., Ciais, P., Hauglustaine, D., Peñuelas, J. and Tao, S.: Sources, transport and deposition of iron in the global atmosphere, *Atmos. Chem. Phys.*, 15(11), 6247–6270, doi:10.5194/acp-15-6247-2015, 2015.
- 20 Xu, L. and Penner, J. E.: Global simulations of nitrate and ammonium aerosols and their radiative effects, *Atmos. Chem. Phys.*, 12(20), 9479–9504, doi:10.5194/acp-12-9479-2012, 2012.
- Xu, N. and Gao, Y.: Characterization of hematite dissolution affected by oxalate coating, kinetics and pH, *Appl. Geochemistry*, 23(4), 783–793, doi:10.1016/j.apgeochem.2007.12.026, 2008.
- 25 [Ye, Y. and Völker, C.: On the Role of Dust-Deposited Lithogenic Particles for Iron Cycling in the Tropical and Subtropical Atlantic, Global Biogeochem. Cycles, 31\(10\), 1543–1558, doi:10.1002/2017GB005663, 2017.](#)
- Yoon, T. H., Johnson, S. B., Musgrave, C. B. and Brown, G. E.: Adsorption of organic matter at mineral/water interfaces: I. ATR-FTIR spectroscopic and quantum chemical study of oxalate adsorbed at boehmite/water and corundum/water interfaces, *Geochim. Cosmochim. Acta*, 68(22), 4505–4518, doi:10.1016/j.gca.2004.04.025, 2004.
- 30 Yu, J. Z., Huang, X., Xu, J. and Hu, M.: When Aerosol Sulfate Goes Up, So Does Oxalate: Implication for the

Formation Mechanisms of Oxalate, *Environ. Sci. Technol.*, 39(1), 128–133, doi:10.1021/es049559f, 2005.

Zender, C. S., Bian, H. and Newman, D.: Mineral Dust Entrainment and Deposition (DEAD) model: Description and 1990s dust climatology, *J. Geophys. Res.*, 108(D14), 4416, doi:10.1029/2002JD002775, 2003.

5 Zhang, L., Gong, S., Padro, J. and Barrie, L.: A size-segregated particle dry deposition scheme for an atmospheric aerosol module, *Atmos. Environ.*, 35(3), 549–560, doi:10.1016/S1352-2310(00)00326-5, 2001.

Zhang, Y., Mahowald, N., Scanza, R. A., Journet, E., Desboeufs, K., Albani, S., Kok, J. F., Zhuang, G., Chen, Y., Cohen, D. D., Paytan, A., Patey, M. D., Achterberg, E. P., Engelbrecht, J. P. and Fomba, K. W.: Modeling the global emission, transport and deposition of trace elements associated with mineral dust, *Biogeosciences*, 12(19), 5771–5792, doi:10.5194/bg-12-5771-2015, 2015.

10 Zhu, X., Prospero, J. M., Savoie, D. L., Millero, F. J., Zika, R. G. and Saltzman, E. S.: Photoreduction of iron(III) in marine mineral aerosol solutions, *J. Geophys. Res. Atmos.*, 98(D5), 9039–9046, doi:10.1029/93JD00202, 1993.

Zhuang, G., Yi, Z., Duce, R. A. and Brown, P. R.: Link between iron and sulphur cycles suggested by detection of Fe(n) in remote marine aerosols, *Nature*, 355(6360), 537–539, doi:10.1038/355537a0, 1992.

15

Tables

Table 1. General description of the participating models used for the atmospheric Fe simulations. For multiple year simulations, the average was used.

Model	Simulated year(s)	Horizontal resolution (lon x lat)	Vertical Resolution (sigma levels)	Meteorology	Reference
CAM4	2007-2011	1.9° x 2.5°	56	GEOS-5	Scanza et al. (2018)
GEOS-Chem	01/03/2009-28/02/2010	2.0° x 2.5°	47	GEOS-5	Johnson and Meskhidze (2013)
IMPACT	2014	2.0° x 2.5°	59	GEOS-FP	Ito et al. (2018)
TM4-ECPL	2008	3.0° x 2.0°	34	ERA-Interim	Myriokefalitakis et al. (2015, 2016)

Deleted: Myriokefalitakis et al. (2015, 2016)

Table 2. Iron representation in the models; TFeD: total Fe in mineral dust; TFeC: total Fe in combustion aerosols Fe; LFeD: Labile Fe in mineral dust; LFeC: Labile Fe in combustion aerosols.

Model	Aerosol Fe Species	Aerosol Size Representation	Soil Mineralogy	Atmospheric Processing	Aqueous-phase median
CAM4	TFeD, TFeC, LFeD, LFeC	4 bins for each Fe-type with diameters: 0.1-1.0, 1.0-2.5, 2.5-5.0, and 5.0-10.0 μm	Claquin et al. (1999)	Proton- and ligand-dissolution of dust and combustion aerosols	Aerosol water, Cloud droplets
GEOS-Chem	TFeD, LFeD	4 bins for TFeD with diameters: 0.2–2.0, 2.0–3.6, 3.6–6.0 and 6.0–12.0 μm 1 bulk for LFeD	Nickovic et al. (2012)	Proton- and ligand-dissolution of dust aerosols	Aerosol water, Cloud droplets
IMPACT	TFeD, TFeC, LFeD, LFeC	4 bins for each Fe-type with diameters: <1.26, 1.26–2.5, 2.5–5, and 5–20 μm	Journet et al. (2014)	Proton-, ligand- and photoinduced dissolution of dust and combustion aerosols	Aerosol water
TM4-ECPL	TFeD, TFeC, LFeD, LFeC	2 modes for each Fe-type, with mass median radii (lognormal standard deviation) of 0.34 μm (1.59) and 1.75 μm (2.00) for dust aerosols and 0.04 μm (1.8) and 0.5 μm (2.00) for combustion aerosols	Nickovic et al. (2012)	Proton- and ligand-dissolution of dust aerosols	Aerosol water, Cloud droplets

Table 3. Global mean bias correction factors (median, lower 95% confidence interval and upper 95% confidence interval) derived for each model and each aerosol size (bins or modes) based on state-of-the-art constraints on size-resolved dust loading (Kok et al., 2017), taken into account for the ensemble model calculations.

Model	AEROSOL SIZE			
	Bin 1	Bin 2	Bin 3	Bin 4
CAM4	0.91, 0.55, 1.57	0.89, 0.57, 1.32	0.98, 0.62, 1.46	1.60, 0.97, 2.44
GEOS-Chem	1.37, 0.86, 2.09	0.99, 0.65, 1.44	0.91, 0.56, 1.38	0.24, 0.76, 1.94
IMPACT	0.89, 0.54, 1.38	0.71, 0.45, 1.01	0.91, 0.564, 1.30	1.01, 0.62, 1.49
TM4-ECPL*	Accumulation Mode		Coarse Mode	
	0.37, 0.22, 0.57		0.73, 0.43, 1.05	

*The median correction factors for the corresponding bins 1-4 are 0.134, 0.692, 1.257 and 1.81, respectively (see text).

5

Table 4. Annual budgets ($Tg\text{-Fe yr}^{-1}$) of total (TFe) and labile (LFe) Fe for emissions (EMI), dry deposition (DRY), wet deposition (WET) and sources (SRC; i.e., sum of emissions and atmospheric processing) for dust (TFed, LFed) and combustion (TFec, LFeC) Fe-containing aerosols as calculated by the models, as well as the models' mean (\pm standard deviation; STD).

Model	TFed			TFec			LFed			LFeC		
	EMI	DRY	WET	EMI	DRY	WET	SRC	DRY	WET	SRC	DRY	WET
CAM4	57.1	33.4	23.7	1.9	0.8	1.1	1.0	0.2	0.8	0.1	0.01	0.1
GEOS-Chem	56.5	40.2	16.3	-	-	-	0.8	0.6	0.2	--	-	-
IMPACT	134.1	67.9	66.2	2.7	1.0	1.8	0.7	0.3	0.4	0.1	0.01	0.1
TM4-ECPL	38.1	30.34	7.76	1.8	1.4	0.4	0.3	0.1	0.2	0.2	0.1	0.1
MEAN (\pm STD)	71.5 (\pm 42.69)	43.0 (\pm 17.13)	28.5 (\pm 26.97)	2.1 (\pm 0.51)	1.1 (\pm 0.35)	1.1 (\pm 0.71)	0.7 (\pm 0.28)	0.3 (\pm 0.20)	0.4 (\pm 0.28)	0.1 (\pm 0.05)	0.1 (\pm 0.06)	0.1 (\pm 0.01)

Table 5. Annual deposition fluxes (Tg-Fe yr⁻¹) to different ocean basins of total (TFe) and labile (LFe) Fe, as calculated by the contributing models and the derived ENSEMBLE model.

Ocean Basin	CAM4		GEOS-Chem*		IMPACT		TM4-ECPL		ENSEMBLE	
	TFe	LFe	TFe	LFe	TFe	LFe	TFe	LFe	TFe	LFe
North Atlantic	4.914	0.202	6.407	0.109	7.541	0.065	3.903	0.057	5.07	0.096
South Atlantic	0.681	0.043	2.067	0.017	4.414	0.014	0.455	0.012	1.677	0.02
North Pacific	1.084	0.057	1.653	0.041	0.972	0.021	3.075	0.054	1.496	0.038
South Pacific	0.111	0.007	1.114	0.01	2.337	0.014	0.49	0.012	0.867	0.009
Indian	3.658	0.076	3.818	0.049	6.911	0.09	1.33	0.027	3.644	0.055
Mediterranean	1.596	0.019	2.664	0.043	4.005	0.021	0.234	0.004	1.95	0.018
Baltic Sea	0.011	0.001	0.011	<0.001	0.017	<0.001	0.014	<0.001	0.011	<0.001
Black & Caspian Sea	0.342	0.006	0.398	0.005	0.966	0.009	0.15	0.001	0.439	0.005
Hudson Bay	0.003	<0.001	0.006	<0.001	0.003	<0.001	0.018	<0.001	0.007	<0.001
Arctic (>66N)	0.127	0.008	0.142	0.001	0.063	0.001	0.411	0.004	0.162	0.003
Southern (>60S)	0.010	0.001	0.030	<0.001	0.058	<0.001	0.051	<0.001	0.031	<0.001
Global Ocean	12.538	0.419	18.31	0.275	27.287	0.235	10.131	0.173	15.354	0.246

10 *In GEOS-Chem, only the Fe from mineral dust is considered

Figures

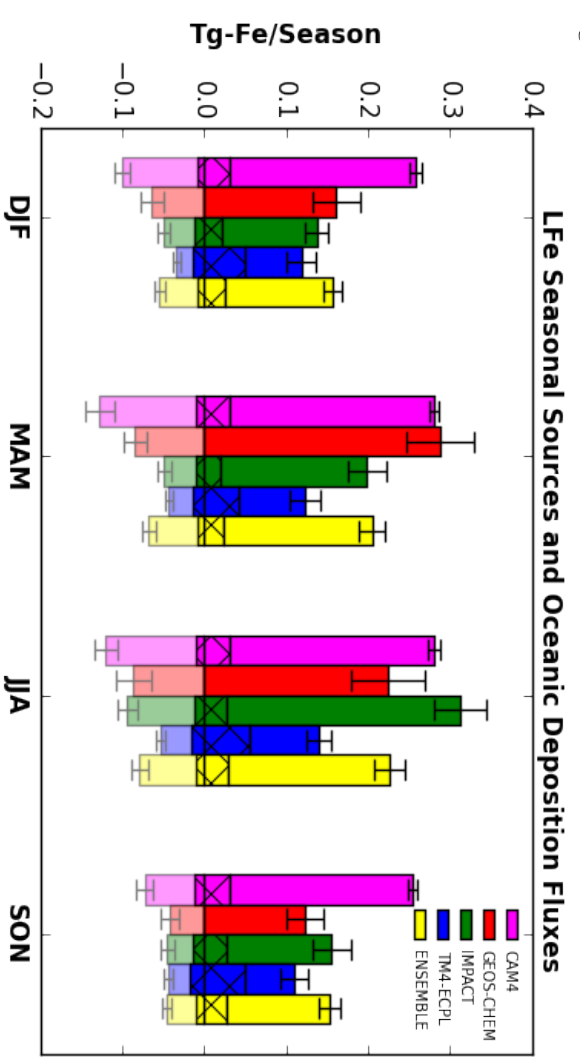
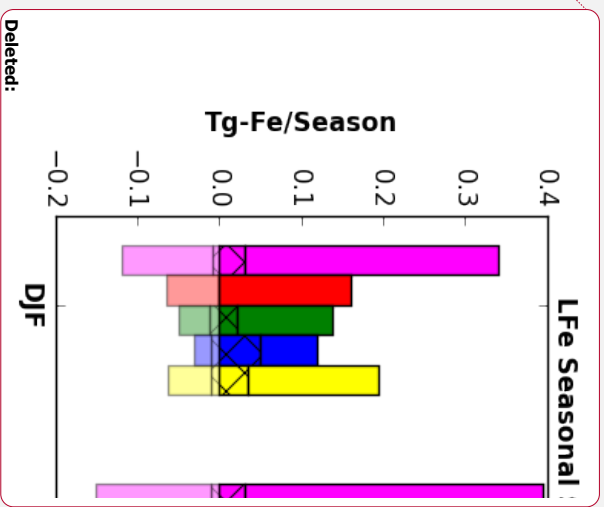
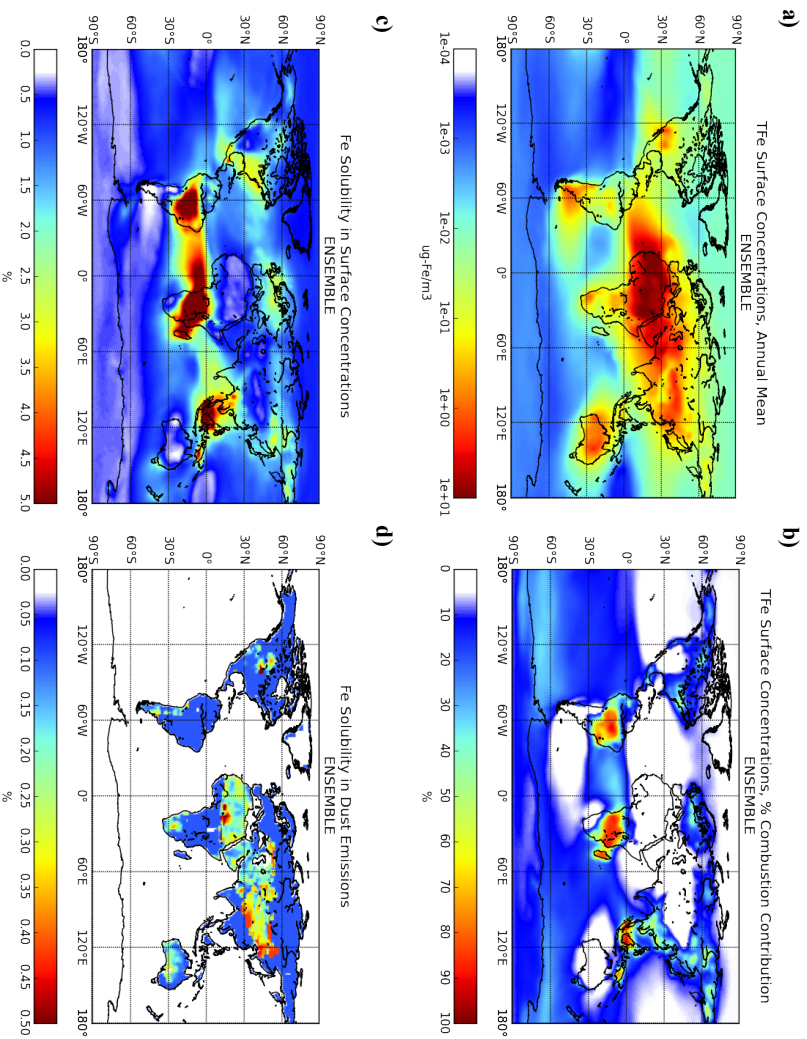


Figure 1: Seasonal LFe sources (positive bars) and oceanic deposition fluxes (negative bars/pale colors) in Tg-Fe Season⁻¹ for December, January and February (DJF); March, April and May (MAM); June, July and August (JJA) and September, October and November (SON), as calculated by each model (CAM4: magenta; GEOS-Chem: red; IMPACT: green and TM4-ECPL: blue), as well as, the ENSEMBLE model (yellow). The hatched areas correspond to the combustion aerosols and the error-bars correspond to the standard deviation of the respective season.

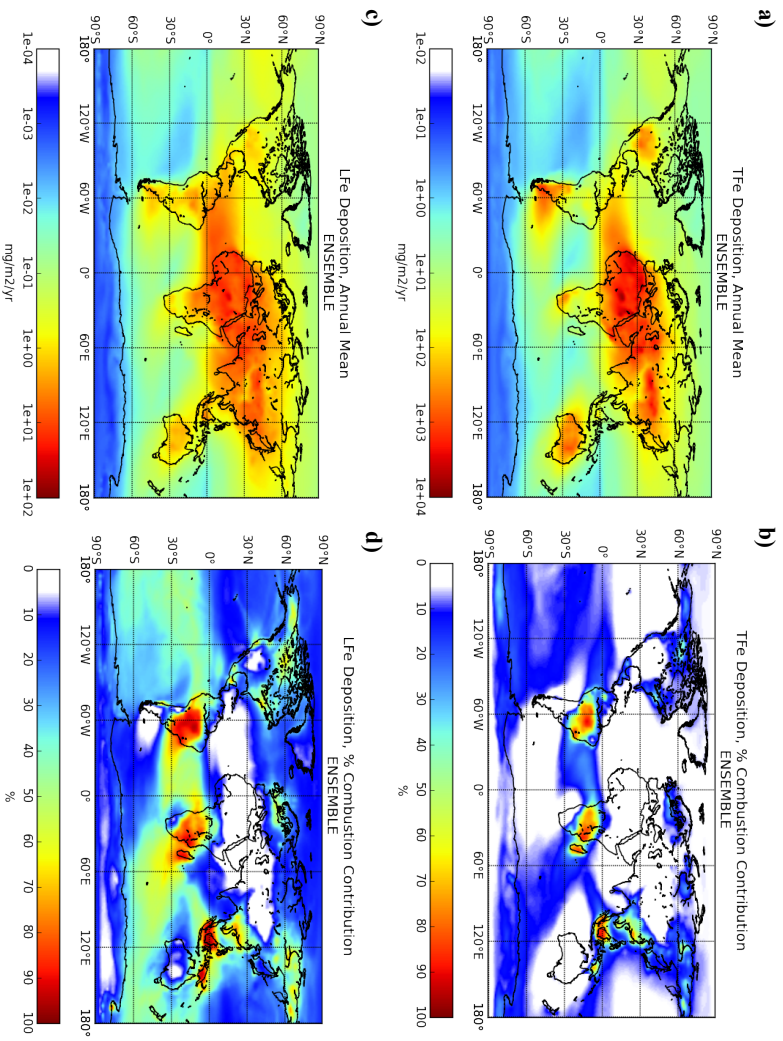
10



Deleted:



5 **Figure 2: ENSEMBLE model results for annual mean (a) surface TFe concentration ($\mu\text{g m}^{-3}$), (b) the percentage contribution (%) of Fe-containing dust aerosols, (c) the Fe solubility (%) in surface TFe concentration and (d) the initial solubility (%) in Fe-containing dust emissions.**



5 **Figure 3: ENSEMBLE model results for annual deposition fluxes ($\text{mg-Fe m}^{-2} \text{ yr}^{-1}$) for (a) TFe and for (c) LFe and their respective percentage contribution (%) of combustion aerosols (b, d).**

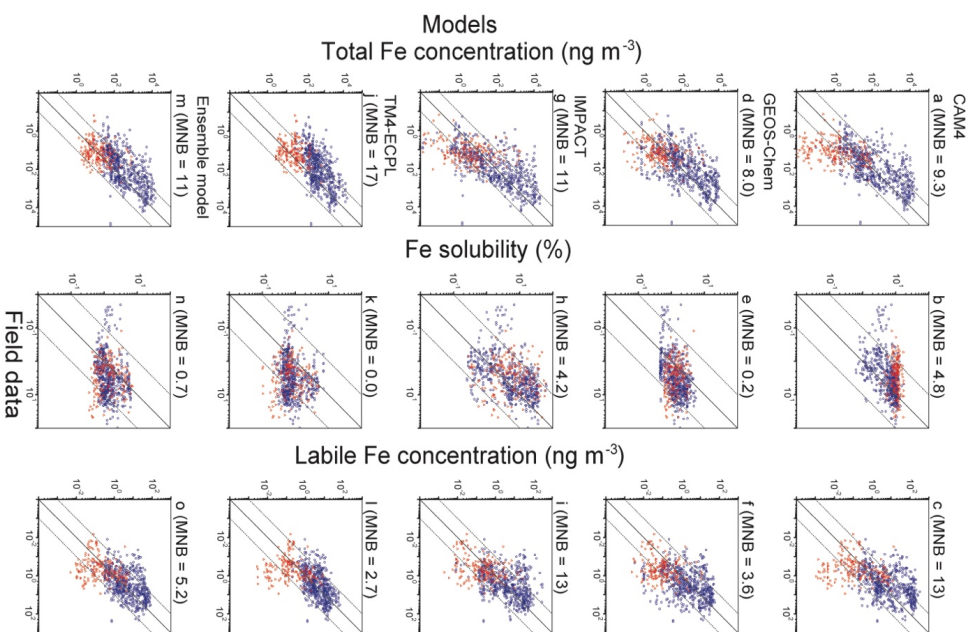


Figure 4: Comparison of simulated and observed TFe concentrations (ng m^{-3}), Fe solubility (%), and LFe concentrations (ng m^{-3}) in the Northern (blue circles) and Southern (red squares) Hemisphere. a, b, and c CAM4; d, e, and f GEOS-Chem; g, h, and i IMPACT; j, k, and l TM4-ECPL; m, n, and o for the ENSEMBLE model. The mean normalized biases (MNB) between the models and observations are presented in parentheses. The solid line represents a 1:1 correspondence and the dashed lines show the 10:1 and 1:10 relationships, respectively. The bias correction in the mineral dust size distribution is applied for the comparison with field data (Kok et al., 2017).

Deleted: loading

Deleted: loading

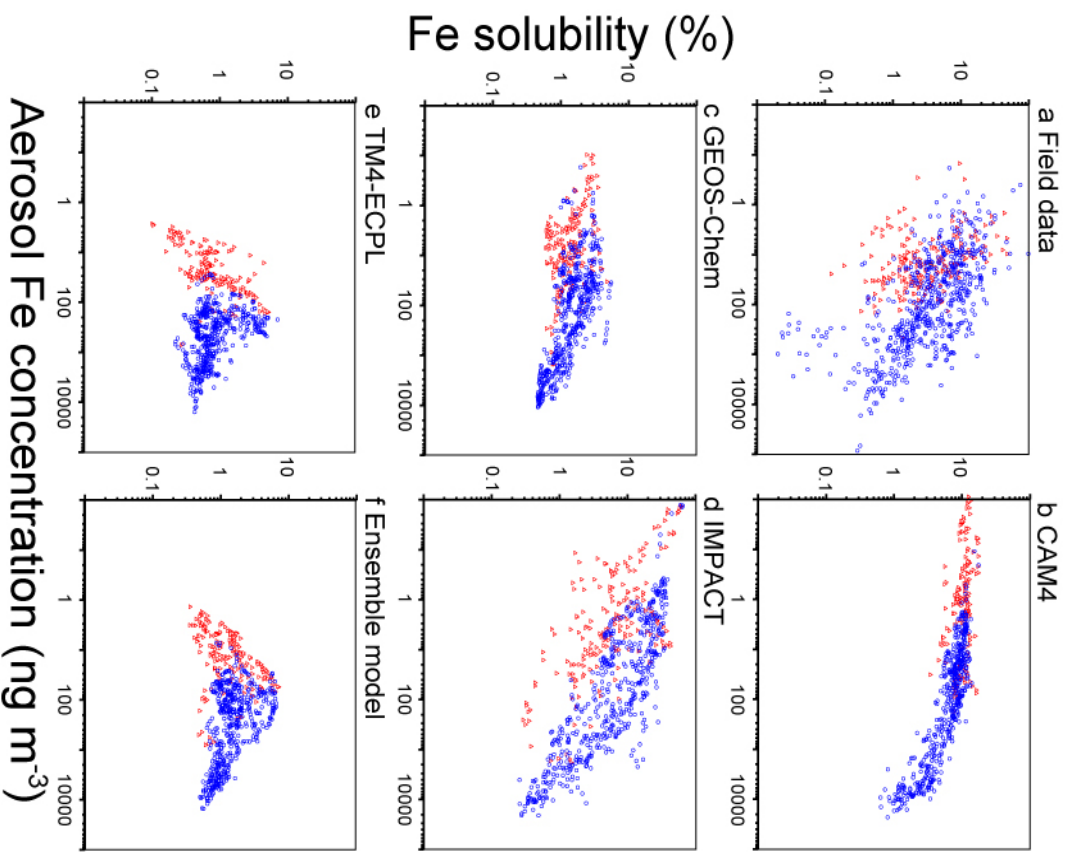


Figure 5: Fe solubility versus atmospheric **concentrations** of aerosol Fe (ng m^{-3}) in the Northern (blue circles) and Southern (red squares) Hemisphere for (a) the measurements, (b) CAM4, (c) GEOS-Chem (d) IMPACT, (e) TM4-ECPL, and (f) the ENSEMBLE model. The bias correction in the mineral dust size distribution is applied for the comparison with field data (Kok et al., 2017).

Deleted: loading

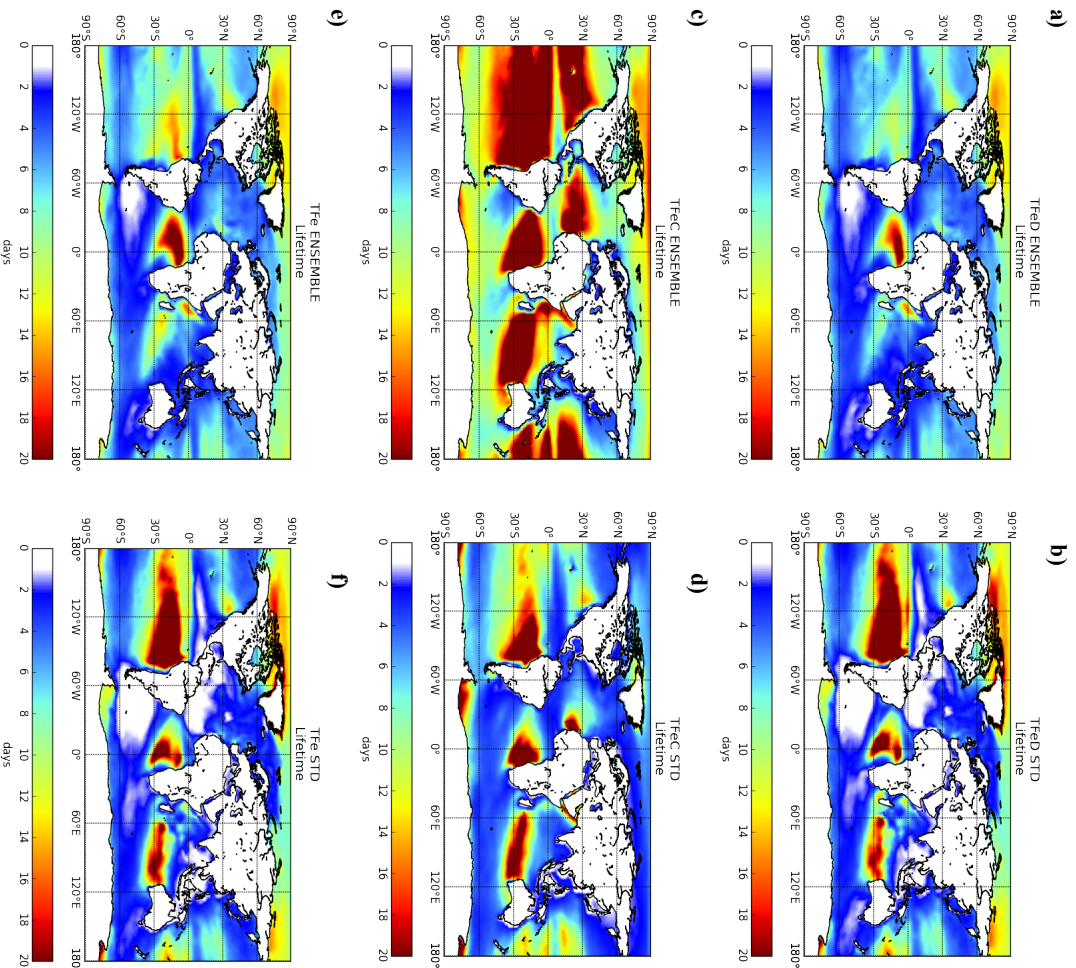


Figure 6: ENSEMBLE model results for TFe lifetime (days) over the ocean originated from a) mineral dust sources c) combustion source and e) total (mineral dust + combustion) and the respective standard deviation (b,d,f). Lifetimes are **atmospheric concentrations** divided by total sinks.

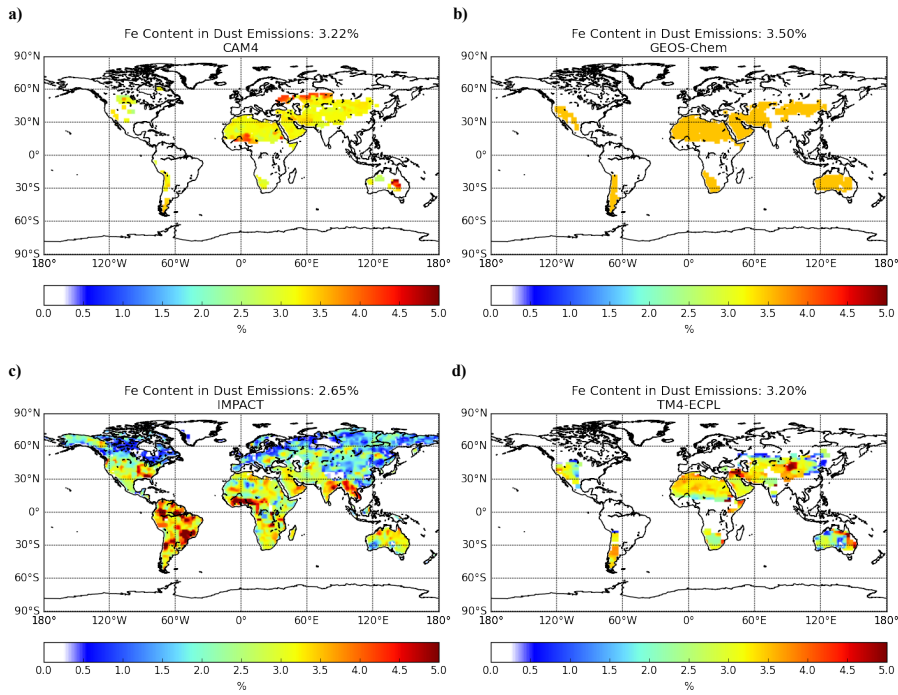


Figure S1: Fe content (%) in mineral dust emissions, taken into account (a) CAM4, (b) GEOS-Chem, (c) IMPACT and (d) TM4-ECPL. The global mean value for each model is also provided in the title.

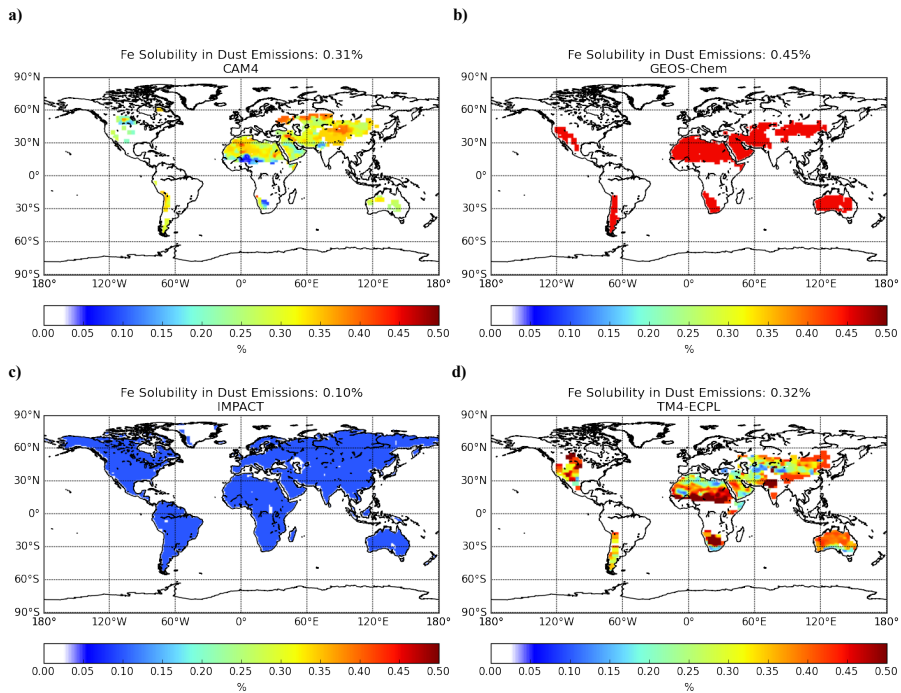


Figure S2: Initial solubility (%) in Fe dust emission, taken into account by (a) CAM4, (b) GEOS-Chem, (c) IMPACT and (d) TM4-ECPL. The global mean value for each model is also provided in the title.

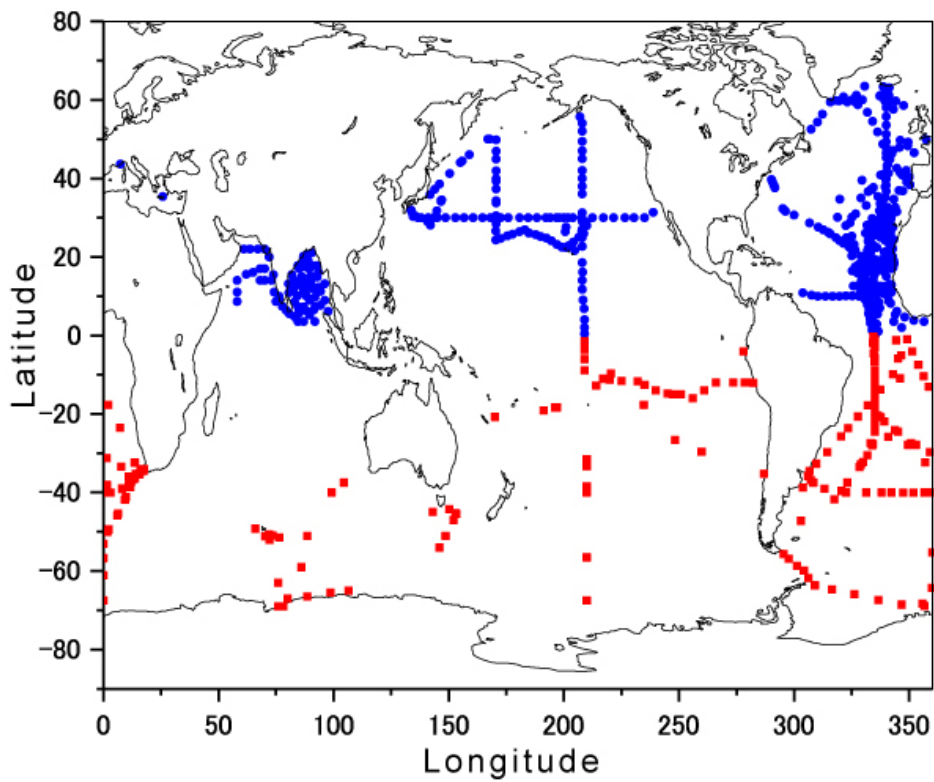
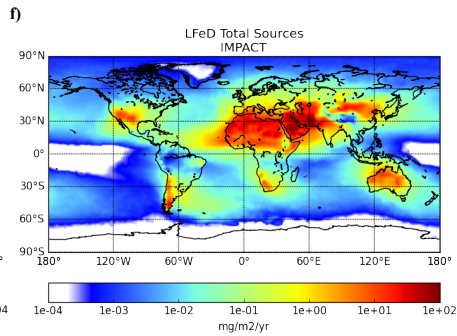
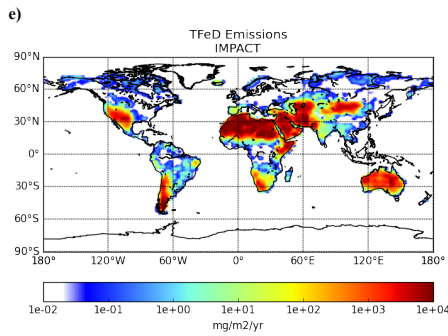
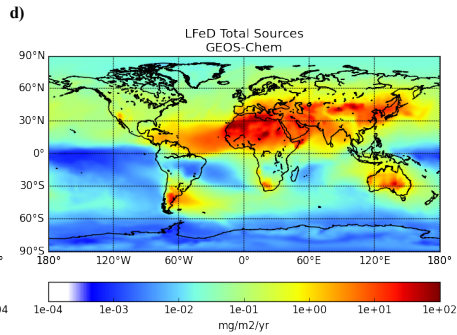
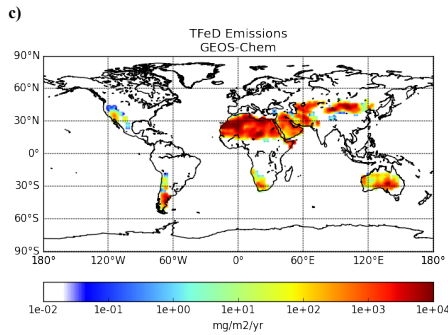
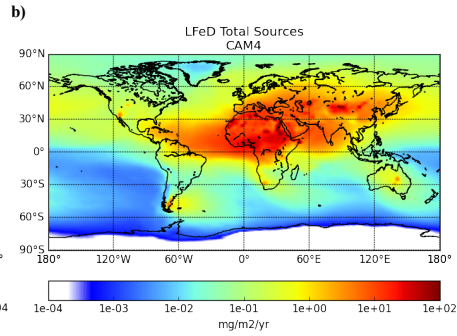
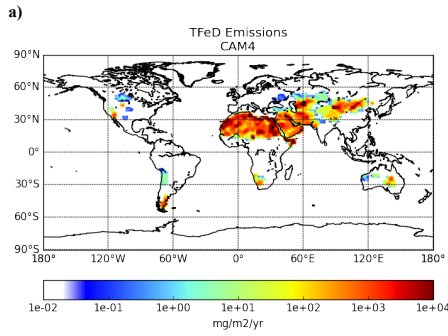


Figure S3: Site location map of observations in the Northern (blue circles) and Southern (red squares) Hemisphere: from Achterberg et al. (2018), Baker et al. (2006a, 2006b, 2007, 2013), Baker and Jickells (2017), Bowie et al. (2009), Buck et al. (2006, 2010, 2013, 2018), Chance et al. (2015), Gao et al. (2013), Guieu et al. (2005, pers. com. 2018), Jickells et al. (2016), Kumar et al. (2010), Longo et al. (2016), Powell et al. (2015), Shelley et al. (2015, pers. com. 2018), Sholkovitz et al. (2012), Srinivas et al. (2012), Srinivas and Sarin (2013), Wagener (2008) and Wagener et al. (2008).



g)

h)

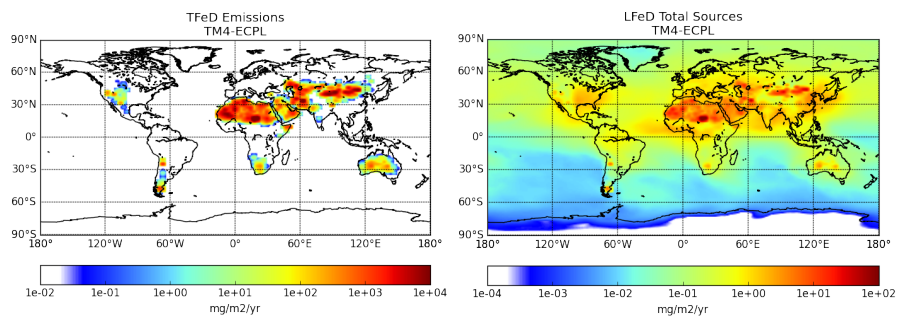


Figure S4: Annual mean TFe emissions and LFe sources (i.e., emissions and atmospheric processing together) (in mg-Fe m⁻² yr⁻¹) from mineral dust, taken into account in (a,b) CAM4, (c,d) GEOS-Chem, (e,f) IMPACT and (g,h) TM4-ECPL.

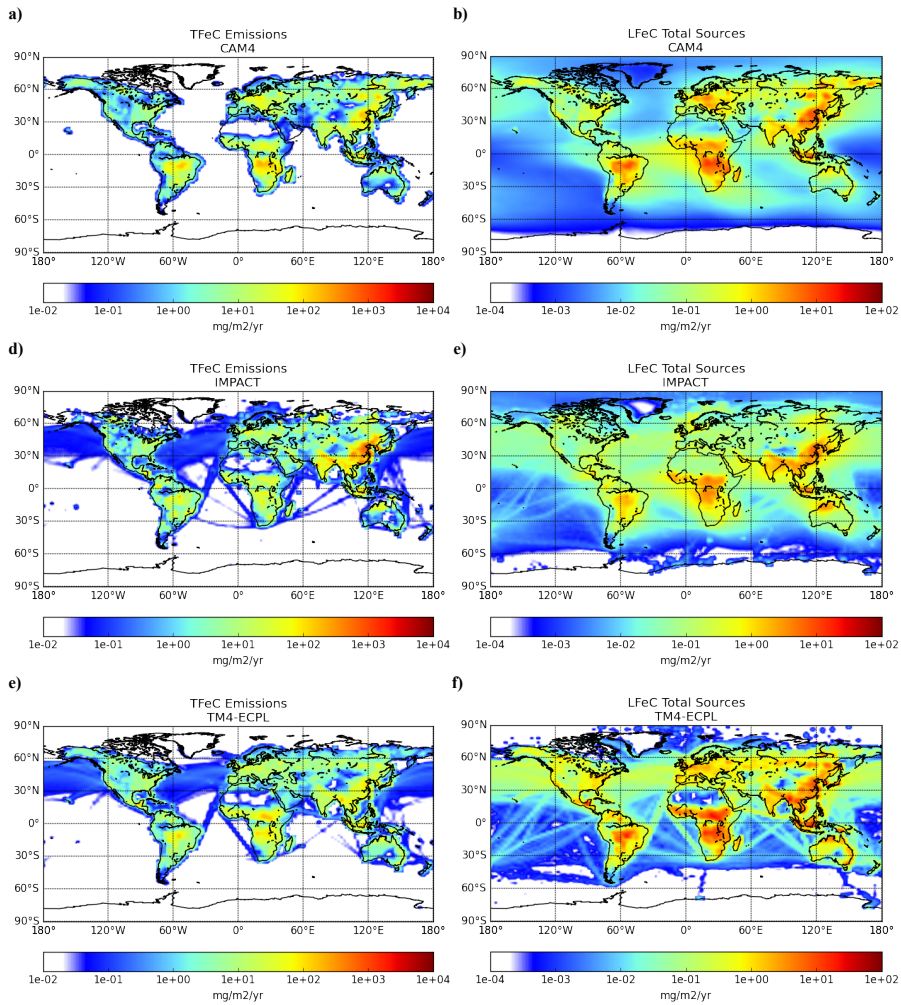
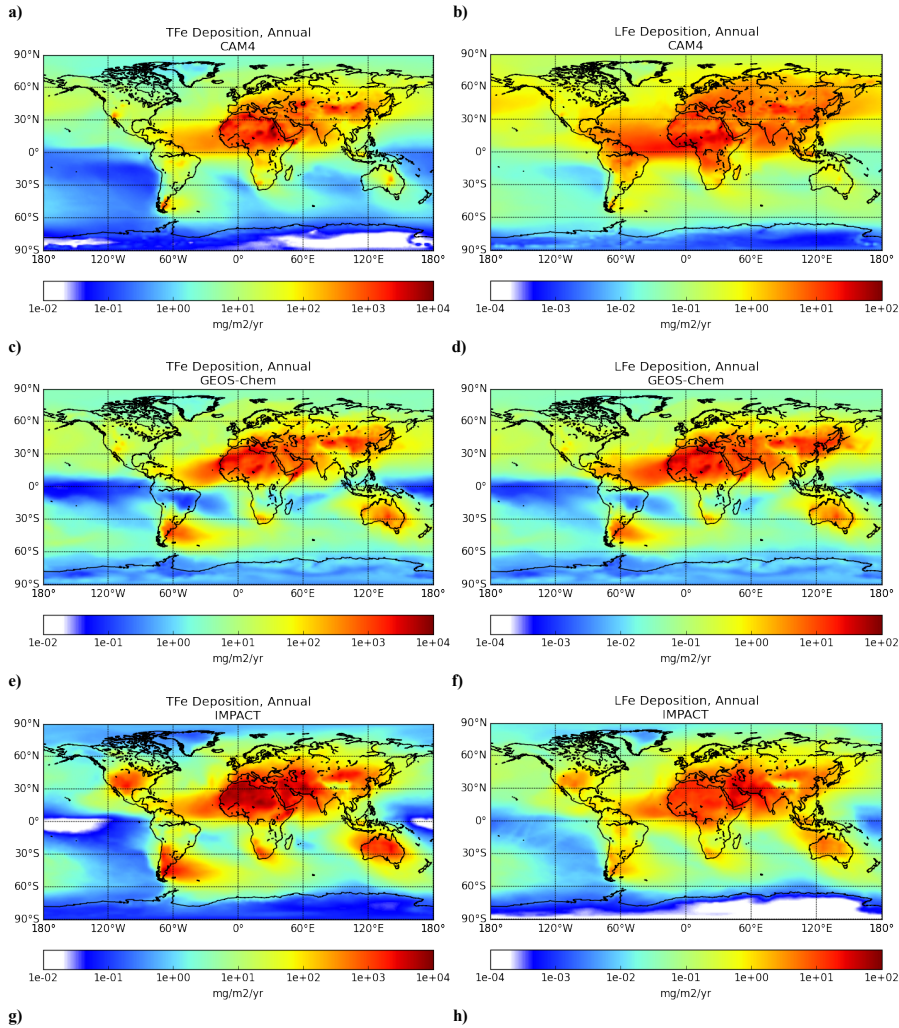


Figure S5: Annual mean TFe emissions and LFe sources (emissions + atmospheric processing) (in $\text{ng-Fe m}^{-2} \text{s}^{-1}$) from combustion processes, taken into account in (a,b) CAM4, (c,d,) IMPACT and (e,f) TM4-ECPL.



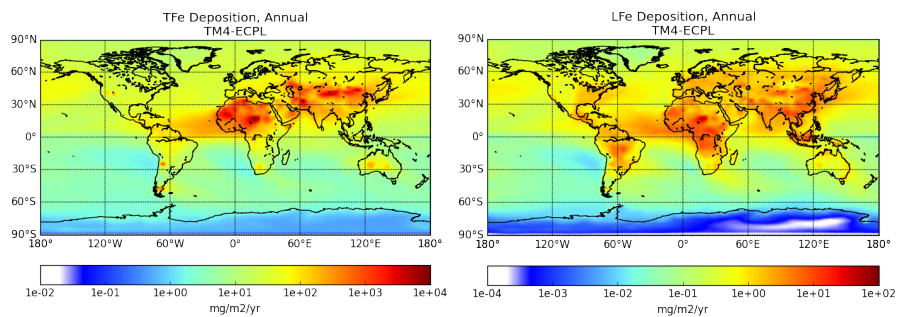


Figure S6: Annual TFe (left) and LFe (right) total (dry+wet) deposition fluxes (in $\text{mg-Fe m}^{-2} \text{ yr}^{-1}$) from mineral dust and combustion sources (in GEOS-Chem only the Fe from mineral dust is considered), as calculated by (a,b) CAM4, (c,d) GEOS-Chem, (e,f) IMPACT and (g,h) TM4-ECPL.

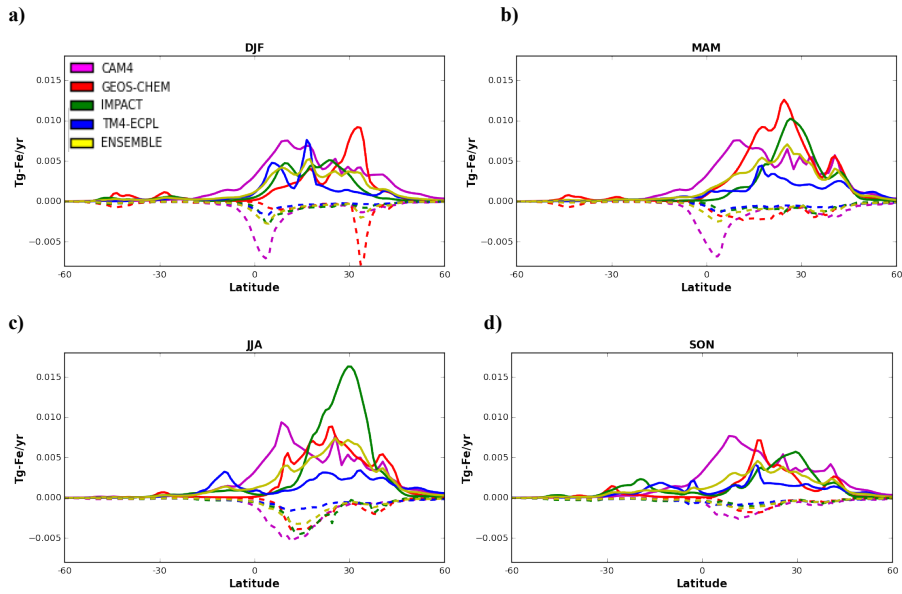


Figure S7: Latitudinal variation of LFe global sources (positive/continuous lines) and oceanic deposition fluxes (negative/dashed lines) in Tg-Fe yr^{-1} , for a) December, January and February (DJF); b) March, April and May (MAM); c) June, July and August (JJA) and d) September, October and November (SON), as calculated by each model (CAM4: magenta; GEOS-Chem: red; IMPACT: green and TM4-ECPL: blue) as well as the ENSEMBLE model (yellow).

Deleted: continues

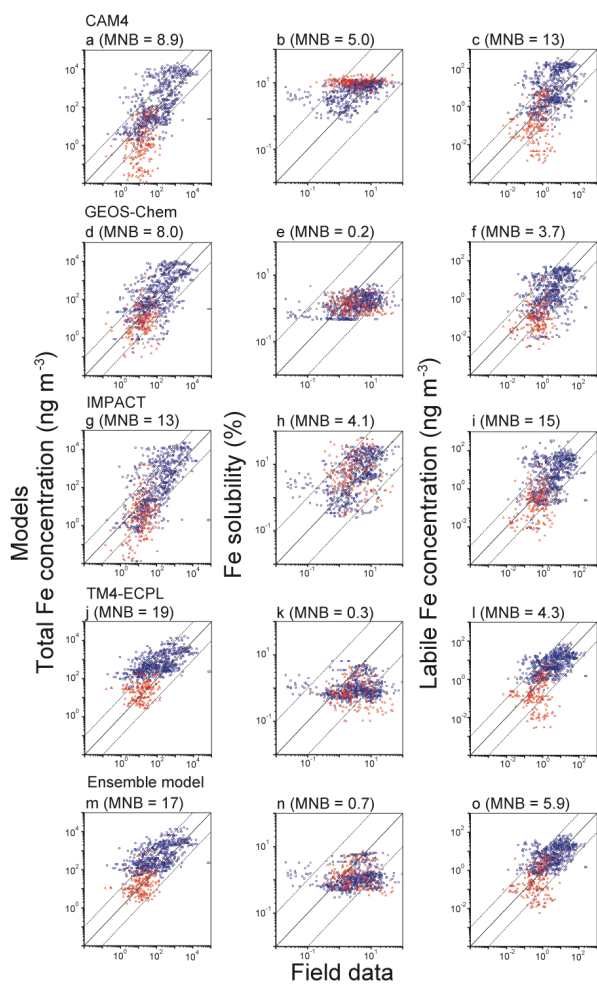


Figure S8: Same as Fig. 4, but the case before the bias correction procedure of Eq. 1. Shown are ensemble model comparisons against observed TFe loading (ng m^{-3}), Fe solubility (%), and LFe loading (ng m^{-3}) in the Northern (blue circles) and Southern (red squares) Hemisphere.

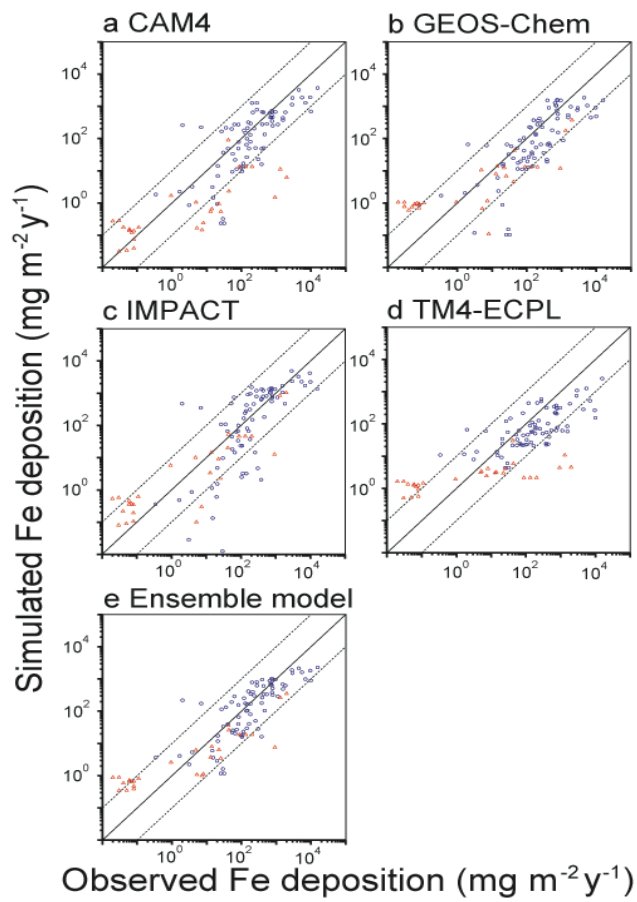


Figure S9: Atmospheric deposition (in mg-Fe m⁻² yr⁻¹) of TFe for (a) the compilation of measurements from Albani et al. (2014), (b) CAM4, (c) GEOS-Chem (d) IMPACT, (e) TM4-ECPL and (f) the ENSEMBLE model. The bias correction in the mineral dust size distribution is applied for the comparison with field data (Kok et al., 2017).

Table S1. Comparison of mineral dust Fe content and their initial Fe solubilities used by the models.

Model	Dust emission (Tg yr⁻¹)	Fe Content (wt %)	Fe solubility (wt %)
CAM4	1767	3.22% ^a	0.31% ^a
GEOS-Chem	1614	3.50%	0.45% ^b
IMPACT	5070	2.65% ^a	0.10% ^c
TM4-ECPL	1181	3.20% ^a	4.3% (kaolinite), 3% (feldspars) ^d

^a global average; ^b Shi et al. (2012); ^c Ito and Shi (2016); ^d Ito and Xu (2014)

Table S2. Comparison of combustion sources of Fe and their initial Fe solubilities used by the models.

Model	Source			Reference
	Biomass Burning	Coal Combustion	Oil Combustion	
CAM4	4% ^a	4%	4% ^c	Luo et al. (2008)
GEOS-Chem	-	-	-	-
IMPACT	0%	0%	58±22% ^d	Ito (2015)
TM4-ECPL	12%	8% ^b	81% ^d	Ito (2013) ^b , Luo et al. (2008) ^b

^a wildfires and biofuel; ^b Luo et al., 2008 (coal & biomass); ^c excluding shipping emissions; ^d only on shipping emissions

Table S3. Summary of total Fe loading (ng m⁻³), Fe solubility (%), and labile Fe loading (ng m⁻³) in aerosols. Dashes (-) correspond to data that are not available.

Latitude	Longitude	Month	Fe (ng m ⁻³)	Fe solubility	labile Fe (ng m ⁻³)	Reference
32.24	-64.87	7	238.61	2.230%	5.321	Longo et al. (2016)
32.24	-64.87	8	414.23	2.130%	8.823	Longo et al. (2016)
32.24	-64.87	8	265.87	3.140%	8.348	Longo et al. (2016)
32.24	-64.87	8	521.94	1.690%	8.821	Longo et al. (2016)
32.24	-64.87	9	128.19	2.790%	3.577	Longo et al. (2016)
32.24	-64.87	9	153.46	2.310%	3.545	Longo et al. (2016)
32.24	-64.87	10	23.66	8.940%	2.115	Longo et al. (2016)
32.24	-64.87	5	37.29	6.480%	2.416	Longo et al. (2016)
35.32	25.67	12	578.30	1.090%	6.303	Longo et al. (2016)
35.32	25.67	2	596.40	4.300%	25.645	Longo et al. (2016)
35.32	25.67	3	734.60	0.830%	6.097	Longo et al. (2016)
35.32	25.67	3	1213.70	1.190%	14.443	Longo et al. (2016)
35.32	25.67	4	2009.00	0.390%	7.835	Longo et al. (2016)
35.32	25.67	11	323.60	1.200%	3.883	Longo et al. (2016)
35.32	25.67	12	1798.40	1.480%	26.616	Longo et al. (2016)
13.1	80.3	12	908.91	7.650%	69.530	Kumar et al. (2010)
15.49	81.8	12	666.51	5.810%	38.694	Kumar et al. (2010)
13.15	83	12	429.88	6.830%	29.370	Kumar et al. (2010)
12.88	84.95	12	772.88	4.300%	33.205	Kumar et al. (2010)
17.09	85	12	1317.11	6.010%	79.149	Kumar et al. (2010)
20.19	86.96	1	1650.57	3.560%	58.725	Kumar et al. (2010)
19.49	86.78	1	1649.05	3.320%	54.717	Kumar et al. (2010)
17.43	87.48	1	492.99	2.540%	12.499	Kumar et al. (2010)
13.34	87.55	1	198.15	4.690%	9.294	Kumar et al. (2010)
12	87.63	1	127.02	9.450%	12.002	Kumar et al. (2010)

13.62	90.01	1	253.88	6.860%	17.410	Kumar et al. (2010)
17.91	90	1	1270.34	6.220%	78.964	Kumar et al. (2010)
21	90.56	1	897.73	7.250%	65.113	Kumar et al. (2010)
17.8	92.5	1	460.62	1.400%	6.443	Kumar et al. (2010)
14.83	92.88	1	213.00	5.180%	11.032	Kumar et al. (2010)
13.09	96.1	1	339.31	7.470%	25.341	Kumar et al. (2010)
8.88	96.1	1	382.02	14.580%	55.687	Kumar et al. (2010)
6.16	97.54	1	355.43	8.610%	30.590	Kumar et al. (2010)
7.62	94.37	1	329.19	5.660%	18.622	Kumar et al. (2010)
11.22	94.37	1	306.33	12.730%	39.010	Kumar et al. (2010)
12.27	93.37	1	259.56	9.300%	24.137	Kumar et al. (2010)
10.91	92.84	1	253.89	7.110%	18.053	Kumar et al. (2010)
7.29	92	1	230.24	10.390%	23.915	Kumar et al. (2010)
3.5	91.9	1	30.59	3.220%	0.986	Kumar et al. (2010)
5.28	89.5	1	95.11	23.890%	22.718	Kumar et al. (2010)
8.94	89.5	1	209.71	11.880%	24.916	Kumar et al. (2010)
7.24	87	1	195.86	3.510%	6.871	Kumar et al. (2010)
3.5	86.85	1	220.00	2.730%	6.008	Kumar et al. (2010)
3.5	84.52	1	169.35	6.870%	11.630	Kumar et al. (2010)
7.3	84.5	1	95.76	6.570%	6.290	Kumar et al. (2010)
8.47	83	1	112.78	3.050%	3.442	Kumar et al. (2010)
4.73	83	1	159.00	5.220%	8.300	Kumar et al. (2010)
6.4	79.31	1	91.41	3.450%	3.156	Kumar et al. (2010)
17.77	84.5	3	807.36	5.270%	42.518	Bikkina et al. (2012)
20.39	88.16	3	1116.06	4.310%	48.076	Bikkina et al. (2012)
19	88.94	3	798.68	6.210%	49.564	Bikkina et al. (2012)
18.32	86.08	3	937.64	4.280%	40.158	Bikkina et al. (2012)
16.99	89.46	3	1009.73	6.590%	66.554	Bikkina et al. (2012)

16.07	93.25	3	1220.98	4.150%	50.696	Bikkina et al. (2012)
15.02	89.81	3	945.62	6.970%	65.900	Bikkina et al. (2012)
15	86.16	3	705.76	3.240%	22.844	Bikkina et al. (2012)
14.01	82.83	3	545.69	3.800%	20.729	Bikkina et al. (2012)
13	86.31	3	599.64	3.780%	22.672	Bikkina et al. (2012)
11.51	86.78	3	420.89	11.970%	50.388	Bikkina et al. (2012)
11.51	82.33	3	420.11	7.240%	30.419	Bikkina et al. (2012)
10.82	80.56	4	272.46	6.850%	18.651	Bikkina et al. (2012)
10.01	84.26	4	242.23	5.640%	13.658	Bikkina et al. (2012)
9.99	88.19	4	244.64	13.590%	33.247	Bikkina et al. (2012)
12	90.41	4	668.25	2.950%	19.708	Bikkina et al. (2012)
9.67	91.81	4	183.96	5.180%	9.528	Bikkina et al. (2012)
6.5	91.36	4	149.62	11.120%	16.638	Bikkina et al. (2012)
6.31	87.94	4	308.70	13.090%	40.416	Bikkina et al. (2012)
5.67	84.8	4	294.48	3.470%	10.231	Bikkina et al. (2012)
5.51	80.74	4	526.84	2.560%	13.499	Bikkina et al. (2012)
7.37	77.81	4	547.05	2.350%	12.847	Bikkina et al. (2012)
8.76	76.48	4	595.43	2.580%	15.336	Bikkina et al. (2012)
9.97	76.23	4	1009.63	0.050%	0.544	Bikkina et al. (2012)
8.57	75	4	976.26	0.020%	0.198	Bikkina et al. (2012)
8.57	58	4	648.26	0.080%	0.541	Bikkina et al. (2012)
11	58	4	314.79	0.040%	0.126	Bikkina et al. (2012)
11	74.16	4	363.78	0.110%	0.385	Bikkina et al. (2012)
14	73	4	380.57	0.030%	0.110	Bikkina et al. (2012)
14	70	4	434.07	0.090%	0.390	Bikkina et al. (2012)
17	70	4	450.20	0.020%	0.109	Bikkina et al. (2012)
17	68	4	953.28	0.040%	0.403	Bikkina et al. (2012)
14	68	4	452.11	0.100%	0.466	Bikkina et al. (2012)

14	58	4	232.10	0.040%	0.096	Bikkina et al. (2012)
22	61	4	92.18	0.430%	0.395	Bikkina et al. (2012)
22	63.7	5	326.82	0.080%	0.257	Bikkina et al. (2012)
15.5	62	5	297.91	0.120%	0.364	Bikkina et al. (2012)
16	65	5	255.08	0.030%	0.075	Bikkina et al. (2012)
22	67	5	152.53	0.030%	0.045	Bikkina et al. (2012)
22	70	5	296.40	0.190%	0.558	Bikkina et al. (2012)
20	72	5	432.04	0.070%	0.295	Bikkina et al. (2012)
15.4	73.8	5	371.86	0.020%	0.087	Bikkina et al. (2012)
30.65	138.68	5	9.72	▼	▼	Buck et al. (2006)
29	140.75	5	210.50	3.350%	7.056	Buck et al. (2006)
28.02	142.02	5	64.46	8.950%	5.768	Buck et al. (2006)
29.98	143.49	5	669.70	5.580%	37.352	Buck et al. (2006)
31.69	144.78	5	490.56	7.390%	36.232	Buck et al. (2006)
34.13	146.67	5	766.64	6.000%	46.032	Buck et al. (2006)
34.46	147.02	5	414.62	7.140%	29.624	Buck et al. (2006)
34.44	146.69	5	212.97	5.420%	11.536	Buck et al. (2006)
35.88	141.85	5	42.11	1.860%	0.784	Buck et al. (2006)
37.17	143.83	5	49.84	4.160%	2.072	Buck et al. (2006)
38.49	145.9	5	30.52	5.500%	1.680	Buck et al. (2006)
41.23	150.33	5	81.76	7.530%	6.160	Buck et al. (2006)
44	155	5	9.69	52.600%	5.096	Buck et al. (2006)
44	155	5	▼	▼	5.529	Buck et al. (2006)
44	155	5	39.70	19.320%	7.672	Buck et al. (2006)
44.38	155.73	5	131.54	11.030%	14.504	Buck et al. (2006)
46.02	158.89	5	234.42	3.250%	7.616	Buck et al. (2006)
47.16	161.16	5	▼	▼	7.316	Buck et al. (2006)

Deleted: NaN
Deleted: NaN

Deleted: NaN
Deleted: NaN

Deleted: NaN
Deleted: NaN

48.85	164.59	5	₹	₹	8.935	Buck et al. (2006)
50	167	5	110.99	4.040%	4.480	Buck et al. (2006)
50	167.76	5	33.43	1.010%	0.336	Buck et al. (2006)
49.76	170.58	5	14.39	4.670%	0.672	Buck et al. (2006)
46.94	170.58	5	15.96	0.350%	0.056	Buck et al. (2006)
44.9	170.58	5	88.09	1.020%	0.896	Buck et al. (2006)
41.88	170.58	5	276.19	1.400%	3.864	Buck et al. (2006)
39.85	170.58	5	35.39	3.320%	1.176	Buck et al. (2006)
39.29	170.57	5	78.62	7.910%	6.216	Buck et al. (2006)
37.31	170.58	5	81.14	7.250%	5.880	Buck et al. (2006)
34.33	170.58	5	79.91	9.320%	7.448	Buck et al. (2006)
33.77	170.57	5	66.14	12.530%	8.288	Buck et al. (2006)
31.37	170.58	5	81.42	₹	₹	Buck et al. (2006)
30.5	170.58	5	63.06	5.770%	3.640	Buck et al. (2006)
28.47	170.5	5	56.67	13.240%	7.504	Buck et al. (2006)
26.59	170.42	5	20.22	31.300%	6.328	Buck et al. (2006)
24.25	170.33	5	35.56	9.610%	3.416	Buck et al. (2006)
24.25	170.33	5	29.29	19.310%	5.656	Buck et al. (2006)
24.27	170.42	5	27.10	13.640%	3.696	Buck et al. (2006)
24.7	172.47	5	41.78	8.580%	3.584	Buck et al. (2006)
25.33	175.45	5	30.13	8.360%	2.520	Buck et al. (2006)
25.78	177.62	5	22.62	7.430%	1.680	Buck et al. (2006)
26.44	-179.19	5	23.69	12.530%	2.968	Buck et al. (2006)
26.92	-176.89	5	26.82	8.140%	2.184	Buck et al. (2006)
26.06	-175.1	5	21.62	10.100%	2.184	Buck et al. (2006)
26	-175	5	28.50	19.840%	5.656	Buck et al. (2006)
25.6	-172.24	5	26.04	19.140%	4.984	Buck et al. (2006)
25.19	-170.12	5	53.70	11.370%	6.104	Buck et al. (2006)

Deleted: NaN
Deleted: NaN

Deleted: NaN
Deleted: NaN

24.76	-167.55	5	16.86	7.310%	1.232	Buck et al. (2006)
24.07	-165.54	5	15.79	10.280%	1.624	Buck et al. (2006)
23.13	-162.98	5	17.42	8.040%	1.400	Buck et al. (2006)
22.48	-160.88	5	35.56	5.670%	2.016	Buck et al. (2006)
22.74	-158.03	5	32.42	5.700%	1.848	Buck et al. (2006)
22.75	-158	5	43.34	6.460%	2.800	Buck et al. (2006)
22.87	-157.76	5	49.39	8.730%	4.312	Buck et al. (2006)
23.74	-155.96	5	65.30	11.920%	7.784	Buck et al. (2006)
24.95	-153.44	6	23.63	5.920%	1.400	Buck et al. (2006)
25.92	-151.39	6	24.98	4.260%	1.064	Buck et al. (2006)
27.99	-150.15	6	14.67	0.380%	0.056	Buck et al. (2006)
28.84	-150.45	6	26.10	6.440%	1.680	Buck et al. (2006)
26.49	-152.17	6	18.14	7.410%	1.344	Buck et al. (2006)
61.9	340	6	9.40	8.590%	0.807	Buck et al. (2010)
60.05	340	6	10.81	14.450%	1.561	Buck et al. (2010)
58.05	340	6	15.59	10.910%	1.700	Buck et al. (2010)
55.75	340	6	7.26	10.350%	0.751	Buck et al. (2010)
53.5	340	6	10.03	20.070%	2.014	Buck et al. (2010)
51.25	340	6	1.42	25.520%	0.362	Buck et al. (2010)
49.3	340	6	2.00	18.930%	0.378	Buck et al. (2010)
47.85	340	6	2.00	12.090%	0.242	Buck et al. (2010)
46.55	340	6	1.68	7.430%	0.125	Buck et al. (2010)
45.25	340	6	1.69	4.720%	0.080	Buck et al. (2010)
41.25	340	7	5.64	46.740%	2.638	Buck et al. (2010)
39.75	340	7	23.10	31.000%	7.160	Buck et al. (2010)
38.25	340	7	28.37	18.060%	5.124	Buck et al. (2010)
36.75	340	7	12.11	22.280%	2.699	Buck et al. (2010)
35.1	339.5	7	8.16	17.780%	1.451	Buck et al. (2010)

33.35	338.5	7	4.00		5.428	Buck et al. (2010)
31.8	337.65	7	4.55	21.890%	0.995	Buck et al. (2010)
30.9	337.8	7	8.00	14.900%	1.192	Buck et al. (2010)
30.8	338.6	7	42.53	11.160%	4.747	Buck et al. (2010)
30	337.5	7	3.34	10.140%	0.338	Buck et al. (2010)
28.3	335.65	7	2.41	27.490%	0.663	Buck et al. (2010)
26.75	334.8	7	3.55	18.660%	0.662	Buck et al. (2010)
25.2	333.95	7	6.06	14.770%	0.894	Buck et al. (2010)
23.7	333.1	7	9.14	13.170%	1.205	Buck et al. (2010)
22.05	332.15	7	106.33	7.170%	7.622	Buck et al. (2010)
20.3	331.3	7	1067.20	17.270%	184.256	Buck et al. (2010)
18.75	331	7	191.31	2.850%	5.460	Buck et al. (2010)
17.15	331	7	243.09	2.970%	7.215	Buck et al. (2010)
15.65	331	7	1865.22	7.340%	136.848	Buck et al. (2010)
14.2	331	7	4168.27	5.100%	212.708	Buck et al. (2010)
12.55	331	7	960.53	7.870%	75.629	Buck et al. (2010)
10.85	331.25	7	45.03	16.900%	7.610	Buck et al. (2010)
9.35	331.85	7	97.98	15.190%	14.888	Buck et al. (2010)
8.1	332.5	7	33.93	19.250%	6.533	Buck et al. (2010)
6.6	333.25	7	19.72	17.690%	3.489	Buck et al. (2010)
4.85	334.1	8	11.63	21.900%	2.547	Buck et al. (2010)
3.15	334.75	8	24.24	13.300%	3.224	Buck et al. (2010)
1.65	335	8	18.15	21.350%	3.874	Buck et al. (2010)
0.3	335	8	16.66	11.870%	1.978	Buck et al. (2010)
-1.2	335	8	9.05	13.780%	1.248	Buck et al. (2010)
-2.5	335	8	6.88	5.440%	0.374	Buck et al. (2010)
-3	335	8	4.55	8.800%	0.400	Buck et al. (2010)
31.87	133.59	6	85.07	3.510%	2.988	Buck et al. (2013)

31.32	133.97	6	44.45	3.240%	1.439	Buck et al. (2013)
30.24	134.48	6	317.60	8.950%	28.421	Buck et al. (2013)
30.38	135.53	6	23.20	3.300%	0.766	Buck et al. (2013)
30	136.61	6	159.96	15.980%	25.568	Buck et al. (2013)
30	137.76	6	79.69	21.880%	17.436	Buck et al. (2013)
30	137.92	6	249.59	9.060%	22.615	Buck et al. (2013)
30	140.98	6	9.83	15.110%	1.485	Buck et al. (2013)
30	142.33	6	12.64	₹	₹	Buck et al. (2013)
30	143.45	6	58.64	7.760%	4.549	Buck et al. (2013)
30.01	144.91	6	54.51	12.610%	6.874	Buck et al. (2013)
30	146.67	6	16.60	₹	₹	Buck et al. (2013)
30	148.61	6	24.17	11.490%	2.776	Buck et al. (2013)
30	150.9	7	31.53	₹	₹	Buck et al. (2013)
30	152.84	7	46.84	10.110%	4.733	Buck et al. (2013)
30	154.6	7	34.65	₹	₹	Buck et al. (2013)
30	156.7	7	29.91	11.570%	3.460	Buck et al. (2013)
30	158.35	7	3.88	₹	₹	Buck et al. (2013)
30	160.6	7	5.03	10.080%	0.507	Buck et al. (2013)
30	162.86	7	16.07	₹	₹	Buck et al. (2013)
30	164.73	7	15.24	6.990%	1.065	Buck et al. (2013)
30	166.68	7	63.30	₹	₹	Buck et al. (2013)
30	168.17	7	33.51	8.320%	2.790	Buck et al. (2013)
30	170.47	7	242.47	₹	₹	Buck et al. (2013)
30	172.47	7	244.70	6.610%	16.171	Buck et al. (2013)
30	174.63	7	31.89	₹	₹	Buck et al. (2013)
30	175.86	7	7.86	10.480%	0.824	Buck et al. (2013)
30	178.45	7	8.82	₹	₹	Buck et al. (2013)
30	180.78	7	9.12	11.200%	1.022	Buck et al. (2013)

Deleted: NaN

30	181.4	7	15.46	₹	₹	Buck et al. (2013)
30	184.48	7	7.44	6.820%	0.508	Buck et al. (2013)
30	186.36	7	10.78	₹	₹	Buck et al. (2013)
30	188.33	7	3.31	16.260%	0.538	Buck et al. (2013)
30	190.29	7	6.53	₹	₹	Buck et al. (2013)
30	192.25	7	20.21	3.150%	0.636	Buck et al. (2013)
30	194.06	7	5.70	6.820%	0.388	Buck et al. (2013)
30	194.32	7	5.35	₹	₹	Buck et al. (2013)
27.89	195.66	7	10.43	₹	₹	Buck et al. (2013)
30	196.16	8	5.55	₹	₹	Buck et al. (2013)
30	196.88	7	3.84	9.660%	0.371	Buck et al. (2013)
30	197.99	8	9.40	5.590%	0.526	Buck et al. (2013)
23.97	199.43	7	₹	₹	0.834	Buck et al. (2013)
30	199.88	8	12.59	5.290%	0.666	Buck et al. (2013)
26.45	200.51	8	14.58	3.160%	0.460	Buck et al. (2013)
22.33	200.76	8	9.73	5.500%	0.535	Buck et al. (2013)
27.54	200.92	8	6.17	11.470%	0.708	Buck et al. (2013)
30	201.76	8	15.09	17.420%	2.630	Buck et al. (2013)
30	203.81	8	16.43	10.060%	1.652	Buck et al. (2013)
30	205.86	8	12.87	₹	₹	Buck et al. (2013)
30	207.84	8	10.00	8.470%	0.846	Buck et al. (2013)
30	209.73	8	6.66	₹	₹	Buck et al. (2013)
30	212.44	8	8.12	8.610%	0.699	Buck et al. (2013)
30	214.66	8	6.36	₹	₹	Buck et al. (2013)
30	217.11	8	6.42	15.150%	0.973	Buck et al. (2013)
30	219.36	8	6.37	₹	₹	Buck et al. (2013)
30	221.61	8	10.29	5.590%	0.575	Buck et al. (2013)
30	224.36	8	6.94	₹	₹	Buck et al. (2013)

Deleted: NaN

27	208	3	34.85	11.190%	3.901	Buck et al. (2013)
29	208	3	39.27	13.550%	5.322	Buck et al. (2013)
31.2	208	3	131.21	14.590%	19.141	Buck et al. (2013)
36	208	3	91.23	10.770%	9.822	Buck et al. (2013)
38	208	3	79.75	9.200%	7.340	Buck et al. (2013)
40	208	3	98.09	7.170%	7.034	Buck et al. (2013)
42	208	3	33.57	13.760%	4.619	Buck et al. (2013)
45	208	3	23.64	8.690%	2.055	Buck et al. (2013)
47	208	3	48.36	10.260%	4.962	Buck et al. (2013)
49.4	208	3	75.29	9.980%	7.511	Buck et al. (2013)
52	208	3	48.60	10.140%	4.929	Buck et al. (2013)
54	208	3	9.08	9.820%	0.892	Buck et al. (2013)
55.7	207.05	3	17.93	8.360%	1.499	Buck et al. (2013)
-4.07	278.01	10	32.81	2.420%	0.793	Buck et al. (2018)
-12.01	280.8	10	61.56	2.000%	1.229	Buck et al. (2018)
-12.05	282.34	11	129.74	1.270%	1.653	Buck et al. (2018)
-11.99	278.5	11	34.65	1.930%	0.670	Buck et al. (2018)
-11.99	273.5	11	4.62	4.750%	0.149	Buck et al. (2018)
-12	266	11	2.60	1.550%	0.040	Buck et al. (2018)
-14	261	11	2.80	0.940%	0.026	Buck et al. (2018)
-16	256	11	3.20	0.690%	0.022	Buck et al. (2018)
-15	250.81	11	2.93	0.560%	0.016	Buck et al. (2018)
-14.99	247.25	11	1.22	1.470%	0.018	Buck et al. (2018)
-14.77	245	11	2.62	0.830%	0.022	Buck et al. (2018)
-14	240	11	3.76	0.490%	0.019	Buck et al. (2018)
-12.54	235	12	6.36	0.350%	0.022	Buck et al. (2018)
-11.67	232	12	3.11	1.270%	0.039	Buck et al. (2018)
-11.6	225	12	1.41	1.220%	0.017	Buck et al. (2018)

-11.31	220	12	4.86	1.680%	0.058	Buck et al. (2018)
-11.03	217.05	12	4.27	0.690%	0.030	Buck et al. (2018)
38.32	-9.66	10	147.43	1.910%	2.814	Shelley et al. (2015); in review 2018
38.33	-9.66	10	109.94	3.660%	4.018	Shelley et al. (2015); in review 2018
36.77	-12.83	10	61.88	4.820%	2.984	Shelley et al. (2015); in review 2018
34.65	-16.79	10	6.89	20.690%	1.426	Shelley et al. (2015); in review 2018
32.7	-19.58	10	19.13	1.700%	0.325	Shelley et al. (2015); in review 2018
29.32	-21.94	10	4.05	2.090%	0.085	Shelley et al. (2015); in review 2018
25.77	-22.01	10	7.79	2.910%	0.227	Shelley et al. (2015); in review 2018
20.68	-20.13	10	2155.00	0.510%	11.023	Shelley et al. (2015); in review 2018
17.36	-18.66	10	2100.49	0.450%	9.442	Shelley et al. (2015); in review 2018
17.36	-18.66	10	1920.00	0.270%	5.132	Shelley et al. (2015); in review 2018
17.35	-20.42	10	3770.00	0.270%	10.077	Shelley et al. (2015); in review 2018
17.36	-20.85	10	4910.00	0.200%	9.822	Shelley et al. (2015); in review 2018
17.35	-21.85	10	1800.00	0.570%	10.308	Shelley et al. (2015); in review 2018
17.35	-21.85	11	1030.00	0.140%	1.479	Shelley et al. (2015); in review 2018
17.37	-24.53	11	267.57	0.420%	1.134	Shelley et al. (2015); in review 2018
39.71	-69.84	11	25.72	3.200%	0.824	Shelley et al. (2015); in review 2018
39.53	-69.67	11	80.25	2.730%	2.189	Shelley et al. (2015); in review 2018
39	-69.37	11	36.64	0.840%	0.306	Shelley et al. (2015); in review 2018
38.35	-68.87	11	38.28	2.270%	0.869	Shelley et al. (2015); in review 2018
37.97	-68.63	11	17.51	5.640%	0.988	Shelley et al. (2015); in review 2018
37.62	-68.38	11	8.17	3.090%	0.253	Shelley et al. (2015); in review 2018
31.89	-64.31	11	3.15	8.780%	0.277	Shelley et al. (2015); in review 2018
31.65	-63.8	11	1.71	3.530%	0.060	Shelley et al. (2015); in review 2018
30.62	-60.1	11	3.23	5.090%	0.164	Shelley et al. (2015); in review 2018
28.64	-53.23	11	0.95	17.620%	0.167	Shelley et al. (2015); in review 2018
27.57	-49.59	11	0.90	4.390%	0.040	Shelley et al. (2015); in review 2018

26.93	-47.47	11	1.87	16.510%	0.309	Shelley et al. (2015); in review 2018
26.21	-45.07	11	1.59	11.360%	0.181	Shelley et al. (2015); in review 2018
25.86	-44.22	11	14.25	2.490%	0.355	Shelley et al. (2015); in review 2018
24.85	-41.88	11	13.64	2.370%	0.323	Shelley et al. (2015); in review 2018
24.15	-40.22	12	3.70	4.830%	0.179	Shelley et al. (2015); in review 2018
23.43	-38.48	12	1.34	7.590%	0.101	Shelley et al. (2015); in review 2018
22.53	-36.3	12	494.10	0.380%	1.857	Shelley et al. (2015); in review 2018
22.37	-35.87	12	2245.00	0.310%	7.000	Shelley et al. (2015); in review 2018
21.63	-34.12	12	623.48	0.410%	2.571	Shelley et al. (2015); in review 2018
20.16	-31	12	1580.00	0.310%	4.944	Shelley et al. (2015); in review 2018
19.43	-29.38	12	2529.85	0.420%	10.608	Shelley et al. (2015); in review 2018
18.78	-27.76	12	3655.00	0.220%	8.211	Shelley et al. (2015); in review 2018
17.58	-24.92	12	5645.14	0.430%	24.370	Shelley et al. (2015); in review 2018
40.33	-10.04	5	5.08	2.870%	0.146	Shelley et al. (2015); in review 2018
40.86	-13.05	5	12.68	3.390%	0.430	Shelley et al. (2015); in review 2018
41.38	-13.89	5	18.66	4.290%	0.801	Shelley et al. (2015); in review 2018
41.38	-13.89	5	14.26	4.650%	0.663	Shelley et al. (2015); in review 2018
42.58	-15.46	5	14.28	3.380%	0.483	Shelley et al. (2015); in review 2018
46.17	-19.38	5	6.27	5.160%	0.323	Shelley et al. (2015); in review 2018
48.78	-21.43	6	6.01	3.490%	0.210	Shelley et al. (2015); in review 2018
51.85	-23.84	6	6.37	6.680%	0.425	Shelley et al. (2015); in review 2018
54.47	-25.89	6	7.39	19.570%	1.447	Shelley et al. (2015); in review 2018
56.86	-28.22	6	8.95	11.670%	1.044	Shelley et al. (2015); in review 2018
58.7	-32.25	6	4.99	7.730%	0.385	Shelley et al. (2015); in review 2018
59.41	-36.87	6	0.67	5.810%	0.039	Shelley et al. (2015); in review 2018
59.71	-40.48	6	0.68	21.320%	0.145	Shelley et al. (2015); in review 2018
59.8	-42	6	0.57	12.500%	0.071	Shelley et al. (2015); in review 2018
59.39	-44.31	6	1.40	9.420%	0.131	Shelley et al. (2015); in review 2018

56.32	-47.79	6	0.19	6.740%	0.012	Shelley et al. (2015); in review 2018
54.32	-49.78	6	9.71	3.310%	0.321	Shelley et al. (2015); in review 2018
52.46	-52.62	6	3.14	1.900%	0.060	Shelley et al. (2015); in review 2018
-45.01	142.98	1	10.80	0.470%	0.051	Bowie et al. (2009)
-54	145.98	2	6.50	1.350%	0.088	Bowie et al. (2009)
-50.99	148.57	2	16.80	0.190%	0.032	Bowie et al. (2009)
-47	152.07	2	6.70	1.480%	0.099	Bowie et al. (2009)
-45.5	153.2	2	5.00	1.620%	0.081	Bowie et al. (2009)
-45.27	153.01	2	6.00	2.520%	0.151	Bowie et al. (2009)
-44.24	150.2	2	5.10	17.650%	0.900	Bowie et al. (2009)
-37.5	104.5	11	8.10	40.740%	3.300	Gao et al. (2013)
-59	86	11	10.00	27.000%	2.700	Gao et al. (2013)
-69	76	12	14.00	23.570%	3.300	Gao et al. (2013)
-66.5	88.5	1	20.00	6.500%	1.300	Gao et al. (2013)
-65	106.5	1	56.00	1.140%	0.640	Gao et al. (2013)
-65.5	98.5	1	31.00	0.740%	0.230	Gao et al. (2013)
-67	80	1	14.00	3.430%	0.480	Gao et al. (2013)
-69	78	2	20.00	1.650%	0.330	Gao et al. (2013)
-69	77	2	30.00	1.470%	0.440	Gao et al. (2013)
-69	77	2	22.00	5.450%	1.200	Gao et al. (2013)
-69	76	2	29.00	9.310%	2.700	Gao et al. (2013)
-63	76	2	11.00	1.270%	0.140	Gao et al. (2013)
-51	88.5	3	38.00	0.760%	0.290	Gao et al. (2013)
-40	99	3	15.00	0.870%	0.130	Gao et al. (2013)
17	-17.5	3	3031.60	0.680%	20.474	Sholkovitz et al. (2012)
17.25	-17	3	1184.56	1.020%	12.095	Sholkovitz et al. (2012)
18.25	-16.85	3	867.12	0.990%	8.566	Sholkovitz et al. (2012)
19	-17.3	3	516.98	1.820%	9.405	Sholkovitz et al. (2012)

20.55	-17.95	3	39.60	13.380%	5.299	Sholkovitz et al. (2012)
19.55	-17.15	3	273.92	2.410%	6.607	Sholkovitz et al. (2012)
19.9	-17.75	3	28.56	15.580%	4.450	Sholkovitz et al. (2012)
17.8	-17.1	3	194.51	2.500%	4.853	Sholkovitz et al. (2012)
17.3	-20.55	4	198.17	2.940%	5.823	Sholkovitz et al. (2012)
18.75	-17	4	192.08	2.210%	4.243	Sholkovitz et al. (2012)
18.5	-18	4	173.97	2.280%	3.962	Sholkovitz et al. (2012)
34.82	-21.69	6	506.96	1.590%	8.074	Baker et al. (2013)
10.59	-31.3	6	473.93	0.920%	4.354	Baker et al. (2013)
3.17	-26.88	5	191.09	2.260%	4.316	Baker et al. (2013)
23.15	-33.89	6	240.38	1.820%	4.380	Baker et al. (2013)
28.03	-28.36	6	93.94	3.340%	3.133	Baker et al. (2013)
-30.58	-28.21	5	147.35	0.550%	0.809	Baker et al. (2013)
-6.37	-25	5	130.03	1.250%	1.624	Baker et al. (2013)
-27.67	-25.79	5	28.14	6.960%	1.959	Baker et al. (2013)
16.38	-34.81	6	46.54	3.270%	1.522	Baker et al. (2013)
-32.83	-31.03	5	34.15	1.350%	0.462	Baker et al. (2013)
-11.68	-24.89	5	46.51	2.360%	1.096	Baker et al. (2013)
43.34	-19.32	6	29.40	1.990%	0.586	Baker et al. (2013)
-15.58	-25	5	48.31	3.130%	1.514	Baker et al. (2013)
-23.67	-25.01	5	43.11	2.480%	1.069	Baker et al. (2013)
-19.52	-25	5	69.17	1.240%	0.861	Baker et al. (2013)
18.68	-18.45	9	5418.87	0.520%	28.267	Baker et al. (2013)
20.52	-19.17	9	4816.81	0.500%	23.959	Baker et al. (2013)
24.31	-20.72	9	644.80	1.670%	10.773	Baker et al. (2013)
15.05	-19.95	9	858.47	0.580%	5.017	Baker et al. (2013)
10.76	-21.56	9	817.28	0.850%	6.937	Baker et al. (2013)
41.24	-20.59	9	427.94	5.290%	22.618	Baker et al. (2013)

6.93	-22.79	9	417.71	1.350%	5.626	Baker et al. (2013)
27.22	-20.82	9	246.86	1.350%	3.335	Baker et al. (2013)
44.88	-18.33	9	56.73	8.800%	4.993	Baker et al. (2013)
-1.48	-24.86	9	114.68	2.240%	2.565	Baker et al. (2013)
-5.83	-25	9	22.64	9.270%	2.099	Baker et al. (2013)
2.87	-24.1	9	11.24	8.080%	0.909	Baker et al. (2013)
-22.08	-25	10	22.44	6.710%	1.506	Baker et al. (2013)
31.4	-21.49	9	23.97	6.160%	1.476	Baker et al. (2013)
35.34	-23.59	9	16.62	2.470%	0.410	Baker et al. (2013)
-27.39	-26.72	10	2.03	11.960%	0.242	Baker et al. (2013)
-33.49	-31.7	10	2.15	7.430%	0.160	Baker et al. (2013)
-39.55	-39.57	10	2.26	9.950%	0.225	Baker et al. (2013)
-18.2	-25	10	4.24	16.090%	0.682	Baker et al. (2013)
-9.88	-25	9	4.27	34.020%	1.454	Baker et al. (2013)
-14.04	-24.99	10	4.30	13.890%	0.597	Baker et al. (2013)
6.7	-27.56	5	452.29	1.610%	7.302	Baker et al. (2013)
10.31	-28.95	5	309.12	1.940%	5.998	Baker et al. (2013)
-0.84	-25.08	5	81.77	2.360%	1.929	Baker et al. (2013)
35.38	-23.66	5	87.18	4.870%	4.246	Baker et al. (2013)
2.59	-25.98	5	133.74	1.800%	2.413	Baker et al. (2013)
37.82	-20.51	5	71.21	4.620%	3.289	Baker et al. (2013)
21.73	-33.49	5	88.99	2.050%	1.823	Baker et al. (2013)
13.99	-30.38	5	164.10	2.390%	3.929	Baker et al. (2013)
33.08	-28.68	5	87.54	2.650%	2.323	Baker et al. (2013)
18.02	-31.99	5	52.24	3.580%	1.869	Baker et al. (2013)
25.28	-34.98	5	120.97	2.360%	2.854	Baker et al. (2013)
28.58	-35.74	5	96.36	2.200%	2.119	Baker et al. (2013)
30.91	-33.35	5	67.40	4.740%	3.197	Baker et al. (2013)

-41.69	-42.45	5	31.56	0.730%	0.229	Baker et al. (2013)
49.19	-10.43	5	36.68	1.900%	0.697	Baker et al. (2013)
41.28	-19.03	5	46.42	2.880%	1.339	Baker et al. (2013)
-16.58	-24.99	5	16.84	2.610%	0.440	Baker et al. (2013)
49.89	-2.66	5	16.52	10.200%	1.685	Baker et al. (2013)
-8.85	-24.99	5	92.87	2.010%	1.871	Baker et al. (2013)
-37.51	-36.87	5	10.70	1.000%	0.107	Baker et al. (2013)
-32.15	-30.04	5	12.22	1.540%	0.189	Baker et al. (2013)
-24.49	-25	5	13.59	1.310%	0.178	Baker et al. (2013)
-28.08	-26.03	5	19.27	0.700%	0.135	Baker et al. (2013)
-20.87	-24.99	5	22.90	2.260%	0.517	Baker et al. (2013)
21.31	-18.93	10	2673.82	1.200%	32.043	Baker et al. (2013)
21.34	-18.48	10	1625.41	1.800%	29.252	Baker et al. (2013)
20.88	-18.22	9	941.80	1.810%	17.050	Baker et al. (2013)
29.64	-17.93	9	385.58	2.970%	11.434	Baker et al. (2013)
8.41	-23.11	10	159.41	2.100%	3.347	Baker et al. (2013)
21.7	-19.09	9	230.91	3.150%	7.263	Baker et al. (2013)
0.48	-24.79	10	154.35	3.140%	4.845	Baker et al. (2013)
32.25	-20.37	9	44.82	4.910%	2.200	Baker et al. (2013)
5.47	-23.84	10	46.13	3.800%	1.755	Baker et al. (2013)
-13.56	-25	10	28.75	2.740%	0.787	Baker et al. (2013)
2.94	-24.34	10	34.31	5.460%	1.872	Baker et al. (2013)
39.59	-20.25	9	91.39	3.900%	3.560	Baker et al. (2013)
-9.85	-25	10	28.46	3.640%	1.035	Baker et al. (2013)
-2.77	-25	10	33.98	3.720%	1.263	Baker et al. (2013)
-6.33	-25	10	39.31	2.490%	0.977	Baker et al. (2013)

-38.06	1.43	10	26.30	7.450%	1.960	Baker et al. (2013)
-38.21	10.94	10	27.13	2.400%	0.652	Baker et al. (2013)
-32.23	-3.1	10	8.94	6.510%	0.582	Baker et al. (2013)
-24.12	-16.31	10	14.72	2.560%	0.376	Baker et al. (2013)
-20.83	-22.45	10	17.36	2.230%	0.388	Baker et al. (2013)
-27.41	-9.15	10	14.38	2.300%	0.331	Baker et al. (2013)
47.9	-14.27	9	14.08	3.390%	0.477	Baker et al. (2013)
43.15	-19.63	9	17.71	1.850%	0.327	Baker et al. (2013)
48.26	-10.61	9	19.46	3.110%	0.605	Baker et al. (2013)
46.37	-17.57	9	19.47	4.010%	0.781	Baker et al. (2013)
-17.34	-24.99	10	21.00	3.100%	0.652	Baker et al. (2013)
11.21	-30.39	6	2465.28	0.120%	2.945	Baker et al. (2013)
17.48	-33.48	6	658.56	0.880%	5.799	Baker et al. (2013)
5.52	-27.64	6	165.59	0.580%	0.952	Baker et al. (2013)
34.64	-40.26	6	139.95	0.610%	0.851	Baker et al. (2013)
-25.87	-19.15	5	21.16	1.220%	0.259	Baker et al. (2013)
-0.26	-25.58	6	24.52	0.120%	0.030	Baker et al. (2013)
24.32	-36.98	6	36.13	10.150%	3.667	Baker et al. (2013)
-27.84	-10.42	5	8.96	1.630%	0.146	Baker et al. (2013)
30.07	-41.18	6	14.77	10.260%	1.516	Baker et al. (2013)
-14.91	-25	6	20.25	2.990%	0.606	Baker et al. (2013)
-32.37	13.58	5	16.50	3.630%	0.599	Baker et al. (2013)
-29.64	-1.05	5	12.48	2.480%	0.309	Baker et al. (2013)
45.1	-19.12	6	15.64	3.630%	0.568	Baker et al. (2013)
39.52	-30.44	6	9.65	97.960%	9.451	Baker et al. (2013)
13.03	-31.27	11	641.79	1.360%	8.725	Baker et al. (2013)
1.41	-25.68	11	364.66	3.010%	10.978	Baker et al. (2013)
-2.31	-25	11	86.68	2.620%	2.272	Baker et al. (2013)

9.08	-29.23	11	123.34	2.200%	2.714	Baker et al. (2013)
15.9	-32.69	11	184.91	2.280%	4.215	Baker et al. (2013)
36.62	-27.85	10	24.23	1.920%	0.464	Baker et al. (2013)
4.32	-27.06	11	34.76	5.680%	1.974	Baker et al. (2013)
-17.81	-25	11	27.64	1.790%	0.494	Baker et al. (2013)
-6.73	-25	11	43.44	3.660%	1.590	Baker et al. (2013)
-21.86	-20.76	11	30.62	0.910%	0.279	Baker et al. (2013)
-13.79	-25	11	35.98	1.540%	0.554	Baker et al. (2013)
20.26	-34.92	11	28.98	2.100%	0.608	Baker et al. (2013)
-31.26	1.28	11	15.35	1.390%	0.214	Baker et al. (2013)
-27.84	-7.09	11	14.21	1.330%	0.189	Baker et al. (2013)
-24.47	-14.88	11	9.22	2.000%	0.184	Baker et al. (2013)
40.84	-22.48	10	10.96	3.400%	0.373	Baker et al. (2013)
24.86	-37.25	11	13.72	2.070%	0.284	Baker et al. (2013)
47.1	-17.12	10	13.81	3.040%	0.420	Baker et al. (2013)
27.99	-37.64	10	14.18	3.780%	0.536	Baker et al. (2013)
49.73	-13.88	10	17.69	1.540%	0.273	Baker et al. (2013)
37.15	-26.52	10	18.32	7.690%	1.408	Baker et al. (2013)
37.71	-25.62	10	19.20	1.540%	0.295	Baker et al. (2013)
37.09	-26.31	10	20.09	6.460%	1.298	Baker et al. (2013)
30.11	-34.87	10	20.64	1.240%	0.256	Baker et al. (2013)
-20.4	-23.7	11	20.98	1.540%	0.323	Baker et al. (2013)
35	-31	10	22.29	2.250%	0.501	Baker et al. (2013)
44.48	-18.97	10	22.90	2.320%	0.531	Baker et al. (2013)
-33.4	7.74	11	26.80	1.240%	0.333	Baker et al. (2013)
-10.45	-25	11	28.84	3.810%	1.098	Baker et al. (2013)
9.17	-31.05	10	▼	▼	14.539	Baker et al. (2017)

Deleted: NaN
Deleted: NaN

-33.99	17.47	2	61.41	2.080%	1.277	Sholkovitz et al. (2012)
-34.05	16.02	2	6.03	10.050%	0.606	Sholkovitz et al. (2012)
-55.28	-0.03	3	9.76	47.810%	4.665	Sholkovitz et al. (2012)
-41.81	9.39	2	11.61	15.250%	1.771	Sholkovitz et al. (2012)
-35.27	14.17	2	17.17	5.990%	1.029	Sholkovitz et al. (2012)
-38.66	11.64	2	7.02	9.990%	0.701	Sholkovitz et al. (2012)
-50.09	1.8	3	11.57	15.790%	1.827	Sholkovitz et al. (2012)
-45.8	6.01	2	6.91	22.350%	1.544	Sholkovitz et al. (2012)
16.21	-30.66	1	16699.67	0.330%	55.867	Sholkovitz et al. (2012)
20.89	-26.97	1	15048.11	0.480%	72.127	Sholkovitz et al. (2012)
16.22	-30.65	1	12763.37	0.450%	57.655	Sholkovitz et al. (2012)
24.02	-27.68	1	9463.10	0.530%	50.503	Sholkovitz et al. (2012)
16.22	-30.65	1	9441.55	0.580%	54.308	Sholkovitz et al. (2012)
17.78	-27.68	1	8069.10	1.340%	108.367	Sholkovitz et al. (2012)
12.65	-26.81	1	6604.73	0.410%	27.299	Sholkovitz et al. (2012)
12.56	-31.92	1	5527.98	0.700%	38.493	Sholkovitz et al. (2012)
12.61	-29.16	1	4850.03	0.570%	27.832	Sholkovitz et al. (2012)
16.4	-29.73	1	4826.19	0.650%	31.194	Sholkovitz et al. (2012)
16.16	-30.65	1	1290.02	1.670%	21.599	Sholkovitz et al. (2012)
25.77	-27.06	1	968.67	1.140%	11.049	Sholkovitz et al. (2012)
24.91	-21.29	1	874.93	1.090%	9.542	Sholkovitz et al. (2012)
13.85	-25.69	1	850.54	1.640%	13.991	Sholkovitz et al. (2012)
12.54	-34.33	1	761.43	1.200%	9.126	Sholkovitz et al. (2012)
18.07	-24.55	1	564.59	2.000%	11.292	Sholkovitz et al. (2012)
25.74	-24.72	1	466.22	1.470%	6.847	Sholkovitz et al. (2012)
16.36	-24.9	1	421.21	4.320%	18.181	Sholkovitz et al. (2012)
19.42	-25.32	1	397.15	1.620%	6.447	Sholkovitz et al. (2012)
21.6	-26.52	1	250.14	1.610%	4.034	Sholkovitz et al. (2012)

23.96	-27.84	1	34.39	4.710%	1.621	Sholkovitz et al. (2012)
25.99	-29	1	27.78	5.650%	1.569	Sholkovitz et al. (2012)
14.31	-30.64	1	42.27	3.570%	1.508	Sholkovitz et al. (2012)
12.57	-34	1	42.18	3.560%	1.502	Sholkovitz et al. (2012)
12.55	-31.63	1	41.31	3.560%	1.473	Sholkovitz et al. (2012)
26.43	-24.84	2	145.71	2.540%	3.701	Sholkovitz et al. (2012)
26.51	-27.93	1	59.66	9.410%	5.614	Sholkovitz et al. (2012)
-40.02	3.19	10	61.92	0.540%	0.335	Jickells et al. (2016)
-37.59	11.18	11	14.83	1.820%	0.269	Jickells et al. (2016)
-35.42	15.38	10	24.50	1.010%	0.249	Jickells et al. (2016)
-36.67	12.7	11	28.84	0.870%	0.251	Jickells et al. (2016)
-35.16	15.8	11	33.16	0.620%	0.206	Jickells et al. (2016)
-39.1	7.96	10	33.70	0.500%	0.167	Jickells et al. (2016)
-37.27	11.95	10	34.03	0.540%	0.185	Jickells et al. (2016)
-34.51	17.33	11	35.42	2.600%	0.919	Jickells et al. (2016)
-40.01	-0.83	10	41.82	2.120%	0.885	Jickells et al. (2016)
-35.9	10.91	11	49.04	0.720%	0.352	Jickells et al. (2016)
-38.92	0.24	10	137.29	0.340%	0.465	Jickells et al. (2016)
12.58	-22.69	2	5823.34	0.670%	39.171	Powell et al. (2015)
12.58	-23.66	2	5096.88	0.450%	22.764	Powell et al. (2015)
10.88	-25.42	2	3681.33	0.810%	29.930	Powell et al. (2015)
12.42	-24.54	2	3139.56	0.510%	16.165	Powell et al. (2015)
13.48	-28.85	3	2746.91	0.030%	0.938	Powell et al. (2015)
16.47	-28.59	3	1997.33	0.060%	1.116	Powell et al. (2015)
12.87	-17.77	2	2750.85	0.620%	17.097	Powell et al. (2015)
6.85	-25.55	2	2516.99	0.650%	16.416	Powell et al. (2015)
12.58	-18.21	2	2597.83	0.980%	25.541	Powell et al. (2015)
12.56	-20.35	2	1600.85	1.240%	19.815	Powell et al. (2015)

2.92	-25.41	2	1494.29	0.570%	8.536	Powell et al. (2015)
5.53	-27.46	3	832.03	1.430%	11.927	Powell et al. (2015)
-1.94	-25.71	3	468.05	1.360%	6.370	Powell et al. (2015)
2.99	-26.68	3	515.51	1.360%	7.033	Powell et al. (2015)
1.22	-26.04	3	314.02	1.260%	3.962	Powell et al. (2015)
7.89	-28.14	3	452.97	1.170%	5.320	Powell et al. (2015)
10.17	-28.66	3	254.82	1.270%	3.231	Powell et al. (2015)
-1.38	-25.23	3	64.31	2.930%	1.884	Powell et al. (2015)
20.19	-26.84	3	70.52	0.430%	0.304	Powell et al. (2015)
22.34	-24.06	3	75.41	0.430%	0.325	Powell et al. (2015)
-6.56	-25.06	3	75.74	0.430%	0.326	Powell et al. (2015)
18.3	-28.25	3	75.80	0.520%	0.395	Powell et al. (2015)
-5.37	-25.07	3	81.98	0.650%	0.530	Powell et al. (2015)
-4.53	-25.34	3	83.94	1.290%	1.080	Powell et al. (2015)
27.59	-22.76	5	91.86	4.590%	4.213	Powell et al. (2015)
27.63	-23.23	5	122.15	2.680%	3.271	Powell et al. (2015)
27.81	-23.34	5	25.09	4.370%	1.095	Powell et al. (2015)
27.79	-23.34	5	39.55	6.190%	2.449	Powell et al. (2015)
27.81	-22.42	5	52.96	3.530%	1.870	Powell et al. (2015)
27.88	-21.46	5	58.18	4.670%	2.716	Powell et al. (2015)
27.86	-23.07	5	31.43	4.300%	1.351	Powell et al. (2015)
27.86	-21.44	5	83.19	5.100%	4.241	Powell et al. (2015)
19.64	-18.55	5	₹	₹	25.279	Powell et al. (2015)
19.64	-18.11	5	₹	₹	25.126	Powell et al. (2015)
21.49	-17.86	5	₹	₹	25.046	Powell et al. (2015)
21.07	-18.33	5	₹	₹	22.396	Powell et al. (2015)
19.66	-18.8	5	₹	₹	21.728	Powell et al. (2015)
19.78	-18.36	5	₹	₹	18.981	Powell et al. (2015)

- Deleted: NaN

-36.77	-52.81	1	34.91	1.870%	0.651	Jickells et al. (2016)
-35.83	-54.04	1	58.55	1.480%	0.869	Jickells et al. (2016)
17.97	-18.5	9	330.56	1.420%	4.705	Baker et al. (2006b)
-34.5	-53.36	10	84.66	5.170%	4.380	Baker et al. (2006b)
13.06	-18.36	9	323.20	1.730%	5.582	Baker et al. (2006b)
-5.07	-13.45	9	16.19	5.600%	0.907	Baker et al. (2006b)
22.66	-18.3	9	115.35	3.780%	4.361	Baker et al. (2006b)
3.55	-16.76	9	55.30	4.240%	2.346	Baker et al. (2006b)
-23.65	-36.6	10	89.34	5.190%	4.633	Baker et al. (2006b)
-1.2	-15.8	9	54.46	5.590%	3.042	Baker et al. (2006b)
-9.83	-17.04	10	41.72	4.980%	2.076	Baker et al. (2006b)
27.76	-17.53	9	14.88	4.800%	0.715	Baker et al. (2006b)
-32.66	-50.4	10	15.80	8.720%	1.378	Baker et al. (2006b)
-10.91	-13.97	10	17.87	4.230%	0.756	Baker et al. (2006b)
36.86	-14.49	9	18.49	50.830%	9.399	Baker et al. (2006b)
-13.85	-22.62	10	23.37	4.580%	1.070	Baker et al. (2006b)
-5.79	-14.86	9	20.95	5.350%	1.121	Baker et al. (2006b)
42.03	-11.31	9	8.02	14.570%	1.168	Baker et al. (2006b)
-20.68	-32.26	10	8.10	6.190%	0.501	Baker et al. (2006b)
-17.74	-28.09	10	8.32	7.800%	0.649	Baker et al. (2006b)
-47.15	-57.05	10	11.31	4.610%	0.522	Baker et al. (2006b)
-38.75	-56.2	10	12.40	11.320%	1.403	Baker et al. (2006b)
46.56	-7.91	9	8.26	23.020%	1.903	Baker et al. (2006b)
32.61	-16.13	9	5.86	4.600%	0.270	Baker et al. (2006b)
-29.63	-45.61	10	8.15	13.140%	1.071	Baker et al. (2006b)
-25.71	-39.63	10	10.49	10.200%	1.070	Baker et al. (2006b)
11	-19.73	11	3537.46	0.540%	19.167	Baker et al. (2006a)
10.79	-17.99	11	3696.06	0.900%	33.112	Baker et al. (2006a)

9.46	-24.69	11	3124.49	0.630%	19.695	Baker et al. (2006a)
10.16	-19.71	11	1882.73	0.950%	17.920	Baker et al. (2006a)
11.04	-17.75	11	1520.71	1.570%	23.803	Baker et al. (2006a)
11.26	-20.19	11	1261.81	1.960%	24.710	Baker et al. (2006a)
10	-31.78	10	1154.38	0.680%	7.881	Baker et al. (2006a)
10.81	-23.18	11	993.55	1.610%	16.039	Baker et al. (2006a)
10	-43.29	10	397.02	1.200%	4.782	Baker et al. (2006a)
3.76	-7.97	11	277.48	2.290%	6.353	Baker et al. (2006a)
10.28	-52.57	10	324.83	0.710%	2.316	Baker et al. (2006a)
8.15	-18.04	11	485.58	1.960%	9.499	Baker et al. (2006a)
10	-28.92	10	541.67	0.540%	2.950	Baker et al. (2006a)
7.18	-24.38	11	150.50	1.930%	2.902	Baker et al. (2006a)
10.78	-56.2	10	317.82	1.020%	3.241	Baker et al. (2006a)
10.01	-34.82	10	393.79	1.120%	4.396	Baker et al. (2006a)
10.02	-37.62	10	258.87	1.920%	4.969	Baker et al. (2006a)
0.01	-24.74	10	38.94	4.060%	1.581	Baker et al. (2006a)
10	-46.44	10	295.26	1.220%	3.611	Baker et al. (2006a)
3.55	-3.68	11	196.61	2.400%	4.726	Baker et al. (2006a)
10	-49.7	10	33.36	2.220%	0.740	Baker et al. (2006a)
8.5	-26.94	10	203.18	2.000%	4.060	Baker et al. (2006a)
4.68	-11.93	11	181.48	3.190%	5.797	Baker et al. (2006a)
1.03	-23.49	10	35.88	2.230%	0.800	Baker et al. (2006a)
6.13	-15.41	11	170.41	2.960%	5.044	Baker et al. (2006a)
10	-40.31	10	95.69	2.510%	2.400	Baker et al. (2006a)
1.56	-26.1	10	20.01	7.910%	1.582	Baker et al. (2006a)
5.04	-26.34	10	26.65	3.190%	0.851	Baker et al. (2006a)
18.08	-16.76	7	4941.49	0.770%	38.120	Powell et al. (2015)
18.51	-16.5	7	3251.40	1.060%	34.420	Powell et al. (2015)

19.31	-17.8	7	2383.48	0.910%	21.636	Powell et al. (2015)
18.78	-17.84	7	2304.23	0.600%	13.734	Powell et al. (2015)
18.33	-16.51	7	2197.04	1.110%	24.475	Powell et al. (2015)
18	-18.01	7	1563.36	1.570%	24.567	Powell et al. (2015)
20.06	-17.3	7	1312.01	1.020%	13.388	Powell et al. (2015)
18.97	-16.78	7	1107.29	1.460%	16.163	Powell et al. (2015)
19.72	-18.58	7	898.17	1.270%	11.415	Powell et al. (2015)
18	-20.01	7	765.00	1.680%	12.856	Powell et al. (2015)
18	-22.01	7	690.14	1.880%	12.995	Powell et al. (2015)
18.54	-18.42	7	683.92	1.650%	11.264	Powell et al. (2015)
18.37	-17.48	7	557.83	1.360%	7.561	Powell et al. (2015)
18.34	-16.71	7	544.17	1.570%	8.520	Powell et al. (2015)
18.86	-19.23	7	434.04	1.950%	8.448	Powell et al. (2015)
20.14	-17.89	7	370.70	1.580%	5.845	Powell et al. (2015)
17.94	-24.58	7	339.87	1.980%	6.724	Powell et al. (2015)
21.2	-20.77	8	290.13	1.930%	5.601	Powell et al. (2015)
26.18	-18	8	63.00	7.210%	4.545	Powell et al. (2015)
23.97	-19.84	8	172.45	2.930%	5.052	Powell et al. (2015)
19.77	-20.77	8	154.07	2.480%	3.815	Powell et al. (2015)
59.6	-20.18	8	214.30	1.630%	3.503	Sholkovitz et al. (2012)
59.31	-19.1	8	133.97	6.080%	8.143	Sholkovitz et al. (2012)
58.53	-12.43	8	50.28	12.060%	6.064	Sholkovitz et al. (2012)
59.6	-19.72	8	60.34	2.400%	1.446	Sholkovitz et al. (2012)
59.2	-19.85	8	36.53	2.800%	1.021	Sholkovitz et al. (2012)
59.91	-19.34	8	9.80	16.000%	1.567	Sholkovitz et al. (2012)
59.52	-18.99	8	14.75	8.570%	1.264	Sholkovitz et al. (2012)
59.51	-19.89	8	9.08	8.810%	0.800	Sholkovitz et al. (2012)
59.8	-20.6	8	8.57	17.130%	1.468	Sholkovitz et al. (2012)

59.31	-19.48	8	0.41	74.690%	0.303	Sholkovitz et al. (2012)
59.3	-19.68	8	0.42		0.764	Sholkovitz et al. (2012)
59.94	-20.22	8	0.45		0.808	Sholkovitz et al. (2012)
59.62	-19.07	8	0.52	58.490%	0.304	Sholkovitz et al. (2012)
59.22	-19.98	8	4.12	23.150%	0.953	Sholkovitz et al. (2012)
59.71	-15.91	8	4.43	4.860%	0.215	Sholkovitz et al. (2012)
61.16	-18.83	8	7.46	5.080%	0.379	Sholkovitz et al. (2012)
60.74	-20.02	6	₹	₹	1.989	Achterberg et al. (2018)
58.55	-8.68	6	₹	₹	1.941	Achterberg et al. (2018)
57.47	-11.31	6	₹	₹	1.230	Achterberg et al. (2018)
58.26	-16.44	6	₹	₹	1.182	Achterberg et al. (2018)
60.72	-38.49	7	13.62	3.650%	0.498	Achterberg et al. (2018)
61.18	-22.42	8	10.01	5.810%	0.582	Achterberg et al. (2018)
59.42	-33.4	7	10.38	9.630%	1.000	Achterberg et al. (2018)
63.41	-29.44	8	8.46	9.770%	0.826	Achterberg et al. (2018)
60	-38.59	7	2.34	13.370%	0.313	Achterberg et al. (2018)
61.19	-32.98	7	2.58	9.960%	0.257	Achterberg et al. (2018)
63.1	-18.76	5	84748.71	0.300%	253.115	Achterberg et al. (2018)
63.09	-19.08	5	67446.47	0.330%	222.051	Achterberg et al. (2018)
63.39	-21.31	5	2586.49	0.760%	19.620	Achterberg et al. (2018)
62.5	-19.97	5	259.06	4.900%	12.703	Achterberg et al. (2018)
60.98	-22.88	5	195.88	4.540%	8.892	Achterberg et al. (2018)
60	-35.01	4	58.84	3.000%	1.768	Achterberg et al. (2018)
59.98	-30.26	5	38.88	7.440%	2.894	Achterberg et al. (2018)
57.6	-16.82	4	10.57	2.100%	0.222	Achterberg et al. (2018)
44.72	-42.41	5	₹	₹	8.386	unknown
47	-39.65	5	₹	₹	7.726	unknown
59.62	-38.72	5	₹	₹	4.609	unknown

- Deleted: NaN

- Deleted: NaN
- Deleted: NaN
- Deleted: NaN
- Deleted: NaN
- Deleted: NaN

16.92	-21.95	2	501.18	0.530%	2.640	Sholkovitz et al. (2012)
13.44	-26.8	2	78.77	5.290%	4.167	Sholkovitz et al. (2012)
19.32	-28.87	1	86.29	1.780%	1.540	Sholkovitz et al. (2012)
19.3	-26	2	18.01	3.510%	0.633	Sholkovitz et al. (2012)
21.49	-28.21	1	21.82	7.820%	1.706	Sholkovitz et al. (2012)
16.93	-23.37	2	6.86	7.260%	0.498	Sholkovitz et al. (2012)
15.94	-24.8	2	15.58	8.880%	1.384	Sholkovitz et al. (2012)
28.17	-27.61	2	15.35	3.010%	0.462	Sholkovitz et al. (2012)
19.14	-23.59	2	64.16	3.720%	2.388	Sholkovitz et al. (2012)
24.68	-27.6	2	5.87	7.250%	0.426	Sholkovitz et al. (2012)
21.49	-27.6	2	79.91	0.860%	0.690	Sholkovitz et al. (2012)
18.31	-23.73	2	121.91	1.610%	1.961	Sholkovitz et al. (2012)
15.83	-25.16	2	35.74	5.860%	2.095	Sholkovitz et al. (2012)
29.09	-19.44	2	1.66	31.630%	0.524	Sholkovitz et al. (2012)
16.27	-27.97	2	1.73		2.684	Sholkovitz et al. (2012)
22.85	-25.38	1	1.93		3.771	Sholkovitz et al. (2012)
29.82	-26.01	2	1.93	31.640%	0.610	Sholkovitz et al. (2012)
-58.6	-58.78	4	78.80	4.500%	3.544	Sholkovitz et al. (2012)
-41.15	9.84	2	136.13	6.390%	8.697	Sholkovitz et al. (2012)
-68.22	-4.35	2	25.51	2.370%	0.605	Sholkovitz et al. (2012)
-68.59	-13.27	3	32.73	3.640%	1.193	Sholkovitz et al. (2012)
-64.33	-0.24	2	15.09	7.170%	1.082	Sholkovitz et al. (2012)
-61.02	0.02	2	16.99	7.960%	1.353	Sholkovitz et al. (2012)
-67.46	0.06	3	11.28	2.020%	0.228	Sholkovitz et al. (2012)
-61.8	-53.82	3	5.53		6.123	Sholkovitz et al. (2012)
-56.76	0.03	2	11.98	11.730%	1.406	Sholkovitz et al. (2012)
-67.37	-23.54	3	14.87	3.080%	0.458	Sholkovitz et al. (2012)
-53.01	0.02	2	9.19	20.060%	1.843	Sholkovitz et al. (2012)

-65.85	-33.87	3	1.48	43.320%	0.641	Sholkovitz et al. (2012)
-64.7	-43.56	3	2.60	22.600%	0.586	Sholkovitz et al. (2012)
-63.61	-50.98	3	2.90	8.660%	0.251	Sholkovitz et al. (2012)
-59.91	-55.73	4	3.73	9.300%	0.347	Sholkovitz et al. (2012)
-68.94	-3.5	3	7.18	4.070%	0.292	Sholkovitz et al. (2012)
-45.37	6.37	2	7.38	3.690%	0.273	Sholkovitz et al. (2012)
-49.4	2.31	2	7.49	4.020%	0.301	Sholkovitz et al. (2012)
-56.88	-62.3	4	8.38	4.440%	0.372	Sholkovitz et al. (2012)
-55.63	-64.62	4	10.32	13.740%	1.418	Sholkovitz et al. (2012)
-50.63	72.08	1	4.10	☹	☹	Wagener, et al. (2008)
-51.4	76.49	1	43.00	☹	☹	Wagener, et al. (2008)
-50.9	73.53	1	4.50	☹	☹	Wagener, et al. (2008)
-52.11	72.17	2	2.70	☹	☹	Wagener, et al. (2008)
-51.18	70.12	2	17.00	☹	☹	Wagener, et al. (2008)
-49.24	65.85	2	11.00	☹	☹	Wagener, et al. (2008)
-12.77	214.06	10	0.15	9.550%	0.010	Wagener (2008)
-9.62	220.5	10	0.31	11.190%	0.040	Wagener (2008)
-17.68	234.63	11	1.95	2.040%	0.040	Wagener (2008)
-26.6	248.28	11	1.88	0.840%	0.010	Wagener (2008)
-29.58	259.76	11	0.29	2.310%	0.010	Wagener (2008)
-32.81	276.98	11	0.16	☹	☹	Wagener (2008)
-35.21	286.85	12	13.00	5.460%	0.710	Wagener (2008)
43.68	7.33	10	210.35	2.250%	4.740	Wagener (2008)
43.68	7.33	11	69.49	2.800%	1.950	Wagener (2008)
43.68	7.33	12	105.60	3.110%	3.280	Wagener (2008)
43.68	7.33	2	87.59	3.110%	2.720	Wagener (2008)
43.68	7.33	3	68.94	9.870%	6.810	Wagener (2008)

- Deleted: NaN

- Deleted: NaN
- Deleted: NaN

References

- Achterberg, E. P., Steigenberger, S., Marsay, C. M., Lemoigne, F. A. C., Painter, S. C., Baker, A. R., Connelly, D. P., Moore, C. M., Tagliabue, A. and Tanhua, T.: Iron Biogeochemistry in the High Latitude North Atlantic Ocean, *Sci. Rep.*, 8(1), doi:10.1038/s41598-018-19472-1, 2018.
- Albani, S., Mahowald, N. M., Perry, A. T., Scanza, R. A., Zender, C. S., Heavens, N. G., Maggi, V., Kok, J. F. and Otto-Bliesner, B. L.: Improved dust representation in the Community Atmosphere Model, *J. Adv. Model. Earth Syst.*, 6(3), 541–570, doi:10.1002/2013MS000279, 2014.
- Baker, A. R. and Jickells, T. D.: Atmospheric deposition of soluble trace elements along the Atlantic Meridional Transect (AMT), *Prog. Oceanogr.*, 158, 41–51, doi:10.1016/j.pocean.2016.10.002, 2017.
- Baker, A. R., French, M. and Linge, K. L.: Trends in aerosol nutrient solubility along a west–east transect of the Saharan dust plume, *Geophys. Res. Lett.*, 33(7), L07805, doi:10.1029/2005GL024764, 2006a.
- Baker, A. R., Jickells, T. D., Witt, M. and Linge, K. L.: Trends in the solubility of iron, aluminium, manganese and phosphorus in aerosol collected over the Atlantic Ocean, *Mar. Chem.*, 98(1), 43–58, doi:10.1016/j.marchem.2005.06.004, 2006b.
- Baker, A. R., Weston, K., Kelly, S. D., Voss, M., Streu, P. and Cape, J. N.: Dry and wet deposition of nutrients from the tropical Atlantic atmosphere: Links to primary productivity and nitrogen fixation, *Deep Sea Res. Part I Oceanogr. Res. Pap.*, 54(10), 1704–1720, doi:10.1016/j.dsr.2007.07.001, 2007.
- Baker, A. R., Adams, C., Bell, T. G., Jickells, T. D. and Ganzeveld, L.: Estimation of atmospheric nutrient inputs to the Atlantic Ocean from 50°N to 50°S based on large-scale field sampling: Iron and other dust-associated elements, *Global Biogeochem. Cycles*, 27(3), 755–767, doi:10.1002/gbc.20062, 2013.
- Bowie, A. R., Lannuzel, D., Remenyi, T. A., Wagener, T., Lam, P. J., Boyd, P. W., Guieu, C., Townsend, A. T. and Trull, T. W.: Biogeochemical iron budgets of the Southern Ocean south of Australia: Decoupling of iron and nutrient cycles in the subantarctic zone by the summertime supply, *Global Biogeochem. Cycles*, 23(4), GB4034, doi:10.1029/2009GB003500, 2009.
- Buck, C. S., Landing, W. M., Resing, J. A. and Lebon, G. T.: Aerosol iron and aluminum solubility in the northwest Pacific Ocean: Results from the 2002 IOC cruise, *Geochemistry, Geophys. Geosystems*, 7(4), 1–21, doi:10.1029/2005GC000977, 2006.
- Buck, C. S., Landing, W. M., Resing, J. A. and Measures, C. I.: The solubility and deposition of aerosol Fe and other trace elements in the North Atlantic Ocean: Observations from the A16N CLIVAR/CO2 repeat hydrography section, *Mar. Chem.*, 120(1–4), 57–70, doi:10.1016/j.marchem.2008.08.003, 2010.
- Buck, C. S., Landing, W. M. and Resing, J.: Pacific Ocean aerosols: Deposition and solubility of iron, aluminum, and other trace elements, *Mar. Chem.*, 157(2013), 117–130, doi:10.1016/j.marchem.2013.09.005, 2013.
- Buck, C. S., Aguilar-Islas, A. N. A., Marsay, C., Kadko, D. & Landing, W. Trace element concentrations, elemental ratios,

and enrichment factors observed in aerosol samples collected during the US GEOTRACES eastern Pacific Ocean transect (GP16). *Chem. Geol.* in review, (2018).

Chance, R., Jickells, T. D. and Baker, A. R.: Atmospheric trace metal concentrations, solubility and deposition fluxes in remote marine air over the south-east Atlantic, *Mar. Chem.*, 177, 1–12, doi:10.1016/j.marchem.2015.06.028, 2015.

Gao, Y., Xu, G., Zhan, J., Zhang, J., Li, W., Lin, Q., Chen, L. and Lin, H.: Spatial and particle size distributions of atmospheric dissolvable iron in aerosols and its input to the Southern Ocean and coastal East Antarctica, *J. Geophys. Res. Atmos.*, 118(22), 12,634–12,648, doi:10.1002/2013JD020367, 2013.

Guieu, C. C., Bonnet, S., Wagener, T., Lo?e-Pilot, M.-D. and Lo?e-Pilot, M. D.: Biomass burning as a source of dissolved iron to the open ocean?, *Geophys. Res. Lett.*, 32(19), L19608, doi:10.1029/2005GL022962, 2005.

Ito, A.: Global modeling study of potentially bioavailable iron input from shipboard aerosol sources to the ocean, *Global Biogeochem. Cycles*, 27(1), 1–10, doi:10.1029/2012GB004378, 2013.

Ito, A.: Atmospheric Processing of Combustion Aerosols as a Source of Bioavailable Iron, *Environ. Sci. Technol. Lett.*, 2(3), 70–75, doi:10.1021/acs.estlett.5b00007, 2015.

Ito, A. and Shi, Z.: Delivery of anthropogenic bioavailable iron from mineral dust and combustion aerosols to the ocean, *Atmos. Chem. Phys.*, 16(1), 85–99, doi:10.5194/acp-16-85-2016, 2016.

Ito, A. and Xu, L.: Response of acid mobilization of iron-containing mineral dust to improvement of air quality projected in the future, *Atmos. Chem. Phys.*, 14(7), 3441–3459, doi:10.5194/acp-14-3441-2014, 2014.

Jickells, T. D., Baker, A. R. and Chance, R.: Atmospheric transport of trace elements and nutrients to the oceans, *Philos. Trans. R. Soc. A Math. Phys. Eng. Sci.*, 374(2081), 20150286, doi:10.1098/rsta.2015.0286, 2016.

Kok, J. F., Ridley, D. A., Zhou, Q., Miller, R. L., Zhao, C., Heald, C. L., Ward, D. S., Albani, S. and Haustein, K.: Smaller desert dust cooling effect estimated from analysis of dust size and abundance, *Nat. Geosci.*, 10(4), 274–278, doi:10.1038/ngeo2912, 2017.

Kumar, A., Sarin, M. M. and Srinivas, B.: Aerosol iron solubility over Bay of Bengal: Role of anthropogenic sources and chemical processing, *Mar. Chem.*, 121(1–4), 167–175, doi:10.1016/j.marchem.2010.04.005, 2010.

Longo, A. F., Feng, Y., Lai, B., Landing, W. M., Shelley, R. U., Nenes, A., Mihalopoulos, N., Violaki, K. and Ingall, E. D.: Influence of Atmospheric Processes on the Solubility and Composition of Iron in Saharan Dust, *Environ. Sci. Technol.*, 50(13), 6912–6920, doi:10.1021/acs.est.6b02605, 2016.

Luo, C., Mahowald, N., Bond, T., Chuang, P. Y., Artaxo, P., Siefert, R., Chen, Y. and Schauer, J.: Combustion iron distribution and deposition, *Global Biogeochem. Cycles*, 22(1), GB1012, doi:10.1029/2007GB002964, 2008.

Powell, C. F., Baker, A. R., Jickells, T. D., Bange, H. W., Chance, R. J. and Yodle, C.: Estimation of the Atmospheric Flux of Nutrients and Trace Metals to the Eastern Tropical North Atlantic Ocean, *J. Atmos. Sci.*, 72(10), 4029–4045, doi:10.1175/JAS-D-15-0011.1, 2015.

Shelley, R. U., Morton, P. L. and Landing, W. M.: Elemental ratios and enrichment factors in aerosols from the US-GEOTRACES North Atlantic transects, *Deep Sea Res. Part II Top. Stud. Oceanogr.*, 116, 262–272,

doi:10.1016/j.dsr2.2014.12.005, 2015.

Shi, Z., Krom, M. D., Jickells, T. D., Bonneville, S., Carslaw, K. S., Mihalopoulos, N., Baker, A. R. and Benning, L. G.: Impacts on iron solubility in the mineral dust by processes in the source region and the atmosphere: A review, *Aeolian Res.*, 5, 21–42, doi:10.1016/j.aeolia.2012.03.001, 2012.

Sholkovitz, E. R., Sedwick, P. N., Church, T. M., Baker, A. R. and Powell, C. F.: Fractional solubility of aerosol iron: Synthesis of a global-scale data set, *Geochim. Cosmochim. Acta*, 89, 173–189, doi:10.1016/j.gca.2012.04.022, 2012.

Srinivas, B. and Sarin, M. M.: Atmospheric deposition of N, P and Fe to the Northern Indian Ocean: Implications to C- and N-fixation, *Sci. Total Environ.*, 456–457, 104–114, doi:10.1016/j.scitotenv.2013.03.068, 2013.

Srinivas, B., Sarin, M. M. and Kumar, A.: Impact of anthropogenic sources on aerosol iron solubility over the Bay of Bengal and the Arabian Sea, *Biogeochemistry*, 110(1–3), 257–268, doi:10.1007/s10533-011-9680-1, 2012.

Wagener, T.: Le fer à l'interface océan-atmosphère: Flux et processus de dissolution dans l'eau de mer, Université de la Méditerranée. [online] Available from: <https://tel.archives-ouvertes.fr/tel-00270558>, 2008.

Wagener, T., Guieu, C., Losno, R., Bonnet, S. and Mahowald, N.: Revisiting atmospheric dust export to the Southern Hemisphere ocean: Biogeochemical implications, *Global Biogeochem. Cycles*, 22(2), GB2006, doi:10.1029/2007GB002984, 2008.